NASA Contractor Report 168347

Radar Data Smoothing Filter Study

J. V. White

June 1984

National Aeronautics and
Space Administration

Goddard Space Flight Center
Wallops Flight Facility
Wallops Island, Virginia 23337

NASA Contractor Report 168347

Radar Data Smoothing Filter Study

J. V. White

The Analytical Sciences Corporation
One Jacob Way
Reading, MA 01867

Prepared Under Contract No. NAS5-27425

National Aeronautics and
Space Administration

Goddard Space Flight Center
Wallops Flight Facility
Wallops Island, Virginia 23337

FOREWORD

The scope of this study was to plan, develop, and implement methods for analyzing and improving the performance of digital data smoothing filters used in the Radar Data Reduction System at the Wallops Flight Facility (WFF). During the study the following primary objectives were accomplished: (1) The accuracy of the current WFF data smoothing technique was analyzed for a variety of radars and payloads, using tracking data provided by WFF for this purpose; (2) alternative data noise reduction techniques were assessed and recommendations were made for improving radar data processing at WFF; (3) a data-adaptive algorithm, based on Kalman filtering and smoothing techniques, was developed for estimating payload trajectories above the atmosphere from noisy time-varying radar data; (4) the new trajectory estimation algorithm was tested and verified using radar tracking data from Peru provided by WFF.

Significant contributions to this study were made by the following individuals: A.R. Leschack provided the algorithm for computing Keplerian trajectories in Section 5.3 and provided an independent numerical check of the nominal-trajectory algorithm in Section 5.4; J.D. Goldstein provided the discrete-time linearized equations of motion for small perturbations about the Keplerian trajectory used in Section 5.4; and A.E. Rhenals developed software for analyzing the WFF data tapes, performed a significant part of the radar data error analysis under Tasks 1 and 2, and contributed theoretical analyses of the effects of smoothing filters on nominal payload trajectory signals and data noise covariances.

TABLE OF CONTENTS

		Page
FOREWORD		iii
LIST OF FIGURES		ix
LIST OF TABLES		xi
1.	INTRODUCTION	1-1
	1.1 Objectives of the Study	1-1
	1.2 Technical Approach	1-2
	1.3 Organization of Report	1-2
2.	TASK 1 - ANALYSIS OF WFF RADAR DATA	2-1
	2.1 Introduction	2-1
	2.1.1 Objective	2-1
	2.1.2 Radar Data	2-1
	2.1.3 Approach	2-1
	2.1.4 Interpretation	2-2
	2.2 Technical Approach	2-3
	2.2.1 Data Signal Components	2-3
	2.2.2 Data Analysis	2-4
	2.2.3 Example Results	2-6
	2.3 Analysis Results	2-10
	2.3.1 Introduction	2-10
	2.3.2 State-Space Models	2-10
	2.3.3 Applications of State-Space Models	2-12
	2.3.4 Error Models	2-16
	2.4 Summary and Conclusions	2-22
	2.4.1 Summary	2-22
	2.4.2 Conclusions	2-23
3.	TASK 2 - ANALYSIS OF ERROR PROPAGATION INTO POSITIONAL DATA	3-1
	3.1 Introduction	3-1
	3.1.1 Objective	3-1
	3.1.2 Approach	3-1
	3.2 State-Space Filter Equations	3-3
	3.3 Error Covariance Equations	3-6
	3.4 Coordinate Transformation Equations	3-7

TABLE OF CONTENTS (Continued)

		Page
3.5	Analysis Results	3-8
3.5.1	Rms Errors of Smoothed Tracking Data	3-8
3.5.2	Rms Errors in Positional Data Products	3-9
3.6	Smoothing-Filter Trajectory Bias	3-10
3.7	Summary and Conclusions	3-14
3.7.1	Summary of Task 2	3-14
3.7.2	Conclusions	3-14
4.	TASK 3 - ALTERNATIVE NOISE REDUCTION TECHNIQUES	4-1
4.1	Introduction	4-1
4.2	Discussion of Current Filtering Techniques	4-2
4.3	Alternative Noise Reduction Techniques	4-3
4.3.1	Avoiding Filter-Induced Trajectory Bias	4-3
4.3.2	Estimating and Minimizing Noise Levels in Smoothed Data	4-4
4.4	Summary of Recommendations for Improving the Current WFF Noise Reduction Techniques	4-7
5.	TASK 4 - DEVELOPMENT AND VERIFICATION OF AN ALTERNATIVE SMOOTHING ALGORITHM	5-1
5.1	Introduction	5-2
5.1.1	Objective	5-2
5.1.2	Technical Approach	5-2
5.2	Overview of Algorithm	5-4
5.3	Keplerian-Trajectory Module	5-9
5.4	Nominal-Trajectory Module	5-12
5.4.1	Normal Gravitation	5-12
5.4.2	Atmospheric Drag	5-15
5.4.3	Trajectory Corrections	5-17
5.5	Radar-Measurements Module	5-21
5.5.1	Introduction	5-21
5.5.2	Transform to Geocentric Coordinates	5-22
5.5.3	Transform to Topocentric Coordinates	5-24
5.5.4	Transformation to Radar Coordinates	5-25
5.5.5	Outputs	5-25
5.6	Kalman-Filter Module	5-26
5.6.1	Introduction	5-26
5.6.2	Kalman Filter Equations	5-29
5.6.3	State-Space Model	5-31
5.6.4	State Variables	5-32
5.6.5	Transition Matrix ϕ	5-34
5.6.6	State Noise Covariance Q	5-35
5.6.7	Measurement Matrix H	5-35
5.6.8	Measurement Noise Covariance R	5-39
5.6.9	Kalman Filter Outputs	5-43

TABLE OF CONTENTS (Continued)

		Page
5.7	Smoother Module	5-44
	5.7.1 Introduction	5-44
	5.7.2 Smoothing Equations	5-46
	5.7.3 Outputs	5-48
5.8	Verification of the Trajectory Estimation Algorithm	5-50
	5.8.1 Nike-Orion Trajectory	5-50
	5.8.2 Terrier-Malemute Trajectory	5-60
	5.8.3 Conclusions	5-66
5.9	Summary	5-66
6.	SUMMARY, CONCLUSIONS, AND RECOMMENDATIONS FOR FUTURE STUDY	6-1
6.1	Summary	6-1
6.2	Conclusions	6-1
6.3	Recommendations for Future Study	6-3
APPENDIX A	ORTHOGONAL POLYNOMIALS	A-1
APPENDIX B	AUTOGRESSIVE MODELING	B-1
APPENDIX C	STOCHASTIC STATE-SPACE MODELING	C-1
APPENDIX D	COORDINATES, TRANSFORMATIONS, AND COVARIANCES	D-1
APPENDIX E	RADAR MEASUREMENT EQUATIONS	E-1
REFERENCES		R-1

LIST OF FIGURES

Figure		Page
2.2-1	Block Diagram of Data Analysis	2-5
2.2-2	Loki Optical Azimuth Data	2-7
2.2-3	Loki Optical Elevation Data	2-7
2.2-4	Loki Optical Range Data	2-8
2.2-5	Example of Selecting the Trajectory Polynomial, Loki Sphere Tracking Data	2-9
2.3-1	Estimated Power Spectra and Coherences for Residual Zuni Tracking Data, Radar No. 3	2-18
2.3-2	Estimated Power Spectra and Coherences for Loki Optical Residual Tracking Data, Radar No. 3	2-20
2.3-3	Estimated Power Spectra and Coherences for Loki Sphere Residual Tracking Data, Radar No. 5	2-21
3.1-1	Block Diagram of Error Propagation Analysis	3-2
3.6-1	Smoothing-Filter Trajectory Bias	3-11
3.6-2	Filter-Induced Range Bias for Loki Optical Tracking Data, Radar No. 3	3-12
3.6-3	Filter-Induced Azimuth and Elevation Bias for Loki Optical Tracking Data, Radar No. 3	3-13
4.1-1	Review of Current WFF Smoothing Technique	4-1
4.3-1	Estimation of High-Frequency Noise Variance from Power Spectral Density (PSD)	4-6
5.2-1	Block Diagram of Pre-Processing for Trajectory Estimation	5-5
5.2-2	Block Diagram of Kalman Filter/Smoother for Trajectory Estimation	5-7
5.5-1	Radar-Measurements Module	5-22

LIST OF FIGURES (Continued)

Figure		Page
5.6-1	Block Diagram of Data Processing in a Kalman Filter	5-28
5.6-2	Kalman Filter Module	5-44
5.7-1	Smoother Module	5-45
5.8-1	Residual Tracking Data, Nike-Orion 31.027 Trajectory, Radar No. 8	5-51
5.8-2	Kalman Filter Innovations, Nike-Orion 31.027 Trajectory, Radar No. 8	5-53
5.8-3	Smoothed Trajectory Estimates, Nike-Orion 31.027 Trajectory, Radar No. 8	5-54
5.8-4	Residual Tracking Data, Nike-Orion 31.027 Trajectory, Radar No. 41	5-56
5.8-5	Kalman Filter Innovations, Nike-Orion 31.027 Trajectory, Radar No. 41	5-57
5.8-6	Smoothed Trajectory Estimates, Nike-Orion 31.027 Trajectory, Radar No. 41	5-58
5.8-7	Residual Tracking Data, Terrier-Malemute 29.019 Trajectory, Radar No. 8	5-63
5.8-8	Kalman Filter Innovations, Terrier-Malemute 29.019 Trajectory, Radar No. 8	5-64
5.8-9	Smoothed Trajectory Estimates, Terrier-Malemute 29.019 Trajectory, Radar No. 8	5-65
D.1-1	Orientation with Respect to the Earth of the Earth-Centered Inertial Coordinate Axes at Time t - 0.	D-2
D.1-2	Orientation with Respect to the Earth of the Geocentric Coordinate Axes at Time t.	D-2
D.1-3	Spherical Geocentric Coordinates of Point P. λ = East Longitude, ϕ = North Latitude, R = Radial Distance	D-4
D.1-4	Cross-section of Reference Ellipsoid and Point P. Geodetic Coordinates of P are ϕ = North Latitude and h = Height	D-6

LIST OF TABLES

Table		Page
2.1-1	Radar Data Sets Analyzed	2-2
2.3-1	Estimated Rms Noise Levels	2-17
3.5-1	Standard Deviations of Smoothed Residual Tracking Data	3-9
3.5-2	Estimated Rms of Noise-Like Errors in Positional Data	3-10
5.4-1	Geodetic Parameters for Reference Ellipsoid	5-13
5.8-1	Statistics of Differences Between Two Nike-Orion 31.027 Trajectory Estimates	5-60

1. INTRODUCTION

1.1 OBJECTIVES OF THE STUDY

The scope of this study was to plan, develop, and implement methods for analyzing and improving the performance of digital data smoothing filters. These filters are used in the Radar Data Reduction System at the Goddard Space Flight Center/Wallops Flight Facility (GSFC/WFF) to reduce noise levels in radar tracking data. The study had four primary objectives:

- To develop stochastic models for radar tracking data provided by WFF
- To determine the propagation of the radar data errors through the WFF noise-reduction filters into positional data products
- To assess alternative noise reduction techniques and to make recommendations for improving the current filtering techniques
- To develop and verify an algorithm for smoothing radar tracking data to estimate trajectories above the atmosphere.

To meet these objectives, the study was divided into four tasks:

- Task 1 - Analysis of Radar Data
- Task 2 - Analysis of Existing Filters and Error Propagation into Positional Data

- Task 3 - Assessment of Alternative Noise-Reduction Techniques
- Task 4 - Development and Verification of Trajectory Estimation Algorithm.

1.2 TECHNICAL APPROACH

The analysis of WFF radar data and smoothing filters (Tasks 1 and 2) is based on stochastic modeling and covariance analysis of noise-like errors. A combination of autoregressive and state-space techniques is used. The autoregressive models provide a cross-check on the more flexible state-space models. To estimate the root-mean-square (rms) noise levels, state-space covariance analysis is used.

The assessment of alternative smoothing techniques (Task 3) is based on the results of the first two tasks and the theory of Kalman optimal filtering and smoothing.

A new algorithm for processing noisy radar data for trajectories above the atmosphere is developed and verified under Task 4. The algorithm is based on Kalman filtering and smoothing techniques. Radar tracking data from Peru (provided by WFF) are used to verify the effectiveness of the algorithm with real data, including data from two radars simultaneously tracking a single payload.

1.3 ORGANIZATION OF REPORT

Each task of the study is documented in a separate chapter (Chapters 2-5). The report ends with Chapter 6, which

provides a summary of the investigation, the primary conclusions, and recommendations for further study. Supporting mathematical definitions and analyses are presented in Appendices A, B, C, D, and E. In particular, the coordinate systems used in this study are defined in Appendix D.

2. TASK 1 - ANALYSIS OF WFF RADAR DATA

2.1 INTRODUCTION

2.1.1 Objective

The main objective of Task 1 is to develop error models for WFF radar tracking data. The data consist of azimuth, elevation, and range measurements for a variety of payloads and radars as provided by the WFF PASS-1 data processing program (Ref. 1). The noise-like zero-mean errors in the radar data are modeled as stochastic processes. In contrast, the systematic errors in the radar data and the payload trajectories are modeled as polynomials.

2.1.2 Radar Data

The radar data sets analyzed in this study are listed in Table 2.1-1. The first three radars listed in the table (Radars Nos. 3, 5, and 6) correspond to data analyzed under Task 1. The remainder of the data sets (Radars Nos. 8 and 41) are analyzed under Task 4.

2.1.3 Approach

The technical approach for analyzing the radar data consists of three steps:

- Model the nominal trajectory for each time series using least-squares orthogonal polynomial functions of time

TABLE 2.1-1
RADAR DATA SETS ANALYZED

RADAR	RADAR LOCATION N.LATITUDE E.LONGITUDE HEIGHT	TRAJECTORY NAME, MODEL NO., DATE
NO. 3 (WFF)	37.841309 deg -75.485102 deg 14.08 m	ZUNI, E1-0425... 0427, 12/1/82 S. LOKI OPTICAL, (MODEL & DATE UNKNOWN)
NO. 5 (WFF)	37.860229 deg -75.509309 deg 16.66 m	S. LOKI SPHERE, T1-0503, 4/25/83 S. LOKI OPTICAL, (MODEL & DATE UNKNOWN)
NO. 6 (WFF)	37.841585 deg -75.484692 deg 9.43 m	S. LOKI OPTICAL, T1-6615, 12/11/81
NO. 8 (PERU)	-12.4993 deg -76.7965 deg 74.26 m	NIKE-ORION 31.027, TU2-0367, 3/9/83 TERRIER-MALEMUTE 29.019, TU-0364, 3/15/83
NO. 41 (PERU)	-12.4990 deg -76.7954 deg 71.02 m	NIKE-ORION 31.027, TU2-0367, 3/9/83

- Select the appropriate degree for each polynomial by using a spectral analysis of the residual tracking data (residual = data - polynomial)
- Develop stochastic state-space models for the noise-like residual tracking data (azimuth, elevation, and range).

Detailed information about the technical approach is presented in Section 2.2.

2.1.4 Interpretation

The polynomials fitted to the data are nominal estimates of the payload trajectory plus any systematic measurement errors. The residual data (actual measurements minus a polynomial) are

a combination of measurement errors and zero-mean noise-like signals caused by payload dynamics. The statistics of the residual data are used to model the noise in the radar measurements.

2.2 TECHNICAL APPROACH

2.2.1 Data Signal Components

The radar tracking data may be represented as the sum of three signal components:

$$\begin{matrix}\text{Tracking} \\ \text{Data}\end{matrix} = \begin{matrix}\text{Payload} \\ \text{Motion}\end{matrix} + \begin{matrix}\text{Systematic} \\ \text{Error}\end{matrix} + \begin{matrix}\text{Noise-Like} \\ \text{Error}\end{matrix} \qquad (2.2\text{-}1)$$

The goal of the analysis is to estimate the statistics of the noise-like errors in real tracking data. This requires that the noise-like error signals be distinguished from the payload motion and systematic error signals. The following criteria are used to distinguish between the data signals:

Payload Motion and Systematic Error	• Polynomial-like • High Coherence between Azimuth, Elevation, and Range Data
Noise-Like Error	• Zero-Mean Random Noise • Low Coherence between Azimuth, Elevation, and Range Data

These criteria are the logical basis for the data analysis described in the next section.

2.2.2 Data Analysis

The radar tracking data are analyzed in three steps:

- Step 1 - Fit orthogonal polynomials to the raw tracking data. The purpose of this is to estimate the signal components caused by payload motion and systematic error. Orthogonal polynomials are used to avoid numerical problems that can otherwise make it difficult to fit the polynomials accurately.

- Step 2 - Develop stochastic models for the residual tracking data. The residual data (raw data minus polynomial) are expected to consist mostly of noise-like radar measurement errors when the degree of the polynomial is appropriate. The stochastic models for the residuals are developed using autoregressive and state-space modeling techniques.

- Step 3 - Select appropriate polynomial degrees based on power spectra and spectral coherences. The stochastic models developed in Step 2 are used to estimate the spectra and coherences. The appropriate polynomial degree is selected so that the azimuth, elevation, and range residuals have small coherences and nearly flat power spectra at low frequencies.

A block diagram of the data processing is shown in Fig. 2.2-1. Each block in this figure is explained in the following discussion.

Inputs - In Fig. 2.2-1 the inputs are "raw data." This means that the input data are in the form provided by the PASS-1 data processing program used at WFF. After plotting the individual time series for azimuth, elevation, and range data, obviously incorrect data are replaced by reasonable values using simple linear interpolation. If a low-frequency analysis

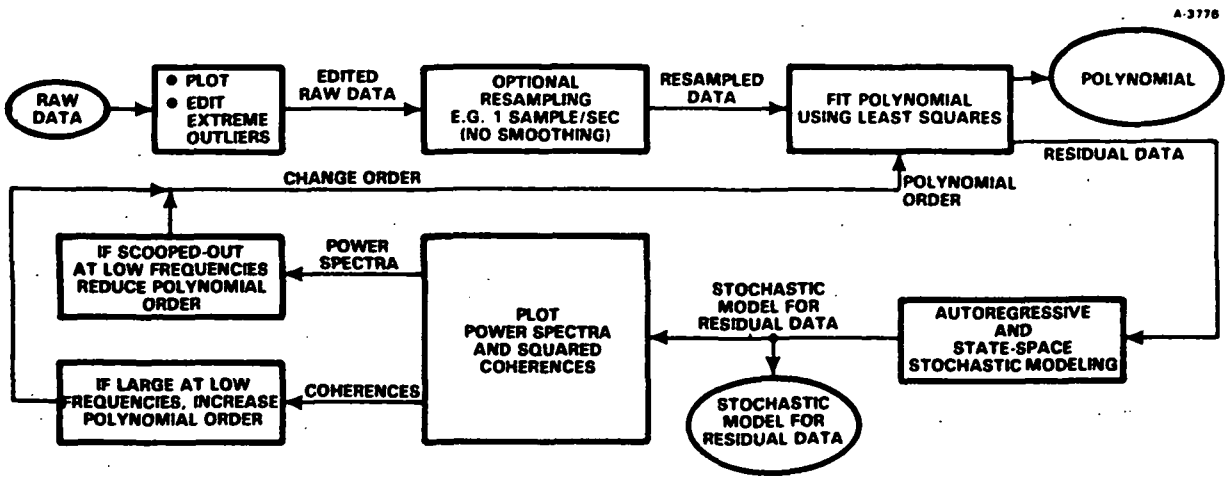

Figure 2.2-1 Block Diagram of Data Analysis

is being performed, the optional resampling is performed at a slower sampling rate than the raw data. No anti-aliasing filter is used in this resampling operation.

Fitting Polynomials - Orthogonal polynomials are fitted to subsets of the resampled data using least squares. The outputs of this procedure are: (1) the coefficients of the polynomial and (2) the residual data. The residuals are defined as the resampled data minus the polynomial. Typical subsets contain 500 measurements, and polynomial degrees usually range from 4 to 10 for the data sets analyzed in this study. The mathematical details of the polynomial fitting are presented in Appendix A.

Modeling Residual Data - The residual data are analyzed using autoregressive and state-space stochastic modeling techniques. (Mathematical discussions of these techniques are presented in Appendices B and C.) The stochastic models are

shaping filters, i.e., difference equations driven by white noise. The steady-state solutions of these difference equations define random processes that are models of the residual radar data. Power spectra and spectral coherences for the models are computed using formulas presented in Appendix B and Section 2.3.3.

Polynomial Degree Selection - The power spectra and spectral coherences are examined to determine if the polynomial degree is too small or too large. If there is significant coherence (>25%) at low frequencies, then the degree is judged to be too small. And if the power spectrum is scooped-out at low frequencies, the degree is judged to be too large. These criteria are consistent with the goal of distinguishing the signals caused by payload motion and systematic error from the signal caused by random measurement noise. As indicated in Fig. 2.2-1, if the degree needs to be changed, then the analysis process is repeated starting with a different polynomial degree.

2.2.3 Example Results

As an example of the results obtained, Figs. 2.2-2 to 2.2-4 depict the raw tracking data and residual data for Radar No. 3 tracking a Super Loki Optical payload. The ejection of the payload occurs at approximately 120 s.

Azimuth Data - Figure 2.2-2 shows that azimuth was nearly constant at 134 degrees (deg). A degree-10 polynomial is appropriate for modeling the payload motion and systematic error over this segment of data. The residuals about this polynomial look like homogeneous random noise. There is no visible anomally caused by the payload ejection.

Elevation Data - Figure 2.2-3 depicts the Loki-Optical elevation data. In this case a degree-8 polynomial was found

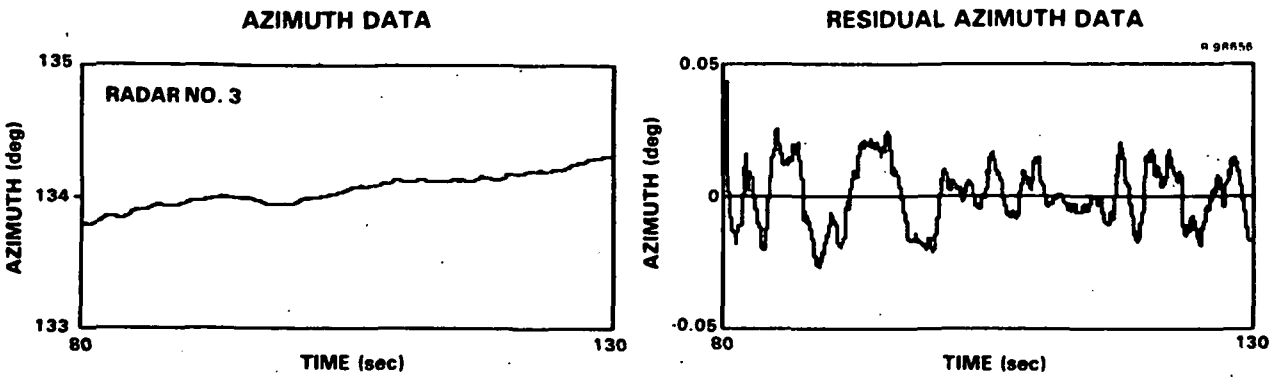

Figure 2.2-2 Loki Optical Azimuth Data

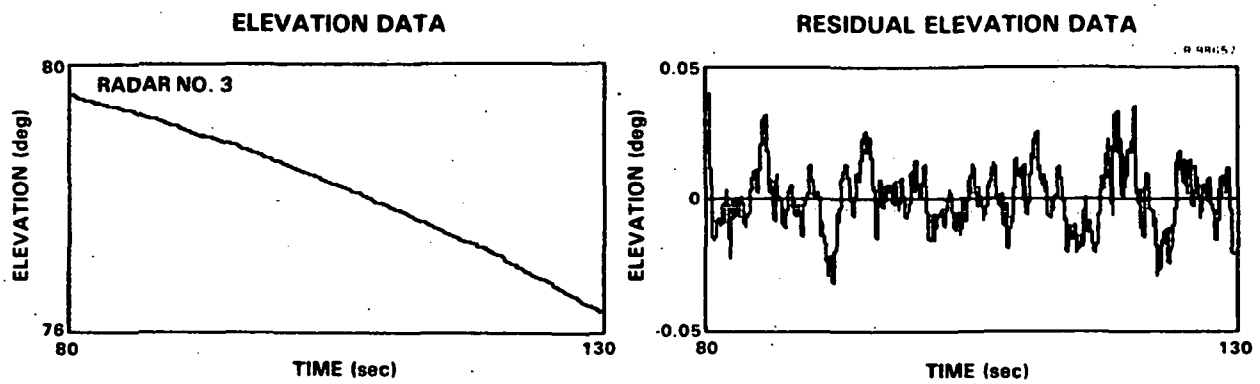

Figure 2.2-3 Loki Optical Elevation Data

to be appropriate. The residuals appear to be more random than the azimuth residuals shown in Fig. 2.2-2, which was confirmed by spectrum analysis. (The more random appearance corresponds to more power at higher frequencies.)

Range Data - The Loki-Optical range data are shown in Fig. 2.2-4. In this case a degree-8 polynomial was appropriate. Although the payload ejection is not visible in the raw range data, a strong localized inhomogeneity caused by the ejection is seen in the residual data. This is an example where the residual data contain a combination of both measurement noise and residual payload motion.

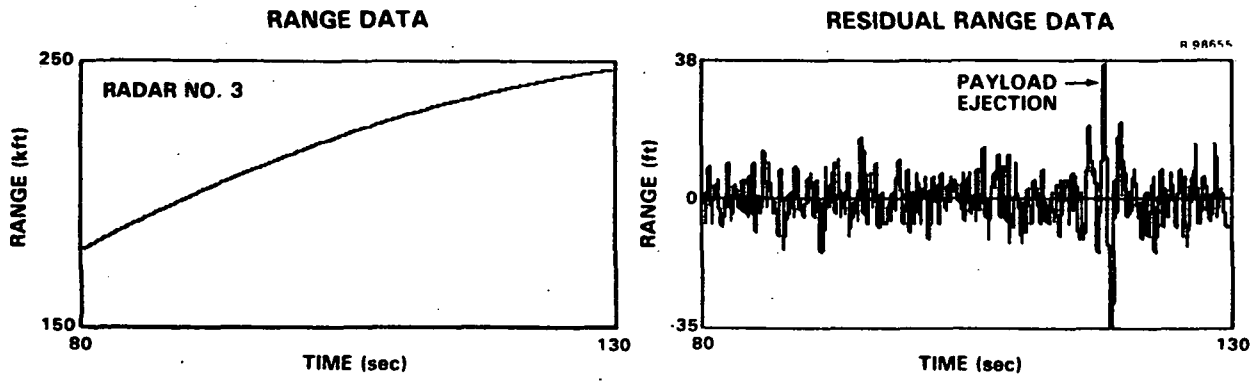

Figure 2.2-4 Loki Optical Range Data

Loki-Sphere Range Data - Figure 2.2-5 shows data from Radar No. 5 tracking a Super Loki Sphere payload. Two sets of analysis results are included for comparison. The pair on the left in Fig. 2.2-5 shows the residual range data for a degree-6 polynomial and the power spectrum estimated from the residual data using the autoregressive modeling technique described in Appendix B. The polynomial degree in this case is not too large because it yields a nearly flat power spectrum at low frequencies. In contrast, the right pair of plots show the results of using a polynomial of degree 15, which is too large. The degree-15 polynomial partially fits the low-frequency randomness of the radar data, as indicated by the dip in the power

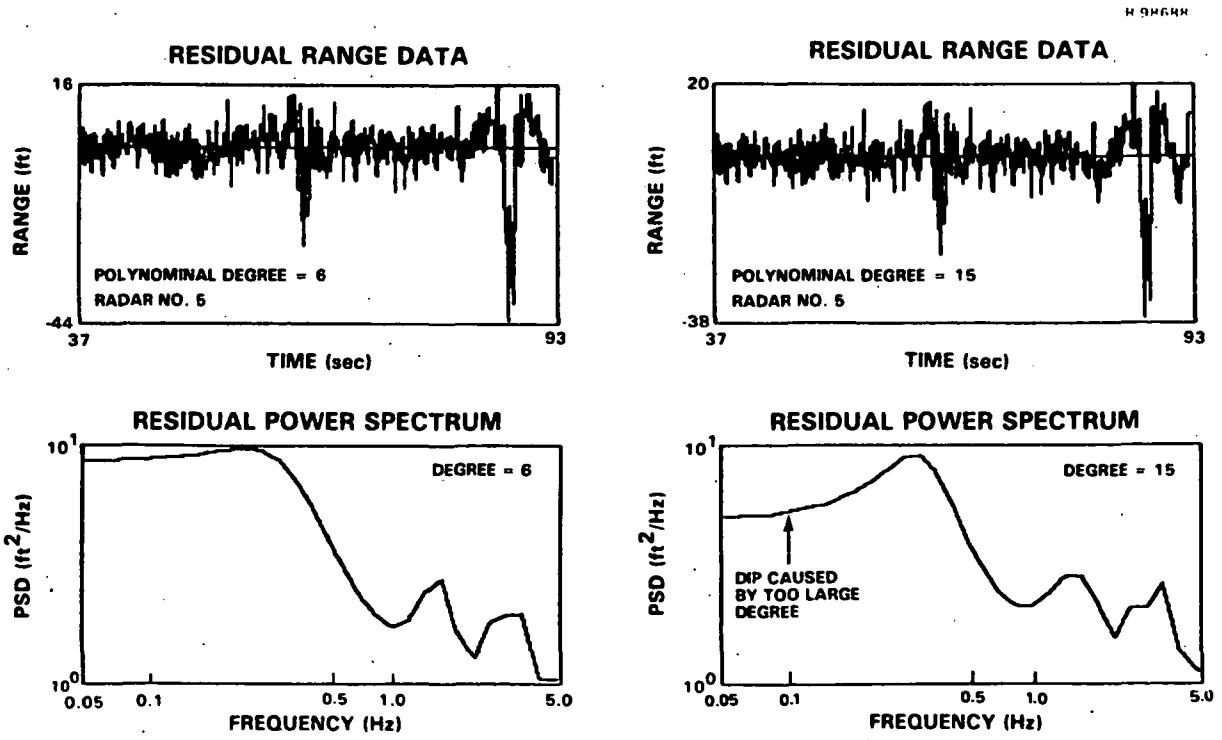

Figure 2.2-5 Example of Selecting the Trajectory Polynomial, Loki Sphere Tracking Data

spectrum. The result of using the degree-15 polynomial would be to slightly underestimate the low-frequency noise in the radar data. Therefore, the degree-6 polynomial is preferred.

2.3 ANALYSIS RESULTS

2.3.1 Introduction

Section 2.3 presents the results of applying the data analysis described in Section 2.2 to a variety of data sets provided by WFF. The principal results of this analysis are stochastic state-space models for residual radar tracking data. These models are used to estimate the power spectra, spectral coherences, and covariance matrices of noise-like errors in the tracking data. The covariance matrices are used in Chapter 3 to estimate the rms random errors in positional data products expressed in latitude, longitude, and height.

2.3.2 State-Space Models

In this secton the concept of a state-space stochastic model is introduced. Mathematical details about the state-space modeling technique used in this study are provided in Appendix C.

State-Space Equations - The residual tracking data consist of three time series, one for each of the azimuth, elevation, and range measurements. The three channels of data are combined to form a 3-vector:

$$\underline{y}_k = \begin{bmatrix} \text{azimuth} \\ \text{elevation} \\ \text{range} \end{bmatrix} \quad \text{at time} \quad k = 1,2,3... \qquad (2.3\text{-}1)$$

A state-space model for the vector random process $\underline{y}_k$ is represented by two equations: (1) a vector difference equation for the states; and (2) an algebraic equation relating the states to the observed process $\underline{y}_k$. The algebraic equation is:

$$\begin{aligned} \underline{y}_k &= H\underline{x}_k + \underline{\nu}_k \\ \underline{x}_k &= n\times 1 \text{ matrix of n state varibles} \\ H &= 3\times n \text{ output matrix} \\ \underline{\nu}_k &= 3\times 1 \text{ matrix of 3 white-noise processes} \\ \text{Cov}(\underline{\nu}_k) &= R = 3\times 3 \text{ covariance matrix} \end{aligned} \qquad (2.3\text{-}2)$$

The white noise $\underline{\nu}_k$ is called the innovations vector because it represents that part of the residual radar data $\underline{y}_k$ which is uncorrelated with the past radar data; the term $H\underline{x}_k$ in Eq. 2.3-2 represents that part of $\underline{y}_k$ which is correlated with the past. The state vector $\underline{x}_k$ contains all necessary information about the past data ($\underline{y}_{k-1}$, $\underline{y}_{k-2}$, ...).

The state vector satisfies the following difference equation:

$$\begin{aligned} \underline{x}_{k+1} &= \phi\underline{x}_k + G\underline{\nu}_k \\ \phi &= n\times n \text{ transition matrix} \\ G &= n\times 3 \text{ noise-gain matrix} \end{aligned} \qquad (2.3\text{-}3)$$

Equations 2.3-2 and 2.3-3 represent a state-space model in the innovations form. There are other forms of state-space models, but this is the form that is appropriate for stochastic modeling based on empirical data.

Modeling - The method of stochastic state-space modeling used in this study is based on a canonical-variates (CV) analysis of the data. (Mathematical details are described in Appendix C.) The canonical variates are used as estimates of the state variables:

$$\underline{x}_k = \begin{bmatrix} \text{1st canonical variate} \\ \text{2nd canonical variate} \\ \vdots \\ \text{nth canonical variate} \end{bmatrix} \begin{matrix} \leftarrow \text{most important state} \\ \leftarrow \text{2nd most important} \\ \\ \leftarrow \text{least important state} \end{matrix} \qquad (2.3\text{-}4)$$

By defining the state variables with the most important state listed first and the least important state listed last, it is straight-forward to compute a family of models by adding one state (canonical variate) at a time. In this way, a CV analysis of the radar data that yields n canonical variates can be used to compute the ϕ, G, H, and R matrices for n+1 different models. Each model contains a different number of state variables, ranging from zero states (a pure white-noise model) to an n-state model of maximum complexity. The Akaike information criterion (AIC) (Refs. 2-4) is then used to select from this family the one model that is best justified by the finite amount of radar data that was used for the analysis. This procedure avoids the problems of under modeling with too few states or over modeling with too many states.

2.3.3 Applications of State-Space Models

Power spectra - In this study, the state-space models are used to estimate power spectra, spectral coherences, and covariances of residual radar data. The power spectral density matrix of the residual radar data $\underline{y}_k$ is a 3×3 matrix:

$$S_{yy} = \begin{bmatrix} S_{AA} & S_{AE} & S_{AR} \\ S_{EA} & S_{EE} & S_{ER} \\ S_{RA} & S_{RE} & S_{RR} \end{bmatrix} \quad \begin{matrix} A \sim \text{AZIMUTH} \\ E \sim \text{ELEVATION} \\ R \sim \text{RANGE} \end{matrix} \qquad (2.3\text{-}5)$$

The elements along the main diagonal (S_{AA}, S_{EE}, and S_{RR}) are the auto spectra for the azimuth, elevation, and range data. The off-diagonal elements are cross spectra between the indicated pairs of measurements. The spectral density matrix is computed as follows using the state-space parameter matrices ϕ, G, H, and R:

$$S_{yy}(F) = \left[H[Ie^{i2\pi F} - \phi]^{-1} G + I \right] R \left[I + G^T [Ie^{-i2\pi F} - \phi^T]^{-1} H^T \right] \qquad (2.3\text{-}6)$$

F = Normalized Frequency [cycle/sampling interval]

I = Identity Matrix (either n×n or 3×3)

The elements of matrix S_{yy} are expressed in the same units as the corresponding elements of the covariance matrix of $\underline{y}_k$. The normalized frequency F ranges from -1/2 to 1/2 [cycle/sampling interval] and is related to the sampling frequency f_{samp} [Hz] and the regular frequency variable f [Hz] as follows:

$$F = f/f_{samp} \qquad (2.3\text{-}7)$$

The spectrum $S_{yy}(F)$ has the units of [variance]. It can be scaled to have the units of [variance/Hz], which are conventionally used for continuous-time signals, and then expressed as $\bar{S}_{yy}(f)$, a function of the frequency variable f [Hz] as follows:

$$\bar{S}_{yy}(f) = \frac{S_{yy}(f/f_{samp})}{f_{samp}} \qquad (2.3\text{-}8)$$

The covariance matrix P_{yy} of $\underline{y}_k$ is equal to the integral of the power spectrum (integration of the spectral density matrix element-by-element):

$$P_{yy} = \int_{-1/2}^{1/2} S_{yy}(F)\, dF = \int_{-f_{samp}/2}^{f_{samp}/2} \bar{S}_{yy}(f)\, df \qquad (2.3\text{-}9)$$

Spectral Coherence - The cross spectra (off-diagonal elements of S_{yy}) are complex valued because they represent the phase of the cross correlations between pairs of measurement processes. To suppress the phase information and focus attention on the magnitudes of the correlations as a function of frequency, the squared coherence (spectral coherence) is computed for each pair of measurement processes. For example, the squared coherence between the azimuth and range measurements, $C_{AR}(F)$, is defined by the formula:

$$C_{AR}(F) = \frac{|S_{AR}(F)|^2}{S_{AA}(F)\, S_{RR}(F)} \qquad (2.3\text{-}10)$$

The coherence between any other pair of measurements is defined in the same way.

The spectral coherence ranges in value from 0% to 100%. It measures how much of the variance of one random process can be explained as a linear transformation of another random process. Put differently, the coherence measures how much power the two processes have in common with each other on the average.

The coherence is a function of frequency and provides more information about the crosscorrelation structure than

simple correlation coefficients. (The squared correlation coefficient is equal to the area under the squared coherence function.) The spectral information contained in the coherence function is used in this study to determine when residual radar data from two different measurements (e.g., azimuth and range) contain correlated low-frequency signals (polynomial-like trajectory signals or systematic error signals). A significant occurrance of these signals produces coherence larger than 25% and indicates that a higher-degree polynomial is appropriate for computing the residual data.

Covariance Matrices - The state-space models are also used to compute covariance matrices for the residual radar data. The method for computing covariances described in this section is much more convenient than evaluating one of the integrals in Eq. 2.3-9. These covariances are used in Task 2 to estimate the rms errors in positional data derived from the radar measurements.

The covariance matrix of the residual radar measurements is denoted P_{yy}. It is computed by solving the following matrix equations, which contain the state-space parameter matrices ϕ, G, H, and R.

$P_{yy} = \text{cov}(\underline{y}_k)$ = Covariance Matrix of Azimuth, Elevation, and Range Data [3×3]

$P_{xx} = \text{cov}(\underline{x}_k)$ = Covariance Matrix of State Vector [n×n]

$$P_{yy} = H\, P_{xx}\, H^T + R \qquad (2.3\text{-}11)$$

$$P_{xx} = \phi\, P_{xx}\, \phi^T + GRG^T \qquad (2.3\text{-}12)$$

A practical way of solving equation 2.3-12 is to set P_{xx} initially equal to the n×n identity matrix and use this

matrix to evaluate the right side of Eq. 2.3-12. Then the new value of P_{xx} is used to evaluate the right side again, etc. until the value of P_{xx} remains unchanged to within the desired computational accuracy. This algorithm converges if ϕ represents a stable state-space model (i.e., all eigenvalues of ϕ have moduli less than unity). Once P_{xx} is computed, P_{yy} is computed using Eq. 2.3-11.

2.3.4 Error Models

In this section state-space models are presented for noise-like radar measurement errors. These models are based on analyses of residual radar data from WFF Radars Nos. 3, 5, and 6, which were tracking Zuni, Loki Optical, and Loki Sphere payloads. Root-mean-square (rms) values, power spectra, and spectral coherences are discussed.

Estimated rms Error Levels - Table 2.3-1 summarizes the rms values of the residual tracking data from four data sets. These rms values are estimates of the rms noise levels in the tracking data. The rms values were computed from stochastic state-space models for residual tracking data and do not include systematic errors in the tracking data. The residual angle data from radars Nos. 3 and 5 have rms values ranging from 2.9 mdeg to 11.4 mdeg, while the rms range data are more tightly clustered from 5.5 ft to 6.8 ft. Radar No. 6 has significantly higher estimated noise levels because it is a wide-band acquisition radar, which is not intended for accurate tracking. The Zuni error model is based on the analysis of three trajectories, while the other models are based on segments from single trajectories. More information about the estimated noise levels is presented in the following discussions of power spectra and spectral coherences.

TABLE 2.3-1

ESTIMATED RMS NOISE LEVELS

DATA SET	NOMINAL PAYLOAD COORDINATES	RMS RESIDUAL TRACKING DATA
ZUNI		
(Radar #3)		
(3 Trajectories)		
Azimuth	132 deg	4.4 mdeg
Elevation	15 deg	6.2 mdeg
Range	27 kft	5.5 ft
LOKI SPHERE		
(Radar #5)		
(37s to 93s)		
Azimuth	137 deg	2.9 mdeg
Elevation	42 deg	4.7 mdeg
Range	27 kft	6.0 ft
LOKI OPTICAL		
(Radar #3)		
(80s to 130s)		
Azimuth	139 deg	11.4 mdeg
Elevation	78 deg	11.4 mdeg
Range	220 kft	6.8 ft
LOKI OPTICAL		
(Radar #6)		
(22-27 min)		
(33-38 min)		
Azimuth	98 deg	53 mdeg
Elevation	18 deg	41 mdeg
Range	260 kft	41 ft

Radar No. 3 Power Spectra and Coherences - Figure 2.3-1 depicts the estimated power spectra (PSDs or power spectral densities) and squared coherences for the errors in the Zuni data from radar No. 3. These graphs were computed from the stochastic model derived from an analysis of the residual tracking data for three trajectories at a sampling rate of 10 samples per second. The coherence plots on the right side of Fig. 2.3-1 indicate that the squared coherences are less than 25% at low

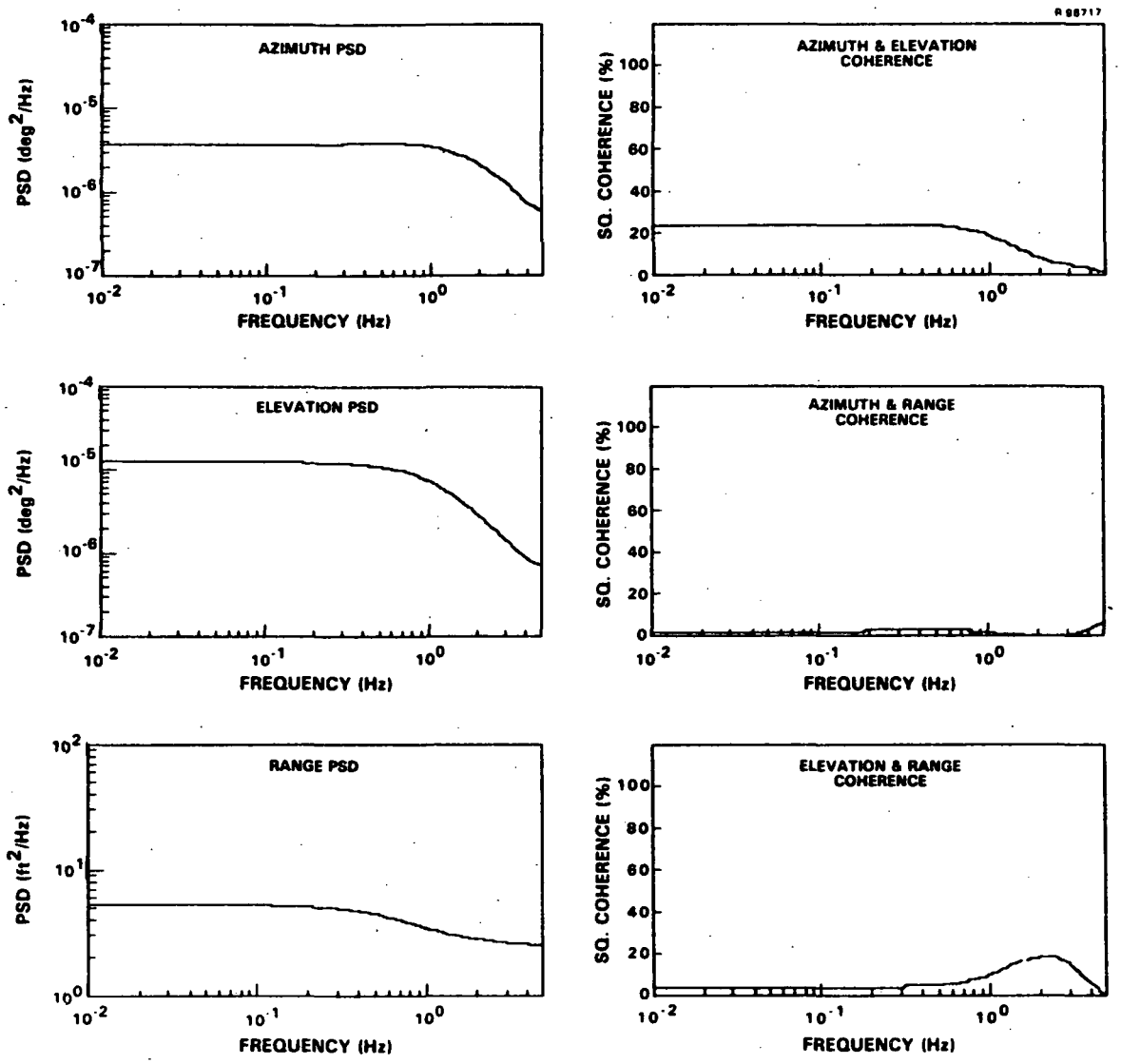

Figure 2.3-1 Estimated Power Spectra and Coherences for Residual Zuni Tracking Data, Radar No. 3

frequencies. At the same time, the spectrum plots on the left side are flat at low frequencies. This verifies that the low-frequency signals caused by payload motion and systematic measurement errors have been appropriately modeled and removed from the residual data.

According to Fig. 2.3-1 the range errors have the most nearly white (flat) spectrum, while the elevation errors are more nearly band limited. The frequency at which the elevation PSD decreases to half its low-frequency value is 1 Hz. The corresponding half-power frequency for the azimuth errors is 2.5 Hz.

Figure 2.3-2 depicts another set of estimated PSDs and coherences for noise-like errors in the data from radar No. 3. In this case, the radar was tracking a Super Loki rocket prior to ejection and its Optical payload after ejection. These plots were computed using a 10-sample/second tracking data shown in Figs. 2.2-2 through 2.2-4. The localized inhomogeniety in the range data (Fig. 2.2-4) is caused by the payload ejection and produces the hump in the range PSD (Fig. 2.3-2) at 0.7 Hz. Aside from this anomaly, the range PSD in Fig. 2.3-2 for the Optical payload is similar to the range PSD in Fig. 2.3-1 for the Zuni trajectories.

The azimuth and elevation PSDs in Fig. 2.3-2 for the Loki Optical tracking errors are significantly different from their Zuni counterparts in Fig. 2.3-1. The Loki Optical error spectra have 10-100 times as much power at low frequencies; while at high frequencies the two sets of PSDs are more nearly equal.

Radar No. 5 Power Spectra and Coherences - Figure 2.3-3 depicts the estimated PSDs and coherences for noise-like errors

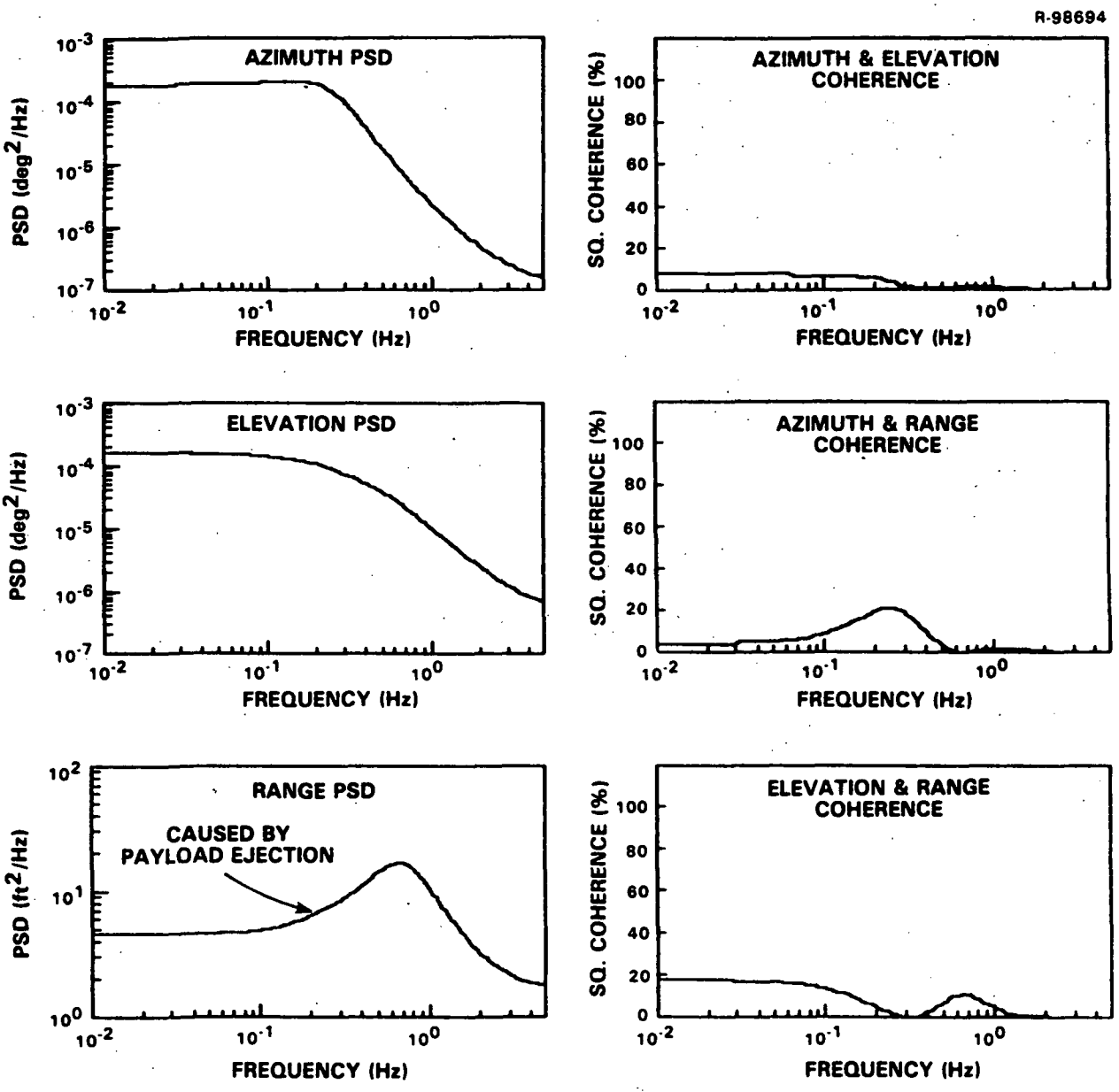

Figure 2.3-2 Estimated Power Spectra and Coherences for Loki Optical Residual Tracking Data, Radar No. 3

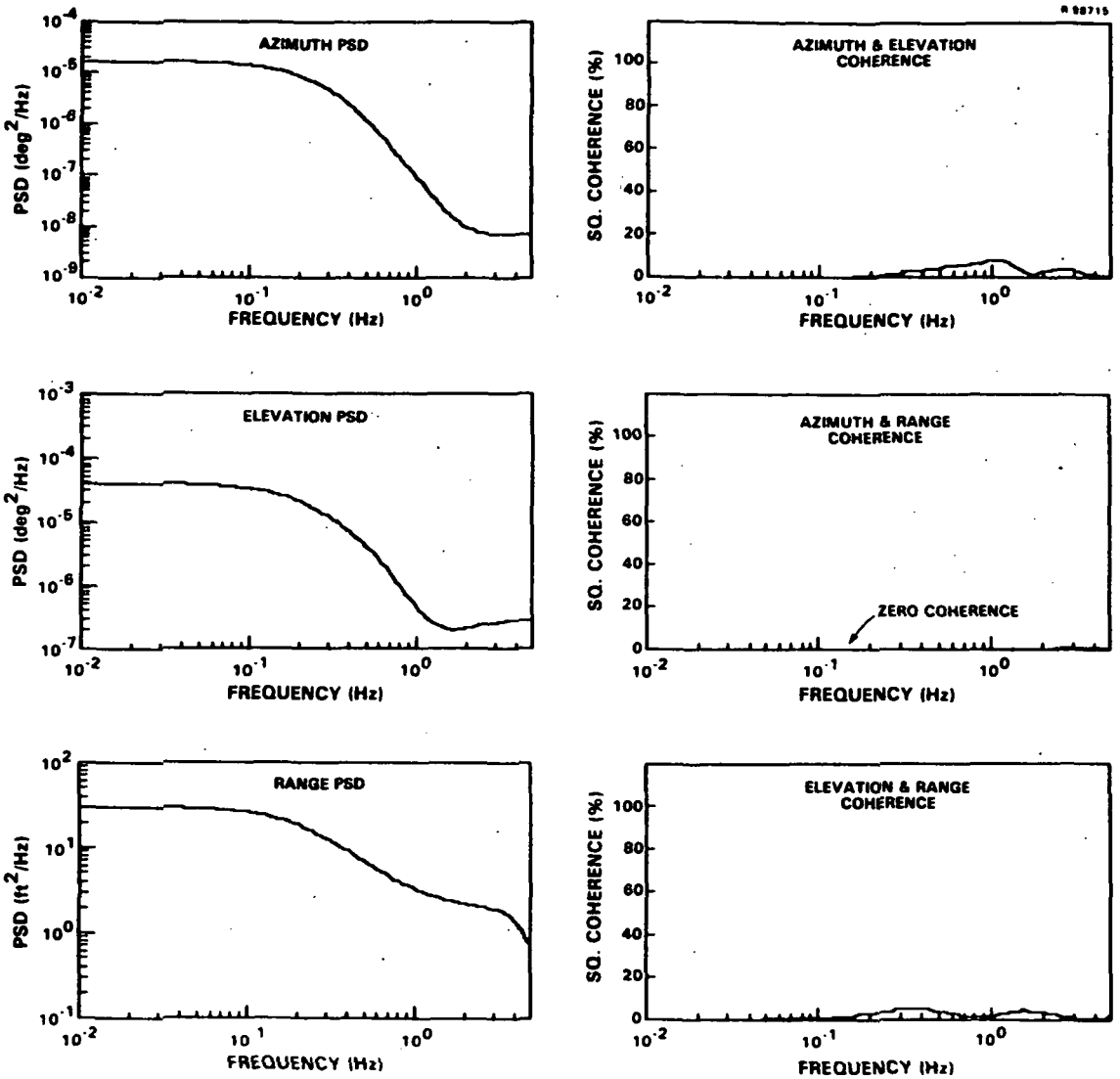

Figure 2.3-3 Estimated Power Spectra and Coherences for Loki Sphere Residual Tracking Data, Radar No. 5

in tracking data from radar No. 5, which was tracking a Super Loki Sphere payload. The state-space model used in this analysis was developed from a segment of the tracking data extending from 37 s to 92.7 s with a sampling rate of 10 samples per second. The small coherences and flat PSDs at low frequencies indicate that polynomials of appropriate degree were used in computing the residual data. The flat portions of the azimuth and elevation PSDs at high frequencies indicate definite white-noise floors in the angular measurements. The magnitudes of these floors denote less high-frequency noise in Radar No. 5 data as compared to corresponding noise levels in Radar No. 3 data represented by Figs. 2.3-1 and 2.3-2. At low frequencies the Radar No. 5 data have noise power levels that are between those estimated for the Loki Optical and Zuni data from Radar No. 3.

2.4 SUMMARY AND CONCLUSIONS

2.4.1 Summary

Under Task 1 of the study, the noise-like errors in radar tracking data were modeled using state-space techniques. The data sets included tracking radars Nos. 3 and 5, and acquisition radar No. 6. The trajectories analyzed were for Zuni, Super Loki Optical, and Super Loki Sphere payloads.

Random measurement noise signals were separated from trajectory signals and systematic tracking errors in the data by subtracting least-squares orthogonal polynomials from segments of the data. The resulting residual data were used as estimates of the noise-like error signals in the tracking data. The appropriate degrees of the polynomials were determined from spectral analyses of the residual data using an autoregressive modeling technique.

2.4.2 Conclusions

The analysis of data from tracking Radars Nos. 3 and 5 and acquisition Radar No. 6, leads to the following conclusions:

- The estimated rms noise levels in tracking data from Radars Nos. 3 and 5 vary from 2.9 millidegree (mdeg) to 11 mdeg in azimuth and elevation, and 5.5 ft to 6.8 ft in range, depending on the radar and the payload (Zuni, Super Loki Optical, and Super Loki Sphere)

- The estimated rms noise levels in Super Loki Optical data from the wide-band acquisition Radar No. 6 are 53 mdeg for azimuth, 41 mdeg for elevation, and 41 ft for range.

3. TASK 2 - ANALYSIS OF ERROR PROPAGATION INTO POSITIONAL DATA

3.1 INTRODUCTION

3.1.1 Objective

The main objective of Task 2 is to determine the propagation of the radar data errors through the WFF noise-reduction filters into positional data products expressed in latitude, longitude, and height. The noise-reduction filters currently used at WFF are digital finite-impulse-response (FIR) smoothing filters (low-pass filters with symmetric impulse responses that produce zero phase shift). The parameters of the filters are manually selected to attenuate the high-frequency noise in the radar tracking data. The radar data are passed through these filters in the SMAD data processing program (Ref. 1), which produces smoothed tracking data as output. These smoothed data are then used as inputs to the MESUP and POSDAT programs (Ref. 1) that generate positional data products. The objective of this task is to estimate the rms noise-like errors in these data products, based on the data error models developed under Task 1.

3.1.2 Approach

The technical approach used in the analysis of error propagation consists of three steps, which are depicted in Fig. 3.1-1 and discussed in the following:

- Step 1 - Develop state-space equations for the WFF smoothing filter being analyzed. The input to this step is the impulse

response of the WFF filter. The output is a set of state-space equations that are mathematically equivalent to the specified impulse response.

- Step 2 - Compute the error covariance matrices of the smoothed radar tracking data. The inputs to this analysis are the equations from Step 1 and the stochastic model for residual tracking data, which was developed under Task 1. The output is the covariance matrix for the noise-like errors in the smoothed residual tracking data.

- Step 3 - Compute the error covariance matrices of positional data products expressed in latitude, longitude, and height. The inputs to this step are the covariances from Step 2, the radar position coordinates, and the nominal payload coordinates. The output is the error covariance matrix of the positional data.

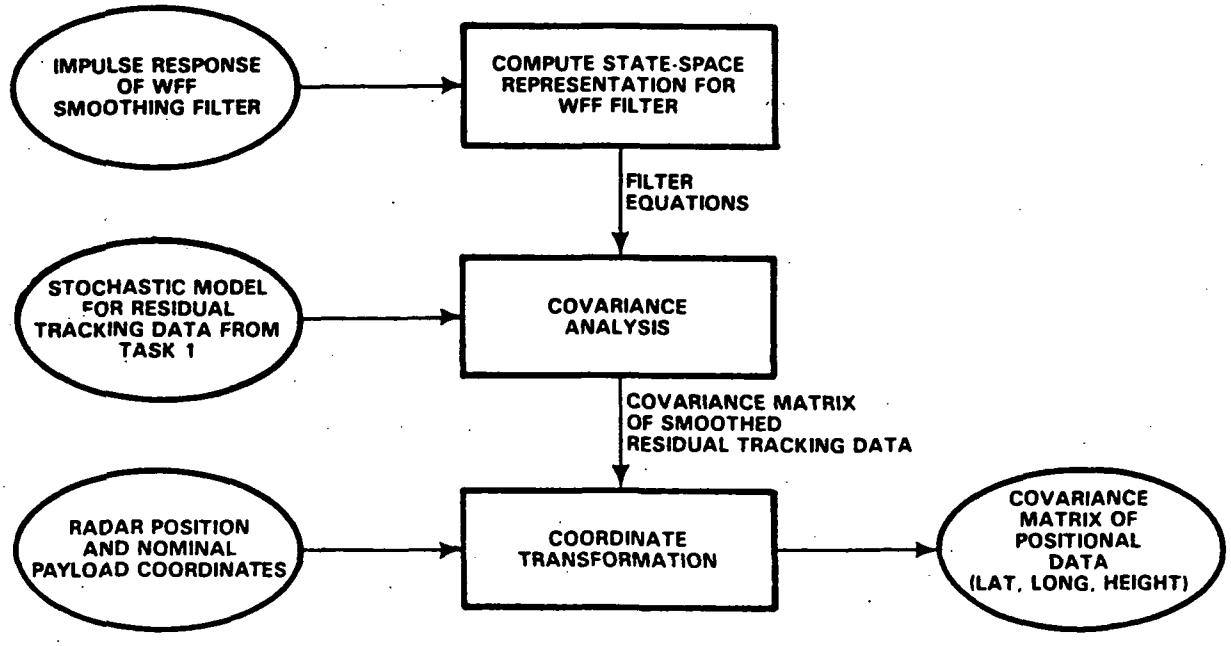

Figure 3.1-1 Block Diagram of Error Propagation Analysis

In addition to the analysis of noise-like errors, a systematic filtering error is also analyzed. This systematic error is caused by the slight distortions suffered by each payload trajectory signal as it is processed by the WFF filters. This error is called filter-induced trajectory bias. It is analyzed in this study by computing the distortions suffered by polynomials (which model nominal payload trajectory signals) when the polynomials are smoothed by the WFF filters.

3.2 STATE-SPACE FILTER EQUATIONS

The purpose of this section is to describe a state-space representation for WFF smoothing filters. This representation is convenient for computing the error covariance matrices of smoothed radar tracking data, given state-space models for the noise in the unsmoothed tracking data.

The impulse response h_k of a FIR filter is represented by the sequence of numbers

$$h_{-L}, h_{-L+1}, \ldots, h_{-1}, h_0, h_1, \ldots, h_{L-1}, h_L \qquad (3.2\text{-}1)$$

In Eq. 3.2-1, L denotes the half-length of the impulse response. The smoothed output y_k (for k = L+1, L+2, ...) produced by an input sequence u_k (for k = 1, 2, ...) may be represented by the following convolution:

$$y_k = \sum_{j=-L}^{L} h_j \, u_{k-j} \qquad (3.2\text{-}2)$$

An equivalent representation, and one that is more convenient than Eq. 3.2-2 for covariance calculations, is the following state-space model with the n'×1 state vector $\underline{x}'_k$ (the number of

states n' equals the number of samples in the support of the filter's impulse response sequence, i.e., n' = 2·L+1):

$$y_k = H'\underline{x}'_k \qquad [1\times 1] \qquad (3.2\text{-}3)$$

$$\underline{x}'_{k+1} = \phi'\underline{x}'_k + G'u_k \qquad [n'\times 1] \qquad (3.2\text{-}4)$$

$$\phi' = \begin{bmatrix} 0 & 1 & 0 & \cdots & \cdots & 0 \\ 0 & 0 & 1 & 0 & \cdots & 0 \\ 0 & 0 & 0 & 1 & 0 & \cdots \\ \vdots & & & \ddots & & \vdots \\ \cdots & & & & 0 & \\ 0 & \cdots & \cdots & 0 & 1 & \\ 0 & \cdots & \cdots & \cdots & 0 & \end{bmatrix} \qquad [n'\times n'] \qquad (3.2\text{-}5)$$

$$G' = \begin{bmatrix} 0 \\ 0 \\ \cdot \\ \cdot \\ 0 \\ 1 \end{bmatrix} \qquad [n'\times 1] \qquad (3.2\text{-}6)$$

$$H' = [h_{-L}\ h_{-L+1}\ \ldots h_0 \ldots h_L] \qquad [1\times n'] \qquad (3.2\text{-}7)$$

Equation 3.2-3 states that the filter output y_k is a linear function of the state vector $\underline{x}'_k$; H' is a 1×n' matrix, which contains the impulse response of the filter as defined by Eq. 3.2-7. Equation 3.2-4 is the state propagation equation in which ϕ' is the n'×n' transition matrix and G' is the n'×1 input matrix.

In Eqs. 3.2-2 and 3.2-4, the input sequence u_k represents the noise-like error signal in radar tracking data (azimuth, elevation, or range measurements). Stochastic state-space models for u_k were developed under Task 1 as discussed in Chapter 2. Such noise models are represented here by the following equations involving the n"×1 state vector $\underline{x}''_k$:

$$u_k = H''\underline{x}_k'' + v_k'' \text{ , variance}(v_k'') = R'' \quad [1\times1] \qquad (3.2\text{-}8)$$

$$\underline{x}_{k+1}'' = \phi''\underline{x}_k'' + G''v_k'' \qquad [n''\times1] \qquad (3.2\text{-}9)$$

Equations 3.2-8 and 3.2-9 are a stochastic model for the radar noise u_k; the scalar white noise v_k'' driving this model is called the innovations and is uncorrelated with $\underline{x}_j''$ for $j \leq k$.

For covariance calculations, the two state-space models for the WFF smoothing filter and the radar noise are combined to form one larger model of the following form, where n = n'+n":

$$\underline{x}_{k+1} = \phi\underline{x}_k + G\underline{w}_k \qquad [n\times1] \qquad (3.2\text{-}10)$$

$$y_k = H\underline{x}_k \qquad [1\times1] \qquad (3.2\text{-}11)$$

The matrices in Eqs. 3.2-10 and 3.2-11 are defined as follows:

$$\underline{x}_k = \begin{bmatrix} \underline{x}_k' \\ \underline{x}_k'' \end{bmatrix} \qquad [n\times1] \qquad (3.2\text{-}12)$$

$$\phi = \begin{bmatrix} \phi' & G'H'' \\ 0 & \phi'' \end{bmatrix} \qquad [n\times n] \qquad (3.2\text{-}13)$$

$$H = [H' \; 0] \qquad [1\times n] \qquad (3.2\text{-}14)$$

$$\underline{w}_k = \begin{bmatrix} 0 \\ v_k'' \end{bmatrix} \qquad [2\times1] \qquad (3.2\text{-}15)$$

$$Q = \text{cov}(\underline{w}_k) = \begin{bmatrix} 0 & 0 \\ 0 & R'' \end{bmatrix} \quad [2\times2] \qquad (3.2\text{-}16)$$

3.3 ERROR COVARIANCE EQUATIONS

The steady-state error variance of the smoothing filter output y_k is denoted var(y). From a covariance analysis of the Eqs. 3.2-10 through 3.2-16 (Ref. 5), it can be shown that the variance of the noise in the filter output may be computed using the following equations:

$$\text{var}(y) = H'P'H'^{T} \qquad [1\times1] \qquad (3.3\text{-}1)$$

$$P' = \phi'P'\phi'^{T} + \phi'SH''^{T}G'^{T} + G'H''S^{T}\phi'^{T} + (G'H'')P''(G'H'')^{T} + G'R''G'^{T} \qquad [n'\times n'] \qquad (3.3\text{-}2)$$

In Eq. 3.3-2, P' is the steady-state error covariance of the filter state vector $\underline{x}'_k$. To solve Eq. 3.3-2 for P', the matrices S and P" are first computed using the following equations:

$$P'' = \phi''P''\phi''^{T} + G''R''G''^{T} \qquad [n''\times n''] \qquad (3.3\text{-}3)$$

$$S = \phi'S\phi''^{T} + G'H''P''\phi''^{T} + G'R''G''^{T} \qquad [n'\times n''] \qquad (3.3\text{-}4)$$

The recommended procedure for solving these equations is to (1) solve Eq. 3.3-3 for P", (2) solve Eq. 3.3-4 for S, (3) solve Eq. 3.3-2 for P', and (4) use Eq. 3.3-1 to compute var(y). Equations 3.3-2 through 3.3-4 are equilibrium equations describing statistical steady-state error covariances. They may be solved by using iteration, e.g., Eq. 3.3-3 may be solved by initially setting P" equal to the n"×n" identity matrix, evaluating the right side of the equation, using the new value for P" to re-evaluate the right side, and continuing until the elements of P" remain unchanged to within the desired numerical accuracy. This iterative method converges to the unique solution of the equation whenever the steady-state covariance exists (i.e., when the eigenvalues of P" have moduli less than unity).

3.4 COORDINATE TRANSFORMATION EQUATIONS

The last step in determining the rms errors in positional data products is to transform the error variances of the smoothed tracking data (azimuth, elevation, and range) into the corresponding error covariances of the positional data (latitude, longitude, and height). The equations for this transformation are discussed in this section, while the mathematical details are presented in Appendix D.

The coordinate transformation is performed in three steps as discussed in the following:

- Step 1 - Transform from radar az-el-range coordinates to topographic north-east-down (NED) coordinates. This is a nonlinear transformation because radar coordinates are not Cartesian.
- Step 2 - Transform from topographic NED coordinates to geocentric Cartesian coordiantes. This is a linear transformation from one Cartesian system to another.
- Step 3 - Transform from geocentric Cartesian coordinates to geodetic lat-long-height coordinates. This is a nonlinear transformation.

The propagation of the error covariance through this sequence of transformations is accurately approximated by linearizing the nonlinear transformations (in Steps 1 and 3) about the nominal payload coordinates. This approximation is accurate because the rms tracking errors are a small fraction of the nominal payload coordinates.

3.5 ANALYSIS RESULTS

This section presents rms error estimates for positional data products expressed in latitude, longitude, and height. The error estimates were computed using the analysis techniques described in Sections 3.2 - 3.4 and the stochastic error models developed under Task 1. The accuracy estimates are for noise-like errors and apply to WFF radars Nos. 3 and 5 tracking Zuni, Super Loki Sphere, and Super Loki Optical payloads.

3.5.1 Rms Errors of Smoothed Tracking Data

Rms error estimates for smoothed radar data (azimuth, elevation, and range measurements) are presented in Table 3.5-1. The first column indicates the payload and data sets used for analysis. (Data from wide-band radar No. 6 are excluded from this comparison because this radar is not intended for precise tracking applications.) The third and fourth columns give the estimated rms noise levels in the data before and after processing with the WFF smoothing filter. (For these data sets, which were analyzed at a sampling rate of 10 samples/second, the appropriate WFF smoothing filter is designated by the code F00.040.10.) The last column in Table 3.5-1 indicates the percent reduction of rms noise in the smoothed data as compared with the rms noise before smoothing.

The data in Table 3.5-1 lead to the following conclusions. The percent reduction in estimated rms noise due to smoothing falls in the range of 71% to 14%. The estimated rms angular errors for Radar No. 3 vary significantly with payload: the Zuni trajectories have rms accuracies of 1.5 mdeg in azimuth and 2.7 mdeg in elevation; in contrast, the Loki Optical payload was tracked with accuracies of 9.5 mdeg in azimuth and 8.2 mdeg

TABLE 3.5-1

STANDARD DEVIATIONS OF SMOOTHED RESIDUAL TRACKING DATA

DATA SET	NOMINAL PAYLOAD COORDINATES	RMS BEFORE SMOOTHING	RMS AFTER SMOOTHING	PERCENT REDUCTION OF RMS
ZUNI (RADAR #3) (3 TRAJECTORIES)				
AZIMUTH	132 deg	4.4 mdeg	1.5 mdeg	66
ELEVATION	15 deg	6.7 mdeg	2.7 mdeg	60
RANGE	27 kft	5.5 ft	1.7 ft	69
LOKI SPHERE (RADAR #5) (ORIGINAL DATA)				
AZIMUTH	137 deg	2.9 mdeg	2.5 mdeg	14
ELEVATION	42 deg	4.7 mdeg	3.8 mdeg	19
RANGE	27 kft	6.0 ft	3.5 ft	42
LOKI OPTICAL (RADAR #3) (ORIGINAL DATA)				
AZIMUTH	139 deg	11.4 mdeg	9.5 mdeg	17
ELEVATION	78 deg	11.4 mdeg	8.2 mdeg	28
RANGE	220 kft	6.8 ft	2.0 ft	71

in elevation. This difference may in part be caused by the much larger nominal slant range for the Optical payload as compared to the Zuni. The rms accuracy for Radar No. 5, tracking a Loki Sphere, is similar to the results for Radar No. 3 tracking the Zuni trajectories.

3.5.2 Rms Errors in Positional Data Products

The rms error estimates for positional data products are presented in Table 3.5-2. The rms latitude errors are in

TABLE 3.5-2

ESTIMATED RMS OF NOISE-LIKE ERRORS IN POSITIONAL DATA

DATA SET	RMS ERROR	MEAN SLANT RANGE
ZUNI (RADAR #3)		
LATITUDE	3 μdeg	
LONGITUDE	5 μdeg	27 kft
HEIGHT	0.4 m	
LOKI SPHERE (RADAR #5) (ORIGINAL DATA)		
LATITUDE	6 μdeg	
LONGITUDE	8 μdeg	27 kft
HEIGHT	0.8 m	
LOKI OPTICAL (RADAR #3) (ORIGINAL DATA)		
LATITUDE	65 μdeg	
LONGITUDE	73 μdeg	220 kft
HEIGHT	2.1 m	

the range from 3 μdeg to 65 μdeg, with the largest error occurring at the largest slant range. The rms longitude errors are similar and range from 5 μdeg to 73 μdeg. Estimated rms height errors range from 0.4 m (1.3 ft) to 2.1 m (6.9 ft). Again, the largest error occurs at the largest slant range.

3.6 SMOOTHING-FILTER TRAJECTORY BIAS

The smoothing filters are intended to reduce high-frequency noise levels in the radar tracking data without

significantly changing the low-frequency signal component representing the payload motion along the trajectory. In practice, the smoothing filter systematically distorts the nominal trajectory slightly. This section describes the results of an analysis of this systematic error component in smoothed tracking data.

The technical approach of this analysis is explained with the aid of Fig. 3.6-1. The raw tracking data (azimuth, elevation, or range measurements) are decomposed into two signal components: a polynomial that represents the nominal trajectory and the residual data that represent the noise-like errors. This decomposition was previously introduced in Chapter 2. The effect of the smoothing filter is to smooth the residual data and to distort slightly the nominal trajectory polynomial. The distortion of the polynomial is termed smoothing-filter trajectory bias because it can produce a systematic bias-like error in the smoothed data.

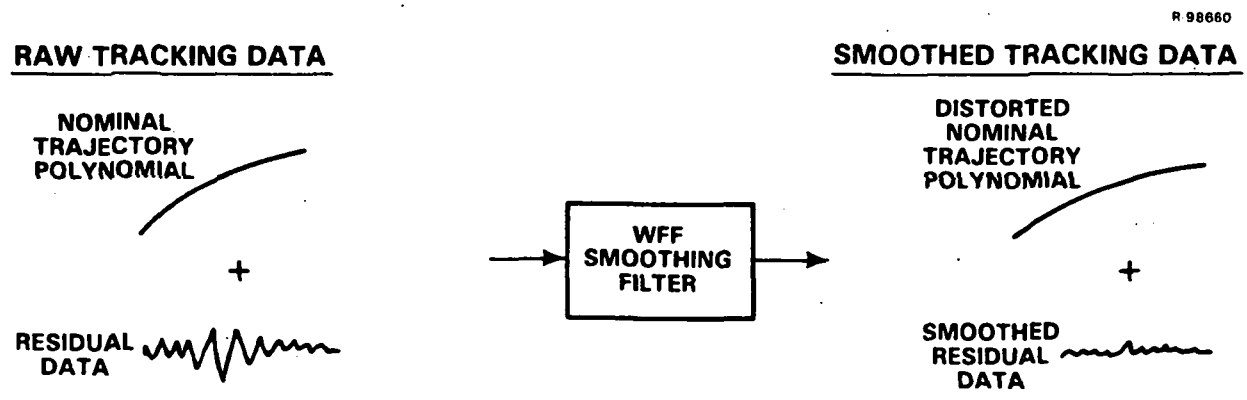

Figure 3.6-1 Smoothing-Filter Trajectory Bias

An example of smoothing-filter trajectory bias is shown in Fig. 3.6-2. The plot on the left depicts the raw range data from Radar No. 3 for a Super Loki Optical payload. To model the trajectory signal, an orthogonal polynomial was fitted to the range data using the technique discussed in Section 2.2. The plot in Fig. 3.6-2 labeled "Range-Bias" shows the distortion of this polynomial that was produced by passing it through the WFF F00.40.10 smoothing filter. More than 3 ft of bias was produced over most of the data segment. This bias is larger than the estimated rms noise level (2.0 ft) in the smoothed data.

Trajectory bias from the smoothing filter does not always produce errors larger than the noise. Figure 3.6-3 shows the azimuth and elevation biases for the Loki Optical data from Radar No. 3. These biases are much less than the rms estimated noise levels (9 mdeg).

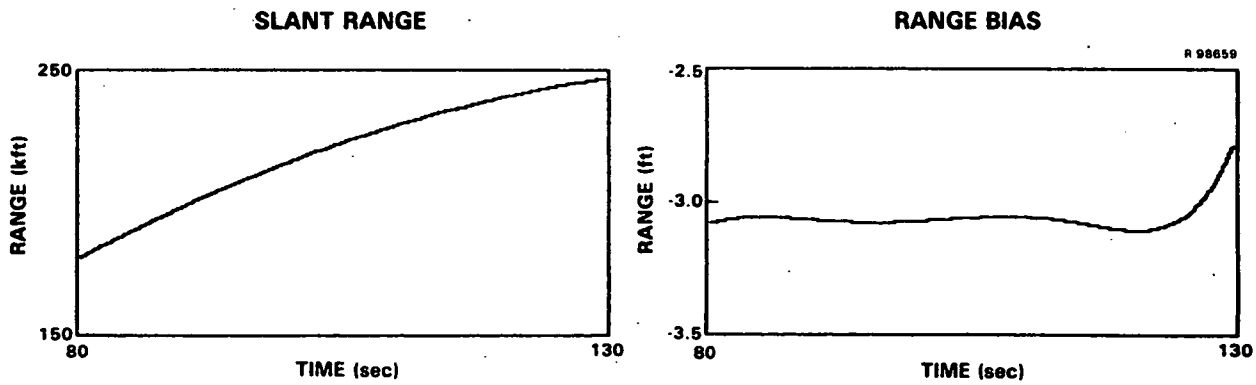

Figure 3.6-2 Filter-Induced Range Bias for Loki Optical Tracking Data, Radar No. 3

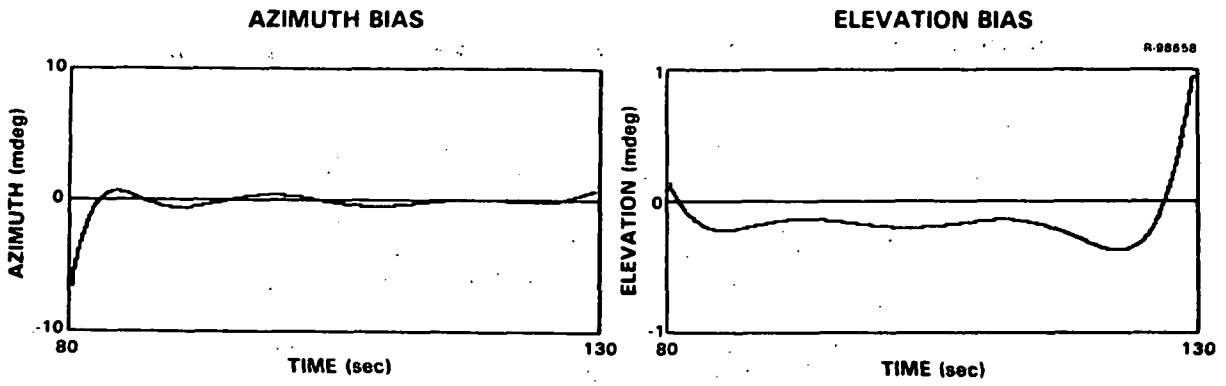

Figure 3.6-3 Filter-Induced Azimuth and Elevation Bias for Loki Optical Tracking Data, Radar No. 3

The analysis of trajectory bias leads to the conclusion that the smoothing filters can produce systematic errors that are larger than the rms noise levels in the smoothed data. A recommended way of avoiding this error is to smooth only residual tracking data and then add the trajectory polynomial to the smoothed residuals at the output of the filter.

3.7 SUMMARY AND CONCLUSIONS

3.7.1 Summary of Task 2

Under Task 2 the following objectives were met:

- The propagation of noise-like errors in radar tracking data into positional data products was analyzed. A state-space covariance analysis was performed based on the stochastic error models developed under Task 1.
- The systematic smoothing error, termed smoothing-filter trajectory bias, was identified and analyzed.

3.7.2 Conclusions

The analysis results of Task 2 lead to the following main conclusions:

- Rms noise-like errors in smoothed tracking data vary with payload for radars No. 3 and 5. The estimated rms noise levels of the smoothed data and positional data products are in the following ranges for the data analyzed in this study:

AZ and EL:	1.5 mdeg to 9.5 mdeg
RANGE:	1.7 ft to 3.5 ft
LAT and LONG:	3 μdeg to 73 μdeg
HEIGHT:	1.3 ft to 6.9 ft

- The bias-like errors caused by WFF smoothing filters can exceed the rms noise levels in smoothed tracking data when raw tracking data are passed through the filters.

4. TASK 3 - ALTERNATIVE NOISE REDUCTION TECHNIQUES

4.1 INTRODUCTION

The purpose of this chapter is to present recommendations for improving the noise reduction techniques currently used at WFF for processing radar tracking data. These recommendations are based on the results of Tasks 1 and 2 of this study and an assessment of practical alternative algorithms.

The current WFF data processing system is depicted in Fig. 4.1-1. At the top of this figure, the radar data tape provides inputs to the PASS 1 program, which produces as its output a working data tape. Data calibration and editing (e.g.,

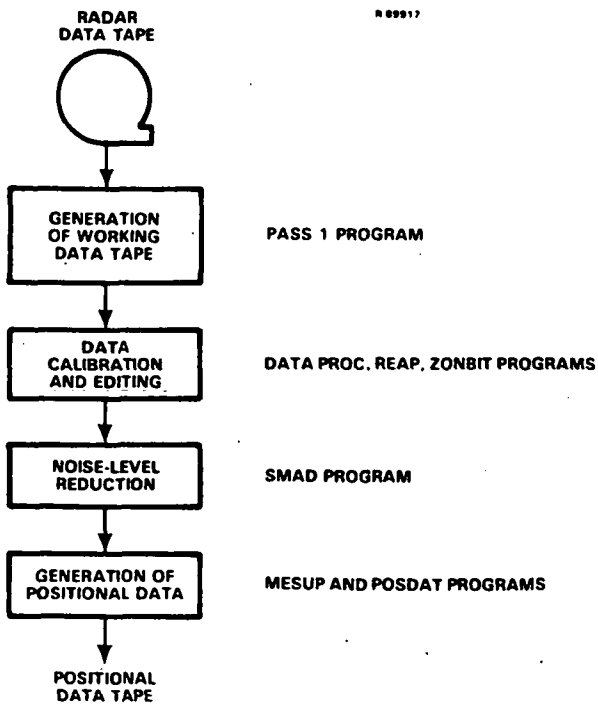

Figure 4.1-1 Review of Current WFF Smoothing Technique

to correct extreme data outliers) are then performed using programs such as DATA PROC and ZONBIT. The calibrated and edited data are next processed using the SMAD program to reduce the noise level in the data. It is in the SMAD program that the smoothing filters (analyzed under Task 2 of this study) are used to process the azimuth, elevation, and range data. The smoothed data are finally processed using the MESUP or POSDAT programs to produce data products, including data on payload position expressed in latitude, longitude, and height. The rms noise levels in these positional data products were estimated in Task 2 of this study.

4.2 DISCUSSION OF CURRENT FILTERING TECHNIQUES

The current WFF smoothing filters are low-pass zero-phase finite-impulse-response (FIR) filters. The parameters of these filters are specified each time the SMAD program is run. Appropriate parameter values depend on the radar, the type of data being processed (azimuth, elevation, or range), the payload, and the portion of the trajectory that is being estimated. For example, data for ECC BALLOON, SUPER LOKI OPTICAL, and ZUNI ROCKETS are usually smoothed with filter parameters designated by the WFF code "F00.040.10." In contrast, THRUSH data may be analyzed using an F00.090.04 filter. For SCOUT and TAURUS ORION data, a variety of different filter parameters may be used, corresponding to different segments of the trajectory.

According to the error analysis presented in Chapter 3, the rms noise levels in ZUNI, SUPER LOKI SPHERE, and SUPER LOKI OPTICAL data are significantly reduced by filter F00.040.10. However, the percent reduction of the noise level varied from 14% to 71% for the data sets analyzed in this study. A main

conclusion to be reached from these results is that the current WFF filters can be effective in reducing rms noise levels, but the final noise levels in the smoothed data vary from data set to data set, and these noise levels are not estimated by the current WFF smoothing techniques.

Another finding from Chapter 3, is that the current WFF smoothing technique can result in a systematic error, called filter-induced trajectory bias. This bias-like error is a slight distortion of the nominal trajectory signal as it is processed by the smoothing filter. For some of the data analyzed, the bias exceeded the rms noise level of the smoothed radar data. This finding can be interpreted positively as a verification that the noise levels are currently low and do not have to be reduced. Or the bias can be viewed as a known error source that should be eliminated. Fortunately, this error can be avoided by a simple modification of the current WFF smoothing procedure, as explained in Section 4.3.

4.3 ALTERNATIVE NOISE REDUCTION TECHNIQUES

4.3.1 Avoiding Filter-Induced Trajectory Bias

The smoothing filter causes trajectory bias because in the SMAD program the nominal trajectory signal is smoothed along with the noise in the data. The nominal trajectory signal is much larger than the noise, and so very small relative distortions of the trajectory signal cause bias-like errors in the filter output. To avoid this bias, a polynomial estimate of the nominal trajectory signal should be subtracted from the radar data to yield residual radar data. The residual data, which consist mostly of measurement noise and only small-scale payload motions, would be smoothed using the current WFF filtering

technique. Finally, the polynomial estimate of the nominal trajectory signal would be added back into the smoothed residual data. By using this technique, the current WFF filters can reduce the noise level without producing significant bias error.

4.3.2 Estimating and Minimizing Noise Levels in Smoothed Data

As discussed in Section 4.2, the current WFF smoothing technique yields no estimate of the noise levels in the smoothed radar data. As a consequence, the noise levels in positional data products are also left unestimated. To correct these deficiencies, a more complicated data processing algorithm is required. In this section, two alternative approaches to estimating noise levels are discussed. The first is the simpler, and requires an additional stage of signal processing to estimate the high-frequency noise levels in the data. The second approach is capable of higher accuracy, but is much more complicated. It is based on Kalman smoothing techniques, which are optimal with respect to prior information about the geometry of the tracking system, the physics of the descending payload, and the statistics of the measurement noise.

Estimating High-Frequency Noise Levels - The high-frequency noise levels in smoothed radar tracking data (outputs from the current SMAD program) can be estimated using the following procedure:

- Step 1 - Select segments of the tracking data for analysis. The lengths of these segments may be as short as a few hundred data samples (e.g., ZUNI data processed under Task 1 of this study typically contained about 300 to 400 measurements per trajectory). For long trajectories spanning tens of thousands of measurements, segments may be selected from the beginning, middle, and end of the trajectory.

- Step 2 - For each segment compute residual azimuth, elevation, and range data by subtracting orthogonal polynomials from each channel of data. The polynomials are fitted to each data segment using least-squares as discussed in Appendix A. The degree of each polynomial is not critical for estimating high-frequency noise levels. Appropriate polynomial degrees for the tracking data analyzed under Tasks 1 and 2 of this study are in the range 6 to 10 for segments containing about 500 data samples.

- Step 3 - Process each channel of residual data with the autoregressive modeling algorithm discussed in Appendix B. The output of this procedure is a stochastic model for the residual data.

- Step 4 - Use the autoregressive models from Step 3 to estimate the power spectra of the azimuth, elevation, and range data for each segment. The rms high-frequency noise level in each data set is inferred from the level of its power spectrum at high-frequencies as indicated in Fig. 4.3-1.

This method for estimating noise levels can be implemented in a new computer program. By running this program on the outputs of SMAD, POSDAT, or MESUP, noise levels can be estimated for smoothed tracking data or positional data products.

An Alternative Smoothing Technique - Optimal estimation techniques can be used instead of the current WFF smoothing procedure. The motive for using optimal smoothing is to obtain the most accurate data products together with reliable error estimates. This requires that the smoothing algorithm be optimized with respect to several kinds of prior information about the tracking system geometry, the physics of the descending payload, and the statistics of the measurement noise and other uncertainties. Incorporating this information optimally requires

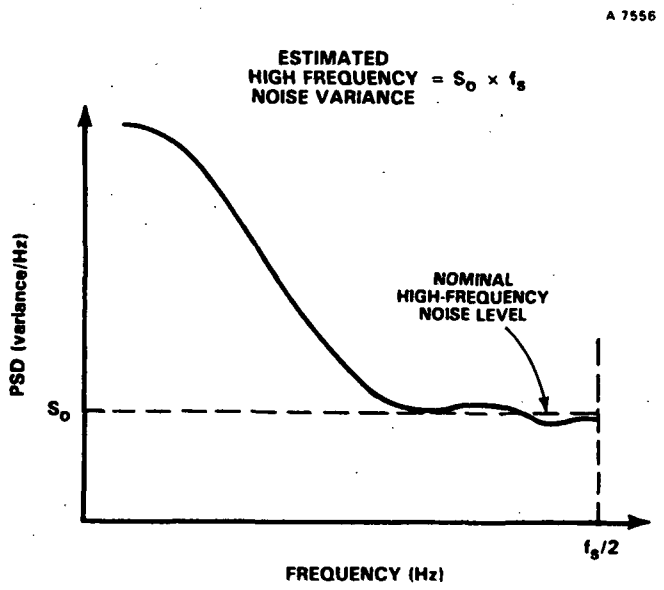

Figure 4.3-1 Estimation of High-Frequency Noise Variance from Power Spectral Density (PSD). f_s = Data Sampling Frequency [Hz] and S_o = Nominal High-Frequency Noise PSD

a much more complicated processing algorithm than the one currently used at WFF. In the majority of cases, where well calibrated low-noise tracking data are being processed, the added complexity of an optimal estimator may not be justified. However, for special cases in which the measurement noise is large, the radar calibration is not precise, or the tracking data contain long gaps due to missing measurements, optimal smoothing may be essential for meeting the objectives of the data analysis.

The recommended way of implementing an optimal estimator for processing radar tracking data is to use Kalman filtering and smoothing algorithms. There is a well developed software technology and mathematical theory to support the design and implementation of Kalman-type processors (e.g., Refs. 5 and 19). Moreover, the mathematical formalism is very flexible,

which makes it possible to improve the accuracy of the processor by adding new or improved error models or additional data inputs to the smoother, without redesigning the software.

Specific examples of tracking data that are candidates for the use of Kalman estimation techniques are NIKE-ORION and TERRIER-MALEMUTE data from Radars Nos. 8 and 41 in Peru. For these examples, the payloads were tracked above the atmosphere (above 50 km) so that the physics of the payload descent can be represented with a relatively simple mathematical model. The primary sources of uncertainty in the estimates of payload position are uncertainties in the radar calibration, random noise in the radar data, and possible data gaps caused by missing measurements or high noise levels. A Kalman smoothing algorithm for these data sets is developed and verified under Task 4 of this study. The detailed specification of the algorithm and examples of its performance with data provided by WFF is presented in Chapter 5.

4.4 SUMMARY OF RECOMMENDATIONS FOR IMPROVING THE CURRENT WFF NOISE REDUCTION TECHNIQUES

Based on the results of (1) the error analyses of the current WFF radar data smoothing fiters (conducted under Tasks 1 and 2 of this study) and (2) an assessment of alternative techniques, the following recommendations are made for improving the noise reduction techniques used at WFF:

- To avoid filter-induced trajectory bias, residual radar data should be smoothed instead of raw radar data. The residual data may be computed by subtracting from the raw data low-degree orthogonal polynomials, which are least-squares estimates of the nominal trajectory signal in the raw data.

- To estimate the high-frequency rms noise levels in smoothed tracking data produced using the existing smoothing filters, residual smoothed data (i.e., either smoothed residual data or smoothed raw data minus an estimated nominal trajectory signal) may be processed with the autoregressive (AR) modeling algorithm discussed in Appendix B. The noise level is estimated from the high-frequency part of the power spectrum of the AR model.

- To process the radar tracking data optimally, an alternative Kalman filter/smoother algorithm is recommended. Optimal estimation is much more complicated than the current smoothing procedure because it uses prior information about tracking system geometry, the physics of the descending payload, and the statistics of the measurement noise, radar calibration errors, and other uncertainties. It is expected that optimal smoothing techniques would be most appropriate for processing tracking data having high noise levels, significant data gaps, or large uncertainties on radar calibration errors.

5. TASK 4 - DEVELOPMENT AND VERIFICATION OF AN ALTERNATIVE SMOOTHING ALGORITHM

This chapter describes the development and verification of a new smoothing algorithm for processing radar tracking data. The algorithm takes as inputs the tracking data (azimuth, elevation, and range) from one radar and provides as outputs estimates of payload position and velocity as functions of time. The algorithm is a Kalman filter/smoother that is optimal (i.e., unbiased and minimum-variance) with respect to prior information about the tracking system geometry, the physics of the payload descent, and the statistics of measurement noise and radar calibration errors. The algorithm, in its present form, is intended for estimating trajectories above the atmosphere (height > 50 km). The algorithm detects and appropriately processes isolated data outliers. Moreover, extended measurement gaps (caused by missing data or high noise levels) are processed optimally when their locations in the data set are specified as input parameters. The performance of the algorithm is verified using tracking data provided by WFF for this investigation.

This chapter is organized as follows. Section 5.1 describes the Task 4 objectives and the technical approach for meeting these objectives. Section 5.2 provides an overview of the algorithm, while the mathematical details are discussed in Sections 5.3 through 5.7. The verification of algorithm performance with tracking data from Radars Nos. 8 and 41 in Peru is presented in Section 5.8. The accomplishments of this task are summarized in Section 5.9.

5.1 INTRODUCTION

5.1.1 Objective

Task 4 has two main objectives:

- Develop an algorithm for processing noisy radar tracking data to estimate payload trajectories above 50 km in altitude. The algorithm should handle data outliers and gaps caused by missing data or high noise levels, and should provide a realistic estimate of rms error for the estimated trajectory.
- Verify the performance of the algorithm using radar data provided by WFF.

5.1.2 Technical Approach

To meet the two objectives, the algorithm was developed using the established theory of Kalman optimal filtering and smoothing (Ref. 5). The technical approach consists of four steps:

- Compute a Nominal Trajectory - The nominal trajectory is computed using (1) a best-guess initial position and velocity for the payload, and (2) deterministic models for normal gravitation and nominal atmospheric drag accelerations.
- Compute Nominal Radar Measurements - The nominal radar measurements are time series for azimuth, elevation, and range corresponding to an ideal radar tracking the nominal trajectory.
- Compute Residual Radar Measurements - The residual radar measurements are defined as the actual measurements minus the nominal measurements computed in Step 2.

- Estimate Corrections to the Nominal Trajectory - The corrections to the nominal trajectory are computed by processing the residual radar data from Step 3 using a Kalman filter/smoother. The final optimal trajectory estimate is then computed by adding these corrections to the nominal trajectory from Step 1. The error covariance matrices of the trajectory estimates are computed by the Kalman smoother.

There are two main advantages to processing residual radar data. The first is that the relation between residual tracking data and residual payload motions about a nominal trajectory can be accurately modeled by linear time-varying state-space difference equations. (The reason for this is that, with high probability, the actual payload motion is a small percent perturbation about the nominal trajectory. This expectation is justified for trajectories above the atmosphere, i.e., height > 50 km, because at high altitudes the accelerations caused by atmospheric drag and gravitation, can be adequately represented using simple models.) The state-space difference equations are precisely the type of mathematical model that is consistent with the recursive Kalman filter/smoother algorithms.

The second advantage to processing residual radar data is that they can be accurately modeled as realizations of zero-mean non-stationary random processes. Moreover, these processes can be represented as outputs from linear time-varying state-space difference equations driven by white noise. This is the type of data for which Kalman filter/smoother algorithms are statistically optimal (i.e., the trajectory estimates are unbiased and have the smallest possible error variances).

5.2 OVERVIEW OF ALGORITHM

The front end of the trajectory estimation algorithm is a pre-processor that (1) computes a nominal trajectory for the payload, and (2) processes the raw radar data (e.g., output data from the WFF PASS 1 program) to produce residual radar data as outputs. Figure 5.2-1 depicts the pre-processor, its inputs, and its outputs. The inputs are:

- Best-Guess Initial State of Payload - The estimated position and velocity of the payload at the initial time expressed in earth-centered Cartesian inertial coordinates
- Nominal Gravitation Model - The normal corrections to a point-mass gravitation model, which account for the oblateness of the earth's gravitational field
- Nominal Atmospheric Drag Acceleration Model - The expected atmospheric drag as a function of altitude and payload velocity, based on the U.S. Standard Atmosphere, 1976 (Ref. 6)
- Geodetic Coordinates of the Tracking Radar - Expressed in terms of latitude, longitude, and height with respect to the reference ellipsoid currently used in the WFF data processing programs
- Actual Radar Measurements - Time series of azimuth, elevation, and range measurements taken at uniformly spaced time intervals.

The outputs of the pre-processor are used by the filtering and smoothing stages of the algorithm. As indicated in Fig. 5.2-1, the outputs are:

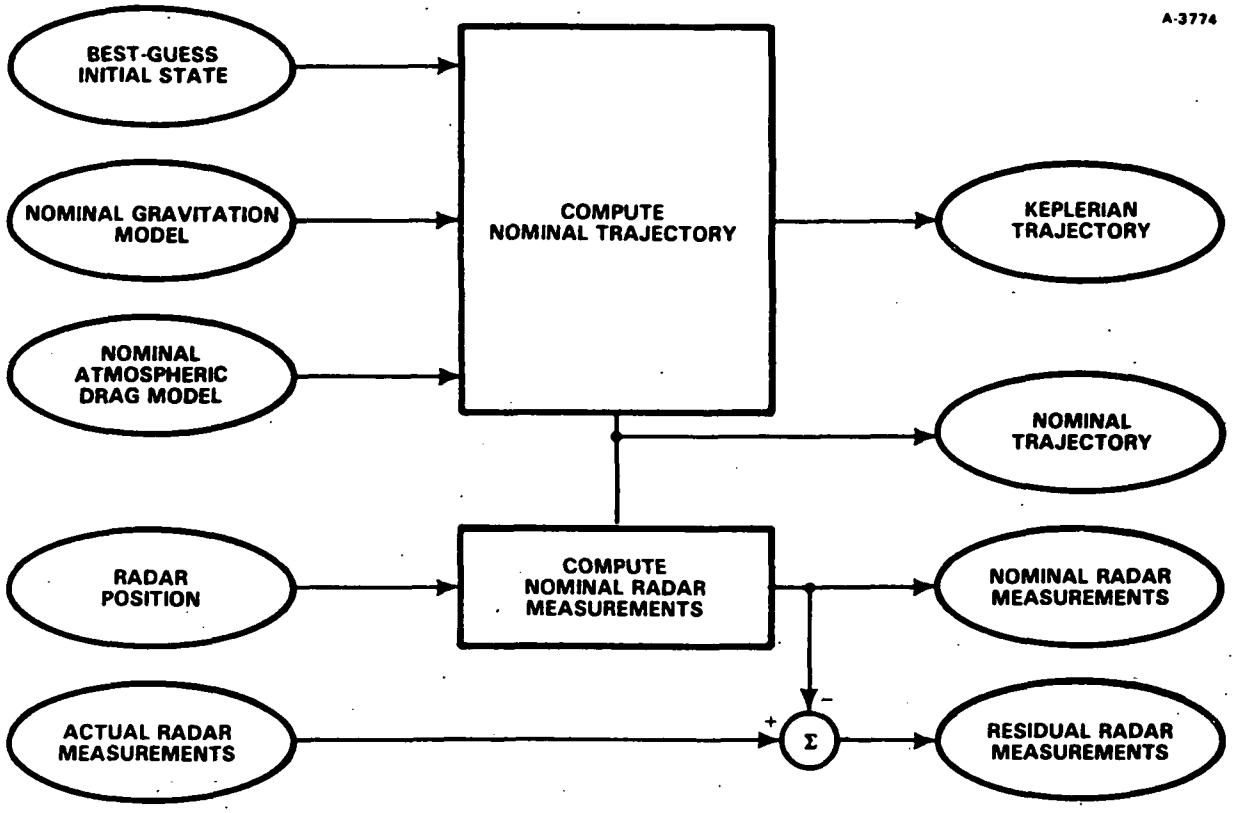

Figure 5.2-1 Block Diagram of Pre-Processing for Trajectory Estimation

- Keplerian Payload Trajectory - The idealized trajectory which the payload would follow if the earth were a point mass, the atmospheric drag accelerations were zero, and the initial position and velocity of the payload were known exactly

- Nominal Payload Trajectory - The expected trajectory for the payload, given the initial estimate of the payload position and velocity at the initial time, the normal gravitation of the earth, and a model for the nominal drag accelerations

- Residual Radar Measurements - The transformed radar data, which contain all available information about the actual departure of the payload trajectory away from the nominal trajectory. The residual data are inputs to the Kalman filter in the second part of the trajectory estimation algorithm.

The second half of the trajectory estimation algorithm is a Kalman filter/smoother. A block diagram of the filter and smoother is presented in Fig. 5.2-2. As shown in this diagram, the Kalman filter algorithm has six inputs:

- The Processing Mode - a parameter that determines whether the algorithm is to be optimal for base-line measurement noise (mode 1), for data gaps caused by missing data or very noisy data (mode 2), or for automatic detection and optimal processing of isolated data outliers (mode 3)

- An Estimate of the Payload's Initial State Vector and the Error Covariance Matrix of this Estimate - the best-guess estimate (before any radar data are processed) of the payload's position and velocity with respect to the nominal trajectory at the initial time

- The Residual Radar Measurements and the Time Between Successive Measurements - the residual radar data computed by the pre-processor

- The Keplerian Trajectory - the trajectory based on a point-mass earth, which is computed by the pre-processor

- The Nominal Radar Measurements - nominal tracking data corresponding to an ideal radar tracking the nominal payload trajectory, which are computed by the pre-processor

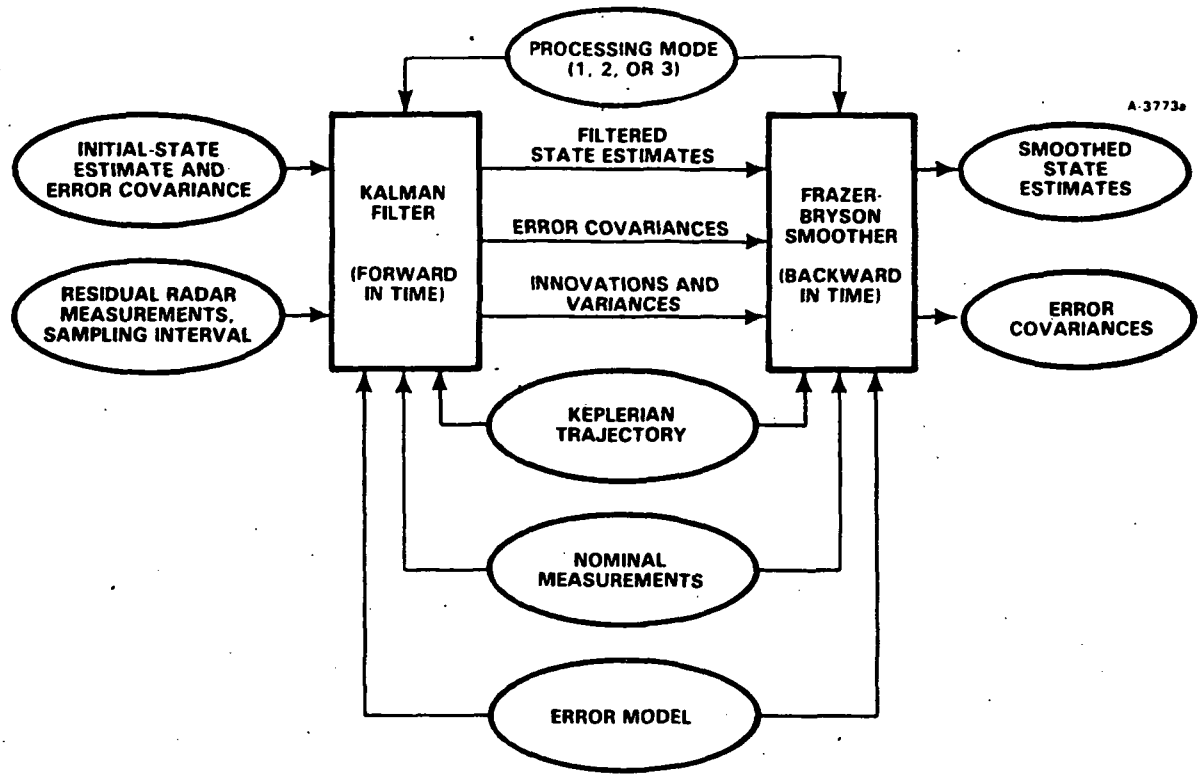

Figure 5.2-2 Block Diagram of Kalman Filter/Smoother for Trajectory Estimation

- The Error Model - a state-space stochastic model for radar measurement noise and radar calibration errors. (The model could also represent acceleration noise caused by small unpredictable perturbations in the gravitational field away from the normal field for an ellipsoidal earth. Based on the results of processing WFF radar data from Peru for Radars Nos. 8 and 41, it was concluded that gravitational errors are much smaller than radar measurement errors. Therefore, an error model for gravitational noise is not included in the present version of the trajectory estimation algorithm.)

The residual radar measurements are processed causally by the Kalman filter, starting with the initial time and proceeding to the end of the data set. The outputs of the Kalman filter are three time series:

- Filtered State Estimates - The estimated position and velocity of the payload with respect to the nominal trajectory as a function of time, together with additional state variables that model radar measurement errors. These estimates are optimal with respect to a causal processing of the data.

- Error Covariances - The error covariance matrices of the filtered state estimates.

- Innovations and Their Variances - The innovations are the prediction errors made by the filter as it predicts what the next residual measurements of azimuth, elevation, and range will be one time-step ahead. In the data-adaptive mode (mode 3) of the trajectory estimation algorithm, the innovations and their variances are used to detect outliers.

As indicated in Fig. 5.2-2, the smoothing algorithm processes the outputs of the Kalman filter. The smoother is also recursive, but it works backward in time, starting at the end of the input time series, and running back to the initial time. Because the smoother runs in reverse, the outputs of the filter are stored in random access files so that they can be accessed in the reverse order to which they were stored.

The outputs of the smoother are optimal estimates of the payload position and velocity (with respect to the nominal trajectory) as a function of time and the error covariances for these estimates. Also included in the outputs of the smoother are estimates of the radar calibration errors that are modeled by the algorithm and their covariances.

In Sections 5.3 through 5.7, the mathematical details of the trajectory estimation algorithm are discussed. The organization of these sections follows the order in which calculations are performed when radar data are being processed.

5.3 KEPLERIAN-TRAJECTORY MODULE

The first step in computing the nominal payload trajectory is to compute a good approximation to it, called the Keplerian trajectory. The Keplerian trajectory is the position and velocity of the payload as a function of time for the idealized model of a point-mass earth and a point-mass payload. Using earth-centered Cartesian inertial coordinates (defined in Appendix D), the payload position $\underline{r}(t)$ and velocity $\underline{v}(t)$ at time t can be expressed as linear combinations of the position and velocity at t=0.

$$\underline{v}(t) = \dot{\underline{r}}(t) = \text{velocity vector} \qquad (5.3\text{-}1)$$

$$\underline{r}(t) = f(t)\underline{r}(0) + g(t)\underline{v}(0) \qquad (5.3\text{-}2)$$

$$\underline{v}(t) = \dot{f}(t)\underline{r}(0) + \dot{g}(t)\underline{v}(0) \qquad (5.3\text{-}3)$$

In Eqs. 5.3-2 and 5.3-3, the scalar functions f(t) and g(t) are known as the "f and g functions" (Refs. 7 and 20). They are computed using the canonical units of length and time, UL and UT, which are defined in terms of the semi-major axis, a [m], of the reference ellipsoid for the earth and the gravitational constant GM [$m^3 \cdot s^{-2}$] of the earth as follows:

$$UL = a \qquad [m] \qquad (5.3\text{-}4)$$

$$UT = \sqrt{\frac{a^3}{GM}} \qquad [s] \qquad (5.3\text{-}5)$$

The initial position $\underline{r}(0)$ and velocity $\underline{v}(0)$ are scaled using the canonical units:

$$\underline{r}_o = \underline{r}(0)/UL \qquad (3.5\text{-}6)$$

$$\underline{v}_o = \underline{v}(0)\cdot UT/UL \qquad (3.5\text{-}7)$$

From these scaled initial conditions, the following parameters are computed (superscript T denotes a matrix transpose):

$$|\underline{r}_o| = \sqrt{\underline{r}_o^T\ \underline{r}_o} \qquad (5.3\text{-}8)$$

$$|\underline{v}_o|^2 = \underline{v}_o^T\ \underline{v}_o \qquad (5.3\text{-}9)$$

$$RV = \underline{r}_o^T\ \underline{v}_o \qquad (5.3\text{-}10)$$

$$\alpha = |\underline{v}_o|^2 - \frac{2}{|\underline{r}_o|} \qquad (5.3\text{-}11)$$

$$c_o = 1 + \alpha\cdot|\underline{r}_o| \qquad (5.3\text{-}12)$$

$$A = (-\alpha)^{-\frac{1}{2}} \qquad (5.3\text{-}13)$$

The parameters defined by Eqs. 5.3-8 to 5.3-13 are used to compute the four additional parameters E_o, e, M_o, and N as follows:

$$\text{If } c_o \neq 0 \text{ then } E_o = \tan^{-1}\left[\frac{RV}{c_o\cdot A}\right] + \pi\cdot(c_o < 0) \qquad (5.3\text{-}14)$$

where the quantity $\pi\cdot(c_o < 0) = \pi$ if $c_o < 0$, and 0 otherwise.

$$\text{If } c_o = 0 \text{ then } E_o = \text{sign}(RV)\cdot\pi/2 \qquad (5.3\text{-}15)$$

where sign(RV) = 1 if RV > 0

sign(RV) = 0 if RV = 0

sign(RV) = -1 if RV < 0

If $\cos(E_o) \neq 0$ then $e = c_o/\cos(E_o)$ (5.3-16)

If $\cos(E_o) = 0$ then $e = \dfrac{RV}{A \cdot \sin(E_o)}$ (5.3-17)

$$M_o = E_o - RV/A \quad (5.3\text{-}18)$$

$$N = A^{-3} \quad (5.3\text{-}19)$$

For each time t of interest, the f and g functions and their derivatives are computed as follows:

$$f(t) = 1 - (1 - \cos[E - E_o]) \cdot \frac{A^2}{|\underline{r}_o|} \quad (5.3\text{-}20)$$

$$g(t) = \left[t/UT - [E - E_o - \sin(E - E_o)]/N\right] UT \quad (5.3\text{-}21)$$

$$\dot{f}(t) = \left[-\frac{A}{r \cdot |\underline{r}_o|} \cdot \sin(E - E_o)\right] \; 1/UT \quad (5.3\text{-}22)$$

$$\dot{g}(t) = 1 - \frac{A^2}{r} \cdot [1 - \cos(E - E_o)] \quad (5.3\text{-}23)$$

In Eqs. 5.3-20 to 5.3-23, the parameters r and E are computed using the following three-step iterative technique:

$$\text{Set } M = M_o + N \cdot t/UT \quad (5.3\text{-}24)$$

$$\varepsilon_{max} = 10^{-8} \quad (5.3\text{-}25)$$

$$E = 0 \quad (5.3\text{-}26)$$

Step 1 set $\varepsilon = M + e \cdot \sin(E) - E$ (5.3-27)

Step 2 if $|\varepsilon| > \varepsilon_{max}$ (5.3-28)

then set $E = E + \varepsilon/1.4$
and go to Step 1

else, go to Step 3

Step 3 set $r = A^2 \cdot [1 - e \cdot \cos(E)]$ (5.3-29)

The algorithm specified by expressions 5.3-24 to 5.3-29 is the recommended way of solving Kepler's equation for E:

$$M = E - e \cdot \sin(E) \quad (5.3\text{-}30)$$

5.4 NOMINAL-TRAJECTORY MODULE

This section discusses the mathematical details of computing a nominal trajectory for the payload at altitudes greater than 50 km. The nominal trajectory is computed by adding small corrections to the Keplerian trajectory defined in Section 5.3. These corrections are based on deterministic models for the normal gravitation of the earth and the expected atmospheric drag force acting on the payload.

The approach is to compute the perturbations in gravitation and the small atmospheric drag forces which the payload would experience if it were to follow the Keplerian trajectory. These small quantities are then used to compute the corrected payload trajectory (nominal trajectory) by using the linearized equations of motion for small departures from the Keplerian trajectory.

5.4.1 Normal Gravitation

The normal gravitation of an ellipsoidal earth model is computed using the reference ellipsoid parameters listed in

Table 5.4-1. These are the parameter values for the reference ellipsoid used in the WFF POSDAT program. The normal gravitational acceleration $\underline{a}_g(\underline{r})$ at position $\underline{r}$ with respect to the center of the reference ellipsoid is expressed as follows:

$$\underline{a}_g(\underline{r}) = -\frac{GM}{|\underline{r}|^3}\cdot\underline{r} + \delta\underline{a}_g(\underline{r}) \qquad [m\cdot s^{-2}] \qquad (5.4\text{-}1)$$

The first term in Eq. 5.4-1 is the gravitation of a point-mass earth model. The second term is the correction for the normal gravitation of the reference ellipsoidal model. The radial and tangential components of the correction are first computed, then they are transformed to Cartesian inertial coordinates. The equations for these calculations are given below:

$$\delta a_{radial} = (3/4)C_2G^2[1 + 3\cdot\cos(2\cdot A_o)] \quad [m\cdot s^{-2}] \qquad (5.4\text{-}2)$$

$$\delta a_{tangnt} = -(3/4)C_2G^2[\cos(3\cdot A_o) - \cos(A_o)]/\sin(A_o) \qquad (5.4\text{-}3)$$

TABLE 5.4-1
GEODETIC PARAMETERS FOR REFERENCE ELLIPSOID

a	=	$6.378166\cdot10^6$ [m]	=	semi-major axis
b	=	$6.356784\cdot10^6$ [m]	=	semi-minor axis
f	=	1/298.3	=	flattening
Ω	=	$7.292115147\cdot10^{-5}$ [rad/s]	=	earth's angular rotation speed
GM	=	$3.986005\cdot10^{14}$ [$m^3\cdot s^{-2}$]	=	earth's gravitational constant

In Eqs. 5.4-2 and 5.4-3, the parameters C_2, G, and A_o are computed as follows:

$$C_2 = 1.082626 \cdot 10^{-3} / (GM/a^2) \qquad (5.4\text{-}4)$$

$$G = GM/|\underline{r}|^2 \qquad (5.4\text{-}5)$$

$$A_o = (\pi/2) - A_1 \qquad (5.4\text{-}6)$$

The parameter A_1 (north latitude) in Eq. 5.4-6 is computed using the earth-centered Cartesian inertial coordinates $\underline{r}$ of the payload position:

$$\underline{r} = [r_1 \; r_2 \; r_3]^T \qquad (5.4\text{-}7)$$

$$r_{12} = \sqrt{r_1^2 + r_2^2} \qquad (5.4\text{-}8)$$

$$|\underline{r}| = \sqrt{r_1^2 + r_2^2 + r_3^2} \qquad (5.4\text{-}9)$$

$$\text{If } r_{12} > 0 \text{ then } A_1 = \tan^{-1}(r_3/r_{12}) \qquad (5.4\text{-}10)$$

$$\text{If } r_{12} = 0 \text{ then } A_1 = \text{sign}(r_3) \cdot \pi/2 \qquad (5.4\text{-}11)$$

In Eq. 5.4-11, the sign(x) function is defined as follows: sign(x) = 1 if x > 0; sign(x) = -1 if x < 0; and sign(x) = 0 if x = 0.

The Cartesian inertial components of the gravitational correction are computed using the radial and tangential components (defined in Eqs. 5.4-2 and 5.4-3) as follows:

$$\delta\underline{a}_g = [\delta a_{g1} \; \delta a_{g2} \; \delta a_{g3}]^T \qquad (5.4\text{-}12)$$

$$\delta a_{g1} = G_{12} \cdot CL \qquad (5.4\text{-}13)$$

$$\delta a_{g2} = G_{12} \cdot SL \qquad (5.4\text{-}14)$$

$$\delta a_{g3} = \delta a_{radial} \cdot \sin(A_1) - \delta a_{tangnt} \cdot \cos(A_1) \qquad (5.4\text{-}15)$$

In Eqs. 5.4-13 to 5.4-15, the parameters G_{12}, CL, and SL, are defined as follows:

$$G_{12} = \delta a_{radial} \cdot \cos(A_1) + \delta a_{tangnt} \cdot \sin(A_1) \qquad (5.4\text{-}16)$$

$$\text{If } r_{12} > 0 \text{ then } CL = r_1/r_{12} \qquad (5.4\text{-}17)$$

$$\text{and } SL = r_2/r_{12} \qquad (5.4\text{-}18)$$

$$\text{If } r_{12} = 0 \text{ then } CL = 0 \qquad (5.4\text{-}19)$$

$$\text{and } SL = 0 \qquad (5.4\text{-}20)$$

5.4.2 Atmospheric Drag

The nominal atmospheric drag force $\underline{f}_d$ acting on the payload at altitudes greater than 50 km is computed as follows:

$$\underline{f}_d(h, \underline{v}_{p/a}) = -(1/2) \cdot C_d \cdot A_p \cdot \rho(h) \cdot |\underline{v}_{p/a}| \cdot \underline{v}_{p/a} \qquad (5.4\text{-}21)$$

The symbols in Eq. 5.4-21 have the following meanings:

$\underline{f}_d$	=	drag force (vector)	[N]
h	=	payload altitude	[m]
$\underline{v}_{p/a}$	=	velocity of payload with respect to the atmosphere	$[m \cdot s^{-1}]$
C_d	=	payload drag coefficient	$[1 \leq C_d \leq 2]$
A_p	=	payload cross-sectional area	$[m^2]$
$\rho(h)$	=	atmospheric mass density	$[kg \cdot m^{-3}]$

The nominal mass density is computed using the following model, which is based on the U.S. Standard Atmosphere, 1976 (Ref. 6):

$$\rho(h) = 2.2 \cdot 10^{-6.5 \cdot 10^{-5} \cdot h} \qquad (5.4\text{-}22)$$

In Eq. 5.4-22, the payload height h above the reference ellipsoid is computed using the ellipsoid parameters (a = semi-major axis, f = flattening, b = (1-f)·a = semi-minor axis) and $|\underline{r}|$, the distance of the payload from the center of the ellipsoid:

$$h = [r_{12}]/\cos(LT)] - N \qquad (5.4\text{-}23)$$

$$LT = . \tan^{-1}[T/(1 - f)^2] \qquad (5.4\text{-}24)$$

$$T = r_3/|\underline{r}| \qquad (5.4\text{-}25)$$

$$N = a^2 \cdot [a^2 \cdot \cos^2(LT) + b^2 \cdot \sin^2(LT)]^{-1/2} \qquad (5.4\text{-}26)$$

In Eq. 5.4-21, the nominal velocity $\underline{v}_{p/a}$ of the payload with respect to the atmosphere is computed from the position of the payload $\underline{r}$ with respect to the center of the earth, the velocity $\underline{v}$ of the payload with respect to an inertial frame, and the angular velocity $\underline{\Omega}$ of the earth with respect to an inertial frame:

$$\underline{v}_{p/a} = \underline{v} - \underline{\Omega} \times \underline{r} \qquad (5.4\text{-}27)$$

The three Cartesian inertial components of $\underline{v}_{p/a}$, $\underline{v}$, and $\underline{\Omega}$ are indicated in the following equations:

$$\underline{v}_{p/a} = [v_{p/a}^{(1)} \; v_{p/a}^{(2)} \; v_{p/a}^{(3)}]^T \qquad (5.4\text{-}28)$$

$$\underline{v} = [v_1 \; v_2 \; v_3]^T \qquad (5.4\text{-}29)$$

$$\underline{\Omega} = [0 \; 0 \; \Omega]^T \qquad (5.4\text{-}30)$$

In Eq. 5.4-30, the first two components of $\underline{\Omega}$ are zero because the first two Cartesian inertial axes span the earth's equatorial plane, while the third axis is the rotational axis of the earth model. (Ω is the earth's rotational rate [rad·s^{-1}].) Using Eqs. 5.4-28 to 5.4-30 in 5.4-27 leads to the following expressions for computing the relative velocity vector $\underline{v}_{p/a}$:

$$v_{p/a}^{(1)} = v_1 + \Omega \cdot r_2 \qquad (5.4\text{-}31)$$

$$v_{p/a}^{(2)} = v_2 - \Omega \cdot r_1 \qquad (5.4\text{-}32)$$

$$v_{p/a}^{(3)} = v_3 \qquad (5.4\text{-}33)$$

By using Eqs. 5.4-22 to 5.4-33, with $\underline{r}$ and $\underline{v}$ evaluated on the Keplerian trajectory, the drag force vector $\underline{f}_d$ is computed from Eq. 5.4-21. The inertial acceleration $\underline{a}_d$ of the payload caused by the drag force $\underline{f}_d$ is then given as follows:

$$\underline{a}_d = (m_p)^{-1} \cdot \underline{f}_d \qquad (5.4\text{-}34)$$

where m_p is the payload mass [kg].

5.4.3 Trajectory Corrections

In this section the equations are presented for computing a nominal payload trajectory, given the Keplerian trajectory defined in Section 5.3, the gravitational correction defined in Section 5.4.1, and the atmospheric drag acceleration defined in Section 5.4.2. The approach is to compute position and velocity corrections that are added to the Keplerian trajectory. These corrections are computed by solving the linearized equations of motion for the payload, which govern small perturbations about the Keplerian trajectory.

The dynamical state of the payload on the nominal trajectory is represented by the state vector $\underline{X}$, which is defined in terms of the nominal payload position $\underline{R}$ and velocity $\underline{V}$. $\underline{R}$ and $\underline{V}$ are measured with respect to the center of the earth and are expressed in earth-centered Cartesian inertial coordinates:

$$\underline{X} = \begin{bmatrix} \underline{R} \\ \underline{V} \end{bmatrix} \tag{5.4-35}$$

$$\underline{R} = [R_1 \; R_2 \; R_3]^T \tag{5.4-36}$$

$$\underline{V} = [V_1 \; V_2 \; V_3]^T \tag{5.4-37}$$

The dynamical state of the payload along the Keplerian trajectory is defined in the same way:

$$\underline{X}^{(K)} = \begin{bmatrix} \underline{r} \\ \underline{v} \end{bmatrix} \tag{5.4-38}$$

In Eq. 5.4-38, the position $\underline{r}$ and velocity $\underline{v}$ are expressed in earth-centered Cartesian inertial coordinates. The nominal and Keplerian state vectors are functions of time t and are related to each other as follows:

$$\underline{X}(t) = \underline{X}^{(K)}(t) + \delta\underline{x}(t) \tag{5.4-39}$$

In Eq. 5.4-39, $\delta\underline{x}(t)$ is the correction that is added to the Keplerian state at time t to account for the influence of normal gravitation and atmospheric drag. In the remainder of this section, equations are presented for computing $\delta\underline{x}(t)$ at uniformly spaced times $t = k \cdot \delta t$, $k = 0, 1, 2, \ldots$, δt = sampling interval [s]. The following notation is used for sampled values:

$$\delta\underline{x}_k \equiv \delta\underline{x}(k\cdot\delta t) \quad \text{for } k = 0, 1, 2, \ldots \tag{5.4-40}$$

The linearized equations of motion for small perturbations about the Keplerian trajectory are as follows:

$$\delta\dot{\underline{x}}(t) = F(t)\delta\underline{x}(t) + \delta\underline{u}(t) \tag{5.4-41}$$

$$\delta\underline{u}(t) = \begin{bmatrix} \underline{0}_3 \\ \delta\underline{a}(t) \end{bmatrix}, \quad \underline{0}_3 \equiv \begin{bmatrix} 0 \\ 0 \\ 0 \end{bmatrix} \tag{5.4-42}$$

In Eq. 5.4-42, the disturbing acceleration $\delta\underline{a}(t)$ is the sum of the gravitational and atmospheric drag accelerations defined in Sections 5.4.1 and 5.4.2:

$$\delta\underline{a}(t) = \delta\underline{a}_g(t) + \delta\underline{a}_d(t) \tag{5.4-43}$$

The matrix F(t) in Eq. 5.4-41 is defined as follows:

$$F(t) = \begin{bmatrix} 0_3 & I_3 \\ J(t) & 0_3 \end{bmatrix} \tag{5.4-44}$$

In Eq. 5.4-44, 0_3 is the 3×3 zero matrix, I_3 is the 3×3 identity matrix, and J(t) is the 3×3 matrix defined as follows in terms of the Keplerian position $\underline{r}(t)$:

$$J(t) = \frac{GM}{|\underline{r}(t)|^3}\left[3\,\frac{\underline{r}(t)[\underline{r}(t)]^T}{|\underline{r}(t)|^2} - I_3\right] \tag{5.4-45}$$

In Eq. 5.4-45, GM is the gravitational constant multiplied by the mass of the earth, and $\underline{r}(t)$ is the position of the payload on the Keplerian trajectory. As shown in an unclassified section of Ref. 8, the sampled values of $\delta\underline{x}(t)$, $t = k\cdot\delta t$, $k = 0, 1, 2, \ldots$, satisfy the following equation:

$$\delta\underline{x}_{k+1} = \phi_k\delta\underline{x}_k + \Gamma_k\delta\underline{a}_k \tag{5.4-46}$$

In Eq. 5.4-46, the 6×6 transition matrix ϕ_k is defined as follows:

$$\phi_k = e^{F \cdot \delta t} = \begin{bmatrix} \phi_{11} & \phi_{12} \\ \phi_{21} & \phi_{22} \end{bmatrix} \tag{5.4-47}$$

The 3×3 submatrices in Eq. 5.4-47 are computed using the following equations:

$$\alpha = \left[\frac{GM}{|\underline{r}(t)|^3} \right]^{1/2} \tag{5.4-48}$$

$$A = \frac{\underline{r}(t) \cdot \underline{r}^T(t)}{|\underline{r}(t)|^2} \tag{5.4-49}$$

$$\phi_{11} = \phi_{22} = [\cosh(\alpha \cdot \delta t \cdot \sqrt{2}) - \cos(\alpha \cdot \delta t)] \cdot A + \cos(\alpha \cdot \delta t) \cdot I_3 \tag{5.4-50}$$

$$\phi_{12} = 1/\alpha \cdot \left[[\frac{1}{\sqrt{2}} \cdot \sinh(\alpha \cdot \delta t \cdot \sqrt{2}) - \sin(\alpha \cdot \delta t)] \cdot A + \sin(\alpha \cdot \delta t) \cdot I_3 \right] \tag{5.4-51}$$

$$\phi_{21} = \alpha \cdot \left[[\sqrt{2} \cdot \sinh(\alpha \cdot \delta t \cdot \sqrt{2}) + \sin(\alpha \cdot \delta t)] \cdot A - \sin(\alpha \cdot \delta t) \cdot I_3 \right] \tag{5.4-52}$$

In Eq. 5.4-46, the 6×3 input weighting matrix Γ_k is defined as follows:

$$\Gamma_k = \begin{bmatrix} \gamma_1 \\ \gamma_2 \end{bmatrix} \tag{5.4-53}$$

$$\gamma_1 = 1/\alpha \cdot \left[\left[\frac{\cosh(\alpha \cdot \delta t \cdot \sqrt{2}) - 1}{2\alpha} + \frac{\cos(\alpha \cdot \delta t) - 1}{\alpha} \right] \cdot A - \frac{\cos(\alpha \cdot \delta t) - 1}{\alpha} \cdot I_3 \right] \tag{5.4-54}$$

$$\gamma_2 = \left[\frac{\sinh(\alpha \cdot \delta t \cdot \sqrt{2})}{\sqrt{2} \cdot \alpha} - \frac{\sin(\alpha \cdot \delta t)}{\alpha} \right] \cdot A + \frac{\sin(\alpha \cdot \delta t)}{\alpha} \cdot I_3 \qquad (5.4\text{-}55)$$

The above equations are used to compute the state corrections $\delta \underline{x}_k$ for k = 0, 1, 2, ..., given the disturbing acceleration $\delta \underline{a}_k$. The sample values $\underline{X}_k$ of the nominal trajectory are then computed by adding the corrections to the Keplerian state:

$$\underline{X}_k = \underline{X}_k^{(K)} + \delta \underline{x}_k \qquad (5.4\text{-}56)$$

5.5 RADAR-MEASUREMENTS MODULE

5.5.1 Introduction

The purpose of this section is to present the mathematical details of the radar-measurements software module. The module is used to compute both nominal radar measurements and residual radar measurements. As depicted in Fig. 5.5-1, this module has the following inputs:

- Nominal Payload Trajectory - expected payload position and velocity expressed in earth-centered Cartesian inertial coordinates
- Radar Position - geodetic coordinates (longitude, latitude, and altitude) of the tracking radar, defined with respect to the reference ellipsoid
- Radar Tracking Data - real tracking data expressed in radar coordinates.

The outputs of this module are (1) a time series of nominal radar measurements and (2) a time series of residual

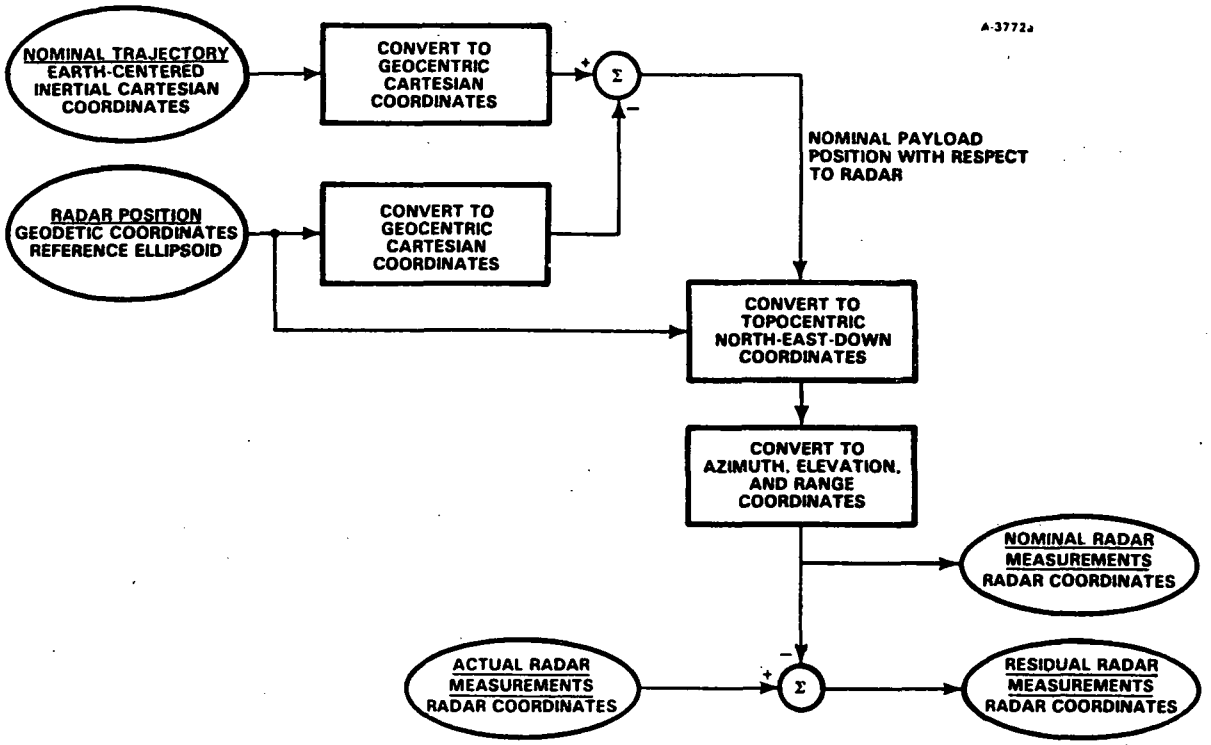

Figure 5.5-1 Radar-Measurements Module

radar measurements, both time series expressed in radar coordinates (azimuth, elevation, and range). The nominal measurements are the data that would be acquired if an ideal radar were to track the payload along the nominal trajectory. The residual measurements are the corrections that are added to the nominal measurements to produce the actual radar measurements.

5.5.2 Transform to Geocentric Coordinates

As indicated in Fig. 5.5-1, the inertial coordinates of the nominal trajectory and the geodetic coordinates of the radar are transformed to geocentric (earth-centered and earth-fixed) Cartesian coordinates. The equations governing these transformations are presented in the following:

$$\underline{r}^{(geo)} = T^{(geo)}_{(in)} \cdot \underline{r}^{(in)} \qquad (5.5\text{-}1)$$

$$\underline{v}^{(geo)} = T^{(geo)}_{(in)} \cdot (\underline{v}^{(in)} - M \cdot \underline{r}^{(in)}) \qquad (5.5\text{-}2)$$

In Eqs. 5.5-1 and 5.5-2, the following definitions are used:

$\underline{r}^{(geo)}$ = payload position vector expressed in geocentric Cartesian coordinates

$\underline{r}^{(in)}$ = payload position vector expressed in earth-centered Cartesian inertial coordinates

$T^{(geo)}_{(in)}$ = inertial-to-geocentric transformation matrix

$\underline{v}^{(geo)}$ = payload velocity expressed in geocentric Cartesian coordinates

$\underline{v}^{(in)}$ = payload velocity expressed in earth-centered Cartesian inertial coordinates

M = Coriolis transformation matrix

The transformation matrices T^{geo}_{in} and M are defined as follows (t = time[s] and Ω = earth's angular rotation speed [$rad \cdot s^{-1}$]):

$$T^{(geo)}_{(in)} = \begin{bmatrix} \cos(\Omega t) & \sin(\Omega t) & 0 \\ -\sin(\Omega t) & \cos(\Omega t) & 0 \\ 0 & 0 & 1 \end{bmatrix} \qquad (5.5\text{-}3)$$

$$M = \begin{bmatrix} 0 & -\Omega & 0 \\ \Omega & 0 & 0 \\ 0 & 0 & 0 \end{bmatrix} \qquad (5.5\text{-}4)$$

The geodetic position coordinates of the tracking radar (LO = east longitude, LA = north latitude, H = height above reference ellipsoid) are transformed to geocentric Cartesian coordinates $\underline{R}^{(radar)}$ using the following equations (a = semi-major axis and b = semi-minor axis of the reference ellipsoid) (Ref. 9):

$$\underline{R}^{(radar)} = \begin{bmatrix} R_1 \\ R_2 \\ R_3 \end{bmatrix} \tag{5.5-5}$$

$$R_1 = (N + H)\cdot\cos(LA)\cdot\cos(L0) \tag{5.5-6}$$

$$R_2 = (N + H)\cdot\cos(LA)\cdot\sin(L0) \tag{5.5-7}$$

$$R_3 = [(b/a)^2\cdot N + H]\cdot\sin(LA) \tag{5.5-8}$$

$$N = a^2\cdot[a^2\cdot\cos^2(LA) + b^2\cdot\sin^2(LA)]^{-1/2} \tag{5.5-9}$$

The nominal payload position relative to the radar, $\underline{r}^{(p/r)}$, is expressed in geocentric Cartesian coordinates as follows:

$$\underline{r}^{(p/r)} = \underline{r}^{(geo)} - \underline{R}^{(radar)} \tag{5.5-10}$$

5.5.3 Transform to Topocentric Coordinates

As depicted in Fig. 5.5-1, the next step in computing nominal radar measurements is to transform the payload position relative to the radar, $\underline{r}^{(p/r)}$, to topocentric Cartesian coordinates $\underline{R}^{(ned)}$ (n = north, e = east, d = down) with the origin located at the radar position. The equations governing this transformation are given in the following:

$$\underline{R}^{(ned)} = T^{(ned)}_{(geo)}\cdot\underline{r}^{(p/r)} \tag{5.5-11}$$

$$T^{(ned)}_{(geo)} = \begin{bmatrix} -\sin(LA)\cdot\cos(L0) & -\sin(LA)\cdot\sin(L0) & \cos(LA) \\ -\sin(L0) & \cos(L0) & 0 \\ -\cos(LA)\cdot\cos(L0) & -\cos(LA)\cdot\sin(L0) & -\sin(LA) \end{bmatrix} \tag{5.5-12}$$

$$\underline{R}^{(ned)} = \begin{bmatrix} R_n \\ R_e \\ R_d \end{bmatrix} = \begin{bmatrix} north \\ east \\ down \end{bmatrix} \qquad (5.5\text{-}13)$$

5.5.4 Transformation to Radar Coordinates

The final transformation indicated in Fig. 5.5-1 is the conversion of Cartesian north-east-down coordinates to spherical radar coordinates (AZ = azimuth, EL = elevation, RA = range). Azimuth is measured positive eastward, with AZ = 0 for due north. Elevation is measured positive toward the zenith, with EL = 0 for the horizontal. Range is measured positive away from the radar, with RA = 0 at the radar. The radar measurements are computed from $\underline{R}^{(ned)}$ using the following equations:

$$R_{ne} = \sqrt{R_n^2 + R_e^2} \qquad (5.5\text{-}14)$$

$$\cos(AZ) = R_n/R_{ne} \qquad (5.5\text{-}15)$$

$$\sin(AZ) = R_e/R_{ne} \qquad (5.5\text{-}16)$$

$$EL = \tan^{-1}(-R_d/R_{ne}) \qquad (5.5\text{-}17)$$

$$RA = \sqrt{R_n^2 + R_e^2 + R_d^2} \qquad (5.5\text{-}18)$$

5.5.5 Outputs

The outputs of the radar-measurements module are the nominal measurement vectors ($\underline{Z}(t)$) and the residual measurement vectors ($\underline{z}(t)$) for each time $t = k \cdot \delta t$, $k = 0, 1, 2, \ldots$, along the nominal trajectory:

$$\underline{Z}_k = \underline{Z}(k\cdot\delta t) = \begin{bmatrix} AZ_k \\ EL_k \\ RA_k \end{bmatrix} \tag{5.5-19}$$

$$\underline{z}_k = \underline{z}(k\cdot\delta t) = \underline{Z}_k^{(actual)} - \underline{Z}_k \tag{5.5-20}$$

where

$$\underline{Z}_k^{(actual)} = \text{vector of actual tracking data at time } t = k\cdot\delta t \tag{5.5-21}$$

5.6 KALMAN-FILTER MODULE

5.6.1 Introduction

This section describes the mathematical details of the Kalman-filter module. The purpose of the filter is to process residual radar tracking data as inputs. The outputs are a time series of filtered estimates of the payload state (position and velocity) relative to the nominal trajectory defined in Section 5.4. Additional outputs are estimates of other state variables representing radar calibration errors, the error covariance matrices for the state estimates, and a time series of innovations data (the one-step-ahead prediction errors of the Kalman filter and their variances).

The Kalman-filter algorithm presented in this section has several important properties (Ref. 5):

- The Kalman filter is a recursive algorithm for computing unbiased minimum-variance estimates of the payload state at time t. These estimates are based on (1) stochastic error models for the radar data, (2) the error covariance of the estimated initial state, and (3) the residual radar measurements up to, but not beyond, time t.

- The filter is linear and time-varying because it estimates small corrections to the nominal dynamical state of the payload as a function of time along the nominal trajectory.

- Missing radar data and isolated outliers are handled optimally. The filter processes missing data by optimally extrapolating over the gaps (this is called mode 2 processing). In mode 3 processing, data outliers are detected automatically by comparing the innovations with their theoretical rms values. When the innovations exceed approximately three standard deviations, the noise variance of the measurement-noise model is continuously and automatically increased, and the new measurement is processed optimally with respect to this higher noise level.

- The filter computes the theoretical rms accuracy of the estimated trajectory based on the radar error model, the uncertainty of the initial position and velocity, and all radar measurements up to the current instant.

- The outputs of the filter are sufficient statistics for computing the final smoothed estimate of the trajectory based on all available radar measurements.

A block diagram of the data processing performed by the Kalman filter is shown in Fig. 5.6-1. The algorithm is recursive, which means that it processes an estimated state vector at time t_1 to produce as output an estimated state vector for the next sampling time t_2 based on the radar measurements at time t_2. As indicated in the upper left corner of Fig. 5.6-1, the filter uses the estimated state vector at time t_1 to predict the states at time t_2. This prediction is optimal and takes into account the physics of the payload dynamics.

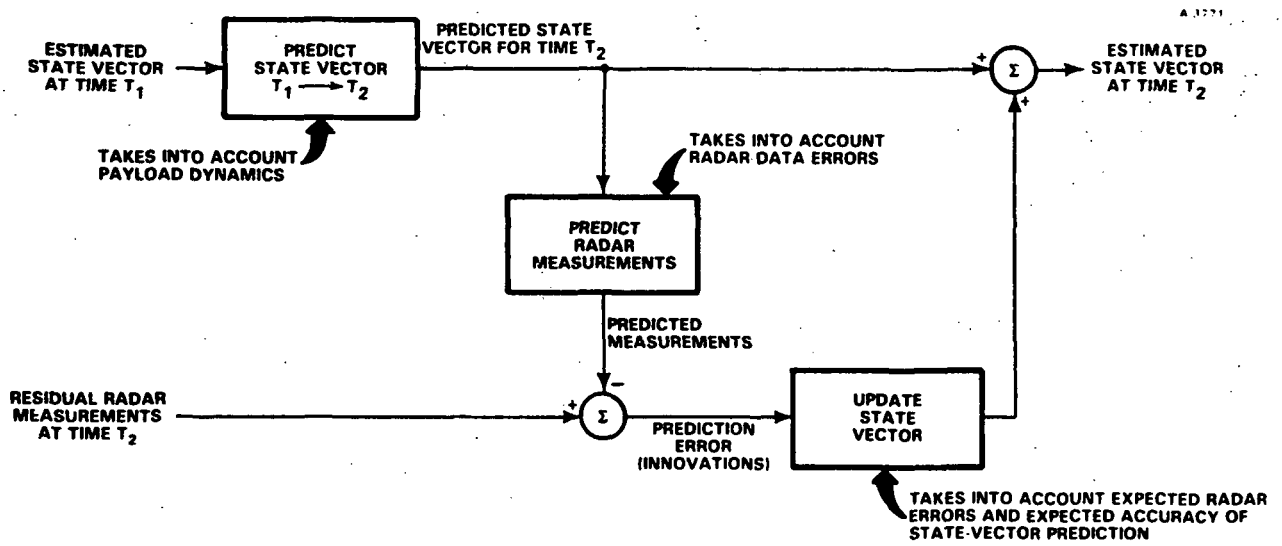

Figure 5.6-1 Block Diagram of Data Processing in a Kalman Filter

Next, the filter uses the predicted state to predict what the radar measurements will be at time t_2. This prediction takes into account the radar error model, which represents both noise and systematic measurement errors.

The differences between the actual residual radar measurements at time t_2 and the predicted measurements are computed. These differences are the one-step-ahead prediction errors of the filter and are known as the innovations. Based on these innovations, the filter computes an optimal update that is added to the predicted state vector for time t_2. This update is optimal; it takes into account the modeled radar error sources and the expected accuracy of the state-vector

prediction. For simplicity, Fig. 5.6-1 does not portray the error covariance calculations that are also performed by the filter at each time step.

5.6.2 Kalman Filter Equations

The Kalman filter processes the sequence of residual radar measurements $\underline{z}_k$, k = 0, 1, 2, ..., which are computed by the radar-measurements module described in Section 5.5. The filter parameters change with time; at time step k they are contained in the following matrices (with n = number of state variables and m = number of scalar radar measurements at each sampling time, e.g., m = 3 for azimuth, elevation, and range data from one radar):

Φ_k =	state transition matrix	[n×n]
Q_k =	state process noise covariance	[n×n]
H_k =	measurement matrix	[m×n]
R_k =	measurement noise covariance	[m×m]

The filter uses these four matrices, together with an initial estimate of the state vector, $\underline{x}_o$, and its error covariance matrix, P_o, to compute the following seven matrices for k = 0, 1, 2, ...:

$\hat{\underline{x}}$ =	one-step-ahead estimate of the state vector	[n×1]
P =	error covariance of $\hat{\underline{x}}$	[n×n]
K =	Kalman gain matrix	[n×m]
$\underline{\nu}_k$ =	innovations vector at time k	[m×1]
C_k =	innovations covariance matrix at time k	[m×m]

$\underline{\hat{x}}_k(+)$ = updated (filtered) estimate of the state vector at time k [n×1]

$P_k(+)$ = error covariance of $\underline{\hat{x}}_k(+)$ at time k [n×n]

The filter computes these matrices using the following recursive formulas (in which M [m×n], MM [n×m], N [n×n] are work arrays):

Initial Conditions

$$P = P_o \quad [n\times n] \quad (5.6\text{-}1)$$

$$\underline{\hat{x}} = \underline{x}_o \quad [n\times 1] \quad (5.6\text{-}2)$$

For k = 0 to kmax

$$M = H_k \cdot P \quad [m\times n] \quad (5.6\text{-}3)$$

$$C_k = M \cdot H_k^T + R_k \quad [m\times m] \quad (5.6\text{-}4)$$

$$K = M^T \cdot C_k^{-1} \quad [n\times m] \quad (5.6\text{-}5)$$

$$N = P - K \cdot M \quad [n\times n] \quad (5.6\text{-}6)$$

$$MM = N \cdot H_k^T \quad [n\times m] \quad (5.6\text{-}7)$$

$$P_k(+) = [N - MM \cdot K^T] + K \cdot R_k \cdot K^T \quad [n\times n] \quad (5.6\text{-}8)$$

$$\underline{\nu}_k = \underline{z}_k - H_k \cdot \underline{\hat{x}} \quad [m\times 1] \quad (5.6\text{-}9)$$

$$\underline{\hat{x}}_k(+) = \underline{\hat{x}} + K \cdot \underline{\nu}_k \quad [n\times 1] \quad (5.6\text{-}10)$$

$$\underline{\hat{x}} = \phi_k \cdot \underline{\hat{x}}_k(+) \quad [n\times 1] \quad (5.6\text{-}11)$$

$$P = \phi_k \cdot P_k(+) \cdot \phi_k^T + Q_k \quad [n\times n] \quad (5.6\text{-}12)$$

Next k [End of For-Next Loop]

In Eqs. 5.6-1 to 5.6-12, the following calculations are performed:

- The initial state estimate and its error covariance are used to initialize $\hat{\underline{x}}$ and P in Eqs. 5.6-1 and 5.6-2
- The innovations covariance C_k and Kalman gain matrix K are computed in Eq. 5.6-4 and Eq. 5.6-5
- The error covariance matrix $P_k(+)$ of the filtered state estimate $\hat{\underline{x}}_k(+)$ is computed (using the Josephson-Bierman update) (Refs. 5 and 10) in Eqs. 5.6-6 to 5.6-8
- The innovations vector $\underline{\nu}_k$ is computed in Eq. 5.6-9
- The filtered state estimate $\hat{\underline{x}}_k(+)$ is computed in Eq. 5.6-10
- The one-step-ahead prediction of the state vector $\hat{\underline{x}}$ and its error covariance P are computed in Eqs. 5.6-11 to 5.2-12.

5.6.3 State-Space Model

The algorithm represented by Eqs. 5.6-1 to 5.6-12 is the optimal filter for estimating the state $\underline{x}_k$ of the following stochastic model for (1) the payload perturbations away from the nominal trajectory and (2) the noisy radar tracking data:

$$\underline{x}_{k+1} = \Phi_k \cdot \underline{x}_k + \underline{w}_k \qquad [n\times 1] \qquad (5.6\text{-}13)$$

$$\underline{z}_k = H_k \cdot \underline{x}_k + \underline{v}_k \qquad [m\times 1] \qquad (5.6\text{-}14)$$

$$E[\underline{w}_k] = \underline{0} \qquad [n\times 1] \qquad (5.6\text{-}15)$$

$$E[\underline{v}_k] = \underline{0} \qquad [m\times 1] \qquad (5.6\text{-}16)$$

$$E[\underline{w}_k \cdot \underline{w}_j^T] = Q_k \cdot \delta_{k-j} \qquad [n\times n] \qquad (5.6\text{-}17)$$

$$E[\underline{v}_k \cdot \underline{v}_j^T] = R_k \cdot \delta_{k-j} \qquad [m\times m] \qquad (5.6\text{-}18)$$

$$E[\underline{w}_k \cdot \underline{v}_j^T] = 0 \qquad [n \times m] \qquad (5.6\text{-}19)$$

for all k and j

$$E[\underline{x}_k \cdot \underline{w}_j^T] = 0 \qquad [n \times n] \qquad (5.6\text{-}20)$$

for all $j \geq k$

$$E[\underline{x}_o] = \underline{0} \qquad [n \times 1] \qquad (5.6\text{-}21)$$

$$E[\underline{x}_o \cdot \underline{x}_o^T] = P_o \qquad [n \times n] \qquad (5.6\text{-}22)$$

Equations 5.6-13 to 5.6-22 have the following interpretation:

- The state vector $\underline{x}_k$ is the solution of the difference Eq. 5.6-13. The initial state vector $\underline{x}_o$ is a random variable with zero mean (Eq. 5.6-21) and covariance matrix P_o (Eq. 5.6-22). Equation 5.6-13 is driven by a white noise vector $\underline{w}_k$.
- The dimension n of the state vector is nine for the filters implemented in this study. Six of the states represent the dynamical state of the payload relative to the nominal trajectory. The remaining three states represent radar measurement biases or ramps caused by radar calibration error. If a bias and a ramp are modeled in each of the three measurement channels then n=12.

5.6.4 State Variables

The state variables (states) are the elements of the state vector $\underline{x}_k$ [n×1]. The first six states are the position $\underline{r}_k$ and velocity $\underline{v}_k$ of the payload relative to the nominal trajectory (expressed in earth-centered Cartesian inertial coordinates). These states form the following 6×1 vector of payload states:

$$\underline{x}_k^{(payload)} = \begin{bmatrix} \underline{r}_k \\ \\ \underline{v}_k \end{bmatrix} \qquad [6\times1] \qquad (5.6\text{-}23)$$

The remaining states are used to model radar measurement biases or ramps caused by radar calibration errors. In this study three radar error states were used to filter and smooth the tracking data provided by WFF from Peruvian radars Nos. 8 and 41. All states used to model radar errors are elements of the following vector of radar error states (in this example there are three error states):

$$\underline{x}_k^{(radar)} = \begin{bmatrix} e_k(1) \\ e_k(2) \\ e_k(3) \end{bmatrix} \qquad [3\times1] \qquad (5.6\text{-}24)$$

The complete state vector $\underline{x}_k$ is organized with the payload states listed first:

$$\underline{x}_k = \begin{bmatrix} \underline{x}_k^{(payload)} \\ \\ \underline{x}_k^{(radar)} \end{bmatrix} \qquad [9\times1] \qquad (5.6\text{-}25)$$

The partitioning of the state vector in Eq. 5.6-25 induces a partitioning of the parameter matrices ϕ_k, Q_k, and H_k as indicated in the following equations:

$$\phi_k = \left[\begin{array}{c:c} \phi_k^{(payload)} \ [6\times6] & 0 \ [6\times3] \\ \hdashline 0 \ [3\times6] & \phi_k^{(radar)} \ [3\times3] \end{array}\right] \qquad [9\times9] \qquad (5.6\text{-}26)$$

$$Q_k = \left[\begin{array}{c:c} \begin{matrix} (\text{payload}) \\ Q_k \quad [6\times6] \end{matrix} & \begin{matrix} 0 \\ [6\times3] \end{matrix} \\ \hdashline \begin{matrix} 0 \\ [3\times6] \end{matrix} & \begin{matrix} (\text{radar}) \\ Q_k \quad [3\times3] \end{matrix} \end{array}\right] \qquad [9\times9] \qquad (5.6\text{-}27)$$

$$H_k = \left[\begin{array}{c:c} \begin{matrix} (\text{payload}) \\ H_k \quad [3\times6] \end{matrix} & \begin{matrix} (\text{radar}) \\ H_k \quad [3\times3] \end{matrix} \end{array}\right] \qquad [3\times9] \qquad (5.6\text{-}28)$$

The definitions of these partitions and the measurement noise covariance matrix R_k are presented in the following sections.

5.6.5 Transition Matrix ϕ

As indicated in Eq. 5.6-26, the transition matrix is block diagonal. This structure occurs because the payload states are independent of radar errors. The payload transition matrix is partitioned into 3×3 submatrices:

$$\phi_k^{(\text{payload})} = \begin{bmatrix} \phi_{11} & \phi_{12} \\ \phi_{21} & \phi_{22} \end{bmatrix} \qquad [6\times6] \qquad (5.6\text{-}29)$$

The 3×3 submatrices in Eq. 5.6-29 are computed using the algorithm specified in Section 5.4.3, Eqs. 5.4-50 to 5.4-52 (the payload state vector $\underline{x}_k^{(\text{payload})}$ in Eq. 5.6-25 plays the role of the state correction $\delta\underline{x}_k$ in Section 5.4.3).

The transition matrix for the radar error states is a 3×3 identity matrix when there are three error states:

$$\phi_k^{(\text{radar})} = \begin{bmatrix} 1 & 0 & 0 \\ 0 & 1 & 0 \\ 0 & 0 & 1 \end{bmatrix} \qquad [3\times3] \qquad (5.6\text{-}30)$$

Equation 5.6-30 is an appropriate transition matrix for modeling systematic (bias and ramp) errors in the radar measurements. In general, if there are n_e (bias and ramp) error states, then

$\phi_k^{(radar)}$ is the $n_e \times n_e$ identity matrix. (For example, if both bias and ramp errors are modeled for azimuth, elevation, and range channels, then $n_e = 6$.)

5.6.6 State Noise Covariance Q

According to the stochastic model used in this study, uncertainty in the payload state at time step k is the result of uncertainty in the payload state at the initial time k=0. Therefore, the state-space model for the payload states is a deterministic difference equation with random initial conditions. Because there is no white noise driving the payload states, the payload Q-matrix in Eq. 5.6-27 is zero:

$$Q_k^{(payload)} = \text{zero matrix} \qquad [6\times6] \qquad (5.6\text{-}31)$$

The radar error states also satisfy a deterministic difference equation with random initial conditions. The uncertainty at the initial time corresponds to uncertainty about the radar calibration errors. The radar errors are modeled as systematic. Therefore, there is no white noise driving the radar error states, and the radar Q-matrix in Eq. 5.6-27 is also zero:

$$Q_k^{(radar)} = \text{zero matrix} \qquad [3\times3] \qquad (5.6\text{-}32)$$

5.6.7 Measurement Matrix H

The payload measurement matrix $H_k^{(payload)}$ in Eq. 5.6-28 models linearly the residual tracking measurements that would be acquired by an ideal radar. According to the analysis in Appendix E, the payload measurement matrix is computed using the following equation:

$$H_k^{(payload)} = \left[H_k^o \quad 0_3 \right] \qquad [3\times6] \qquad (5.6\text{-}33)$$

In Eq. 5.6-33, 0_3 is the 3×3 zero matrix, and the 3×3 matrix H_k^o is computed using the nominal radar measurements $\underline{Z}_k$. (The algorithm for computing $\underline{Z}_k$ is presented in Section 5.5.) The matrix H_k^o is computed as follows:

$$H_k^o = A_k^{-1} \cdot B \cdot C_k \qquad [3\times3] \qquad (5.6\text{-}34)$$

In Eq. 5.6-34, the matrices A_k and C_k depend on the nominal radar measurements (AZ_k = azimuth, EL_k = elevation, and RA_k = range) as follows:

$$\underline{Z}_k = [AZ_k \quad EL_k \quad RA_k]^T \qquad [3\times1] \qquad (5.6\text{-}35)$$

Matrix A_k is computed using the following definitions:

$$CL = \cos(EL_k) \qquad (5.6\text{-}36)$$

$$SL = \sin(EL_k) \qquad (5.6\text{-}37)$$

$$CZ = \cos(AZ_k) \qquad (5.6\text{-}38)$$

$$SZ = \sin(AZ_k) \qquad (5.6\text{-}39)$$

$$RC = RA_k \cdot CL \qquad (5.6\text{-}40)$$

$$RS = RA_k \cdot SL \qquad (5.6\text{-}41)$$

$$A_k = \begin{bmatrix} -RC\cdot SZ & -RS\cdot CZ & CZ\cdot CL \\ RC\cdot CZ & -RS\cdot SZ & SZ\cdot CL \\ 0 & -RC & -SL \end{bmatrix} \qquad (5.6\text{-}42)$$

In Eq. 5.6-34, matrix B depends on the geodetic latitude LA and longitude LO of the tracking radar as follows:

$$B = \begin{bmatrix} -\sin(LA)\cdot\cos(LO) & -\sin(LA)\cdot\sin(LO) & \cos(LA) \\ -\sin(LO) & \cos(LO) & 0 \\ -\cos(LA)\cdot\cos(LO) & -\cos(LA)\cdot\sin(LO) & -\sin(LA) \end{bmatrix} \quad (5.6\text{-}43)$$

Matrix C_k in Eq. 5.6-34 depends on the sampling interval δt [s] of the radar measurements and the earth's angular velocity Ω [rad$\cdot$s^{-1}] as follows:

$$C_k = \begin{bmatrix} \cos(a_k) & \sin(a_k) & 0 \\ -\sin(a_k) & \cos(a_k) & 0 \\ 0 & 0 & 1 \end{bmatrix} \quad (5.6\text{-}44)$$

$$a_k = \Omega\cdot\delta t\cdot k \quad [\text{rad}] \quad (5.6\text{-}45)$$

The radar error states $\underline{x}_k^{(radar)}$ represent biases or ramps in the residual radar measurements. Whether a particular error state represents a bias offset or a linear ramp depends on the radar measurement matrix $H_k^{(radar)}$ in Eq. 5.6-28. For example, in this study three error states were used to process test data from WFF. Therefore, $\underline{x}_k^{(radar)}$ is a 3×1 vector and $H_k^{(radar)}$ is a 3×3 matrix in this case. The radar calibration errors are modeled as being statistically uncorrelated between the azimuth, elevation, and range channels. Therefore, each column of $H_k^{(radar)}$ is filled with zeros except for <u>one</u> entry, which is either a 1 or k. The entry is 1 if the error state models a bias; it is k if the error state models a ramp.

As an example, consider the case where all three measurement channels have bias errors, and ramps are not being modeled. Suppose furthermore, that the first radar error state

corresponds to the bias in the first measurement channel (azimuth), the second error state corresponds to the second measurement channel (elevation), the third error state corresponds to the third measurement channel (range), then

$$H_k^{(radar)} = \begin{bmatrix} 1 & 0 & 0 \\ 0 & 1 & 0 \\ 0 & 0 & 1 \end{bmatrix} \qquad (5.6\text{-}46)$$

If on the other hand, each measurement channel error is modeled as a ramp, and pure bias offsets are not modeled, then

$$H_k^{(radar)} = \begin{bmatrix} k & 0 & 0 \\ 0 & k & 0 \\ 0 & 0 & k \end{bmatrix} \qquad (5.6\text{-}47)$$

As a third example, suppose that the first measurement channel has both bias and ramp errors, the second measurement channel has only a bias error, the third measurement channel has neither bias nor ramp error, then

$$H_k^{(radar)} = \begin{bmatrix} 1 & k & 0 \\ 0 & 0 & 1 \\ 0 & 0 & 0 \end{bmatrix} \qquad (5.6\text{-}48)$$

According to Eq. 5.6-48, the first error state represents a bias in the first measurement channel, the second error state represents a ramp in the first measurement channel, and the third error state represents a bias in the second measurement channel. An alternative to Eq. 5.6-48, which assigns the three error states differently, is the following:

$$H_k^{(radar)} = \begin{bmatrix} 1 & 0 & k \\ 0 & 1 & 0 \\ 0 & 0 & 0 \end{bmatrix} \qquad (5.6\text{-}49)$$

Equations 5.6-48 and 5.6-49 are different ways of representing the same radar error model. The two equations simply assign different physical meanings to the three error states.

If the radar data are to be processed with both bias and ramp errors being modeled for all three measurement channels, then six radar error states are required. In this case $\underline{x}_k^{(radar)}$ would be a 6×1 vector and $H_k^{(radar)}$ would be a 3×6 matrix, which could have the following form:

$$H_k^{(radar)} = \begin{bmatrix} 1 & k & 0 & 0 & 0 & 0 \\ 0 & 0 & 1 & k & 0 & 0 \\ 0 & 0 & 0 & 0 & 1 & k \end{bmatrix} \qquad (5.6\text{-}50)$$

In Eq. 5.6-50, the first two error states represent the bias and ramp errors in the azimuth data, the third and fourth error states represent the bias and ramp errors in the elevation data, and the fifth and sixth error states represent the bias and ramp errors in the range data.

5.6.8 Measurement Noise Covariance R

The measurement noise covariance R_k is a 3×3 diagonal matrix. This models the noise signals in the measurement channels as being uncorrelated with each other, which is consistent with the spectral coherence plots for radar data studied under Task 1 of this investigation. The covariance R_k represents the level of white noise in each channel of the residual radar measurement vector $\underline{z}_k$. By appropriately defining R_k as a function time (k), the Kalman filter will optimally process radar data having time-varying noise and gaps caused by missing observations.

There are three modes in which the Kalman filter is used to process residual radar measurements:

Mode 1 — The noise covariance R_k is constant (i.e., $R_k = R_{baseline}$ for $k = 0, 1, 2, \ldots, k_{max}$)

Mode 2 — The noise variances in R_k are intentionally set to very large values, $R_k = R_{big}$, for pre-specified values of k that correspond to known intervals of missing data or very noisy data.

Mode 3 — Individual noise variances in R_k are automatically increased ($R_k > R_{baseline}$) by the filtering algorithm when an individual azimuth, elevation, or range measurement is an outlier (i.e., the measurement is statistically inconsistent with the noise and error models for which the filter is optimized). The outliers are detected automatically using the innovations data generated by the filter. The amount of increase in R_k is a continuous function of the magnitude of discrepancy between the observed innovation values and their theoretical rms values.

The algorithm can be switched between these three modes at any values of k during the processing of the radar data. The equations for computing the R_k matrix are presented in the following.

Mode 1 for Fixed Noise Model - The baseline value for the measurement noise covariance is used for all k:

$$R_{baseline} = \begin{bmatrix} \sigma_{az}^2 & 0 & 0 \\ 0 & \sigma_{el}^2 & 0 \\ 0 & 0 & \sigma_{ra}^2 \end{bmatrix} \qquad (5.6\text{-}51)$$

$$R_k = R_{baseline} \quad \text{for all } k \qquad (5.6\text{-}52)$$

In Eq. 5.6-51, the sigmas are the nominal rms values of the white noise in the azimuth, elevation, and range data. The baseline covariance matrix is diagonal because the noise is modeled as uncorrelated between the measurement channels.

Mode 2 for Data Gaps - Very large noise variances (R_{big}) are used for pre-specified values of k and pre-specified measurement channels:

$$R_{big} = \begin{bmatrix} \sigma^2_{big\ az} & 0 & 0 \\ 0 & \sigma^2_{big\ el} & 0 \\ 0 & 0 & \sigma^2_{big\ ra} \end{bmatrix} \qquad (5.6\text{-}53)$$

In Eq. 5.6-53, the sigmas are large (e.g., 1000 times larger than the baseline sigmas in Eq. 5.6-51) for each measurement channel that has missing or very noisy data. For example, if the range data are missing or very noisy, but the angle measurements are normal, then a reasonable choice is $\sigma_{big\ ra} = 1000 \cdot \sigma_{ra}$, while $\sigma_{big\ az} = \sigma_{az}$ and $\sigma_{big\ el} = \sigma_{el}$.

$$R_k = R_{big} \quad \text{for prespecified } k \qquad (5.6\text{-}54)$$

Mode 3 for Automatic Outlier Processing - Each diagonal element of R_k is computed on the basis of the innovations $\underline{\nu}_k$ and their variances. The Kalman filter algorithm computes the 3×1 vector $\underline{\nu}_k$ and its covariance matrix C_k as specified in Section 5.6.2. The elements of $\underline{\nu}_k$ are arranged in the same order as the elements of the residual radar measurement vector $\underline{z}_k$ (1st = azimuth, 2nd = elevation, 3rd = range). In this discussion, the following notation is used:

$$\underline{z}_k = [z_1 \; z_2 \; z_3]^T \tag{5.6-55}$$

$$\underline{\nu}_k = [\nu_1 \; \nu_2 \; \nu_3]^T \tag{5.6-56}$$

$$C_k = \begin{bmatrix} c_1 & 0 & 0 \\ 0 & c_2 & 0 \\ 0 & 0 & c_3 \end{bmatrix} \tag{5.6-57}$$

$$R_k = \begin{bmatrix} r_1 & 0 & 0 \\ 0 & r_2 & 0 \\ 0 & 0 & r_3 \end{bmatrix} \tag{5.6-58}$$

$$R_{baseline} = \begin{bmatrix} r_1(bl) & 0 & 0 \\ 0 & r_2(bl) & 0 \\ 0 & 0 & r_3(bl) \end{bmatrix} \tag{5.6-59}$$

When Mode 3 is in effect, the diagonal elements of R_k are computed based on the squares of the innovations and their theoretical expected values. For these computations, the variance function V is defined for i = 1, 2, and 3:

$$V[\nu_i, c_i, r_i(bl)] = \frac{r_i(bl) + 4 \cdot x \cdot [x/A]^7}{1 + [x/A]^7} \tag{5.6-60}$$

where

$$A = 12 \cdot c_i \tag{5.6-61}$$

$$x = \nu_i^2 \tag{5.6-62}$$

Given: (1) the baseline noise covariance $R_{baseline}$; (2) the innovations vector $\underline{\nu}_k$; and (3) the innovations covariance matrix C_k; the covariance matrix R_k is computed using the following algorithm:

For i = 1 to 3

If $x/A > 10$ then $r_i = 4 \cdot x$ (avoids possible overflow in function V) (5.6-63)

Else $r_i = V[\nu_i, c_i, r_i(bl)]$ (5.6-64)

Next i

This algorithm for computing matrix R_k yields a model noise variance r_i that equals the baseline value when the squared innovation ν_i^2 is small compared to $12 \cdot c_i$. When the innovations start exceeding approximately three standard deviations, then the noise variance r_i starts to approach $4 \cdot \nu_i^2$. The result of this is that large innovations (which are improbable under the baseline noise model) cause the filter noise model to be changed automatically so that noise spikes in the data are filtered optimally with respect to the increased noise variance.

5.6.9 Kalman Filter Outputs

Figure 5.6-2 depicts the inputs and outputs of the Kalman filter module for the case in which there are nine state variables: three payload position states, three payload velocity states; and three radar error states. Sixty scalars are stored per time step: nine filtered state estimates; 45 distinct elements of the state error covariance matrix (symmetric 9×9); and six scalars representing the innovations and their variances.

The outputs of the filter module are stored in a random access data store for subsequent processing by the smoothing module. The data store is random access, rather than sequential access, because the smoother processes the data backwards in time. More specifically, the data store should support last-in first-out data accesses.

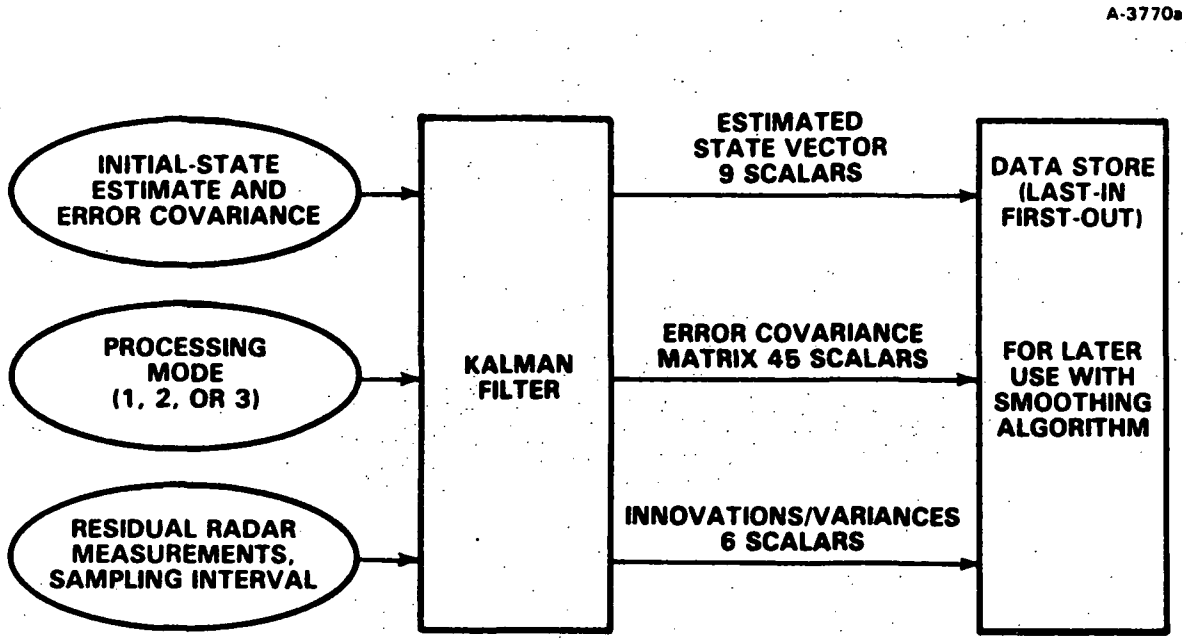

Figure 5.6-2 Kalman Filter Module

5.7 SMOOTHER MODULE

5.7.1 Introduction

The smoother is the last stage of the trajectory estimation algorithm. As indicated in Fig. 5.7-1, the inputs to the smoother module are taken from the data store in which the outputs from the filter module were saved. This data store is used in a last-in first-out mode because the smoothing algorithm processes the data backwards in time. The inputs to the smoother at time step k are the processing mode and the following time series (in this example there are three radar error states):

$\underline{\hat{x}}_k(+)$ = filtered state-vector estimate [9×1] (5.7-1)

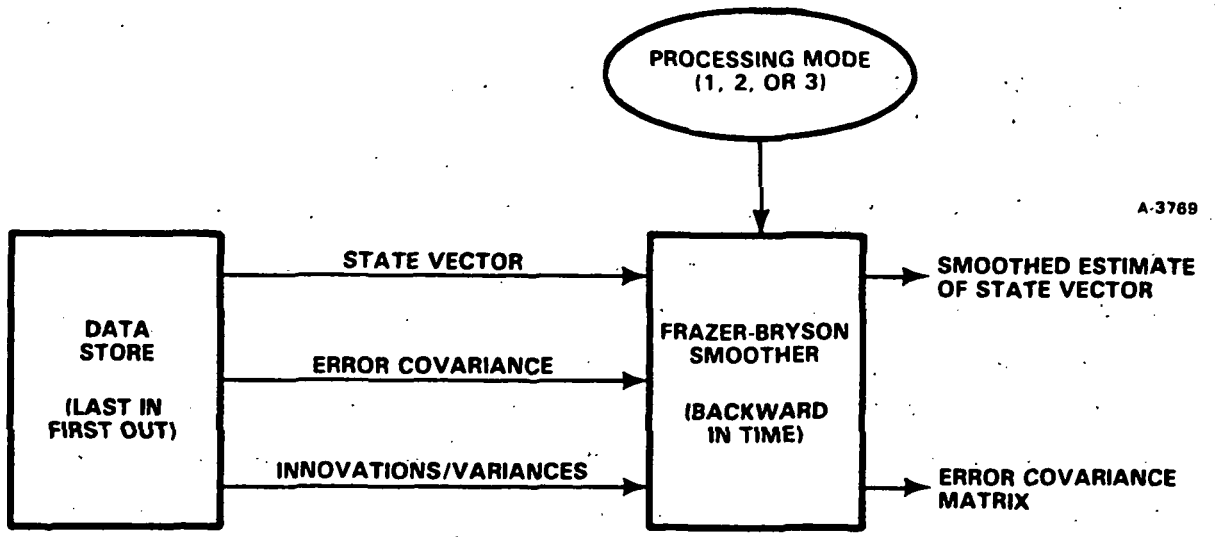

Figure 5.7-1 Smoother Module

$P_k(+)$ = filtered state error covariance [9×9] (5.7-2)

$\underline{\nu}_k$ = innovations vector [3×1] (5.7-3)

C_k = innovations covariance matrix (only 3 diagonal elements are used during mode 3 outlier processing) [3×3] (5.7-4)

These inputs are defined in Section 5.6.2, and the processing modes for missing data and outlier processing are discussed in Section 5.6.8.

The outputs of the smoothing algorithm at each time step k are the smoothed estimate of the state vector and its error covariance:

$\hat{\underline{x}}_k$ = smoothed state-vector estimate [9×1] (5.7-5)

P_k = smoothed state error covariance matrix [9×9] (5.7-6)

In Eq. 5.7-5, the first six elements of the state vector are the smoothed position and velocity coordinates of the payload relative to the nominal trajectory $\underline{X}_k$ defined in Section 5.4. (All coordinates are expressed in earth-centered Cartesian inertial coordinates.) Therefore, the smoothed estimate of the payload position and velocity relative to the center of the earth is computed by adding the first six elements of the smoothed state in Eq. 5.7-5 to the nominal trajectory $\underline{X}_k$ defined by Eq. 5.4-56. The mean-square accuracy of this estimate is represented by the error covariance matrix in Eq. 5.7-6.

The remaining states (there would typically be three to six of them) in the state vector of Eq. 5.7-5 are radar error states. Their covariances are also contained in the covariance matrix P_k.

5.7.2 Smoothing Equations

The algorithm presented in this section is the Frazer-Bryson smoother (Ref. 11). It computes trajectory estimates that are fully optimal (unbiased and minimum-variance) with respect to the stochastic model for radar errors and payload initial state uncertainty. The smoothing algorithm is mathematically equivalent to batch processing optimally all of the available data.

The algorithm operates on the input data backwards in time, working from the final time step $k = k_{max}$ back to the initial step $k = 0$. The equations describing the algorithm

are presented in the following (A [n×n], $\underline{A}_o$ [n×n], $\underline{b}$ [n×1], $\underline{b}_o$ [n×1], B [n×n], C [n×m], and S [n×n] are work arrays):

Initial Conditions

$$\underline{b} = \text{zero vector} \qquad [n\times 1] \qquad (5.7\text{-}7)$$

$$A = \text{zero matrix} \qquad [n\times n] \qquad (5.7\text{-}8)$$

For $k = k_{max}$ to 0 stepping by -1

$$\underline{\hat{x}}_k = \underline{\hat{x}}_k(+) - P_k(+)\cdot\underline{b} \qquad [n\times 1] \qquad (5.7\text{-}9)$$

$$P_k = P_k(+) - P_k(+)\cdot A\cdot P_k(+) \qquad [n\times n] \qquad (5.7\text{-}10)$$

$$C = H_k^T\cdot R_k^{-1} \qquad [n\times m] \qquad (5.7\text{-}11)$$

$$S = C\cdot H_k \qquad [n\times n] \qquad (5.7\text{-}12)$$

$$B = [I_n - P_k(+)\cdot S]\cdot\phi_k \qquad [n\times n] \qquad (5.7\text{-}13)$$

$$\underline{b}_o = B^T\cdot[\underline{b} - C\cdot\underline{\nu}_k] \qquad [n\times 1] \qquad (5.7\text{-}14)$$

$$\underline{b} = \underline{b}_o \qquad [n\times 1] \qquad (5.7\text{-}15)$$

$$A_o = B^T\cdot A\cdot B + \phi^T\cdot S\cdot B \qquad [n\times n] \qquad (5.7\text{-}16)$$

$$A = A_o \qquad [n\times n] \qquad (5.7\text{-}17)$$

Next k

In Eqs. 5.7-7 to 5.7-17, the parameter matrices ϕ_k, H_k, and R_k are computed by using the algorithms specified in Sections 5.6.5, 5.6.7, and 5.6.8. When computing the measurement noise covariance R_k, the smoother should use the same

processing mode (mode 1, 2, or 3 as defined in Section 5.6.8) that is used in the Kalman filter module. For example, if the filter changes from mode 1 to mode 2 at k = 55, then the smoother module should compute R_k using mode 1 for k < 55 and switch to mode 2 processing at k = 55. Using inconsistent modes in the filter and smoother modules can produce covariance matrices having negative elements along their diagonals.

The innovation variances are used only for mode 3 processing. Therefore, when mode 1 or mode 2 processing is used at time k, the innovation covariance matrix C_k is not used by the smoother and is not a required input quantity.

5.7.3 Outputs

The outputs of the smoother module at each time step k are the estimated state vector and its error covariance. The state vector may be written in the following partitioned form, in which the payload states are distinguished from the radar error states:

$$\underline{\hat{x}}_k = \begin{bmatrix} \underline{\hat{x}}_k^{(payload)} \\ \\ \underline{\hat{x}}_k^{(radar)} \end{bmatrix} \qquad [n\times 1] \qquad (5.7\text{-}18)$$

In Eq. 5.7-18, the payload state vector is [6×1], and the radar error state vector is $[n_e \times 1]$, where n_e is number of radar error states in the model. (For processing the WFF radar data from Peru, n_e = 3.) The partition in Eq. 5.7-18 induces the following partitions in the error covariance matrix:

$$P_k = \begin{bmatrix} P_k^{(payload)} & P_k^{(p/r)} \\ \\ P_k^{(r/p)} & P_k^{(radar)} \end{bmatrix} \qquad [n\times n] \qquad (5.7\text{-}19)$$

$$P_k^{(payload)} = \text{error covariance of } \hat{\underline{x}}_k^{(payload)} \quad [6\times6] \qquad (5.7\text{-}20)$$

$$P_k^{(radar)} = \text{error covariance of } \hat{\underline{x}}_k^{(radar)} \quad [n_e \times n_e] \qquad (5.7\text{-}21)$$

$$P_k^{(p/r)} = P_k^{(r/p)^T} = \text{error cross-covariances} \qquad (5.7\text{-}22)$$

The estimated payload state in Eq. 5.7-18 contains the estimated position and velocity of the payload relative to the nominal trajectory $\underline{X}_k$ defined in Section 5.4.3. The position coordinates and velocity coordinates are expressed in earth-centered Cartesian inertial coordinates, with the position coordinates listed first:

$$\hat{\underline{x}}_k^{(payload)} = \begin{bmatrix} \hat{\underline{r}}_k \\ \hat{\underline{v}}_k \end{bmatrix} \qquad [6\times1] \qquad (5.7\text{-}23)$$

$$\underline{X}_k = \begin{bmatrix} \underline{R}_k \\ \underline{V}_k \end{bmatrix} \qquad [6\times1] \qquad (5.7\text{-}24)$$

To compute the estimated payload position and velocity coordinates relative to the center of the earth, $\underline{r}_k^e$ and $\underline{v}_k^e$, the estimated state in Eq. 5.7-23 is added to the nominal state in Eq. 5.7-24:

$$\underline{r}_k^e = \hat{\underline{r}}_k + \underline{R}_k \qquad [3\times1] \qquad (5.7\text{-}25)$$

$$\underline{v}_k^e = \hat{\underline{v}}_k + \underline{V}_k \qquad [3\times1] \qquad (5.7\text{-}26)$$

The error covariances of $\underline{r}_k^e$ and $\underline{v}_k^e$ are given by matrix $P_k^{(payload)}$ in Eq. 5.7-19.

The estimated systematic radar measurement errors (which are modeled by the radar error states) are computed

using the radar measurement matrix $H_k^{(radar)}$. This $3 \times n_e$ matrix is defined by Eq. 5.6-28 and the discussion in Section 5.6.7. The estimated bias and ramp errors in the radar measurements at time step k are computed as follows:

$$\underline{z}_k^{(bias/ramp)} = H_k^{(radar)} \cdot \hat{\underline{x}}_k^{(radar)} \qquad [3\times1] \qquad (5.7\text{-}27)$$

The error covariance matrix of the estimated bias and ramp errors is computed using the following formula:

$$\text{cov}\left[\underline{z}_k^{(bias/ramp)}\right] = H_k^{(radar)} \cdot P_k^{(radar)} \cdot H_k^{(radar)^T} \qquad [3\times3] \qquad (5.7\text{-}28)$$

These equations are applied to the analysis of WFF radar data from Peru in Section 5.8.

5.8 VERIFICATION OF THE TRAJECTORY ESTIMATION ALGORITHM

To verify the performance of the trajectory estimation algorithm, WFF provided tracking data from Radars No. 8 and No. 41 in Peru. The results of processing these data to estimate a Nike-Orion trajectory and a Terrier-Malemute trajectory are discussed in Sections 5.8.1 and 5.8.2.

5.8.1 Nike-Orion Trajectory

The data used in this verification of the trajectory estimation algorithm were obtained from Radars No. 8 and No. 41, which were simultaneously tracking a Nike-Orion (31.027) trajectory. The results of processing data from Radar No. 8 are discussed first. Then the results obtained using data from Radar No. 41 are presented. Section 5.8.1 concludes with a comparison of the two independent estimates of the trajectory.

Radar No. 8 Data - Figure 5.8-1 depicts the residual tracking data from Radar No. 8 used for this test. These plots show the departures of the actual measurements from the nominal measurements. (The nominal measurements would have been obtained if an ideal radar had tracked the nominal trajectory.) The time is measured starting with the nominal apogee, and the initial conditions for the nominal trajectory are consistent with the position and velocity data provided in the WFF documentation. The parameters for the atmospheric drag force model are as follows: drag coefficient = 1.5; payload mass = 286 kg; and payload cross-sectional area = 0.15 m^2.

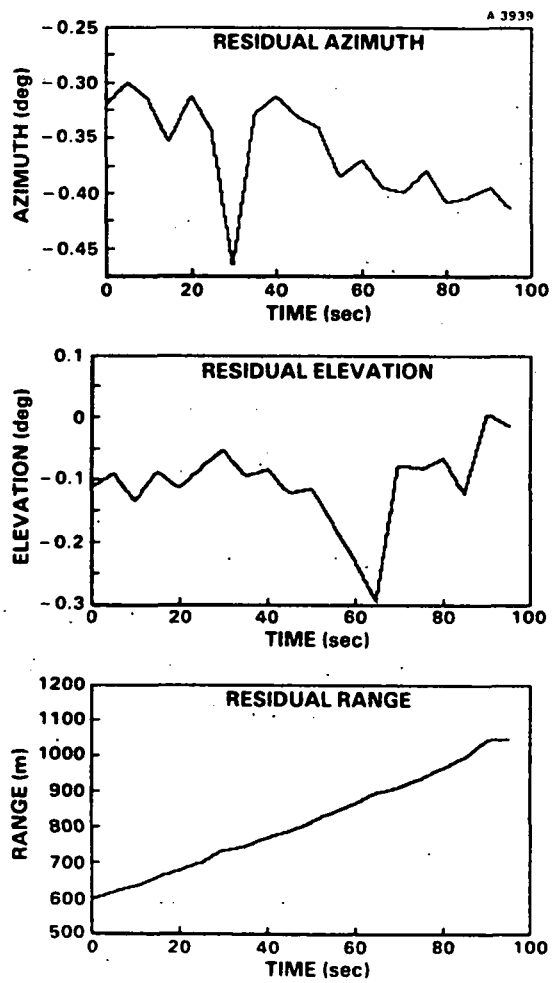

Figure 5.8-1 Residual Tracking Data, Nike-Orion (31.027) Trajectory, Radar No. 8

For these validation tests, the radar data (originally sampled at 1-s intervals) were intentionally undersampled with a sampling time of 5 s between consecutive measurements. This provided a realistic test of the trajectory estimation algorithm while using a reduced number of measurements.

The error model for Radar No. 8 had three state variables: one of the states modeled a bias in the azimuth channel; while the other two states modeled a bias and a ramp in the range channel. The rms a priori uncertainties of these errors were 0.5 deg for the azimuth bias, 1000 m for the range bias, and 6 m/s for the range ramp. In addition to these calibration error uncertainties, each measurement channel was modeled as having random white noise with the following rms values: 0.04 deg in azimuth, 0.09 deg in elevation, and 3.7 m in range. These noise values are the rms of residual tracking data computed from raw measurements by subtracting a least-squares linear trend from each channel of data. For estimating the noise levels, typically 50 to 100 samples of radar data sampled at 1-s intervals were used.

The a priori rms uncertainties of the initial payload position and velocity were 1000 m for each of the three position coordinates and 10 m/s for each of the velocity coordinates. These values were selected to be large but plausible so that the filter/smoother would rely primarily on the tracking data, rather than on the initial conditions, for estimating the trajectory.

The behavior of the Kalman filter can be monitored by observing the innovations data, which are the filter's one-step-ahead predictions of the residual radar data. Figure 5.8-2 depicts the innovations for the Nike-Orion data. In these plots the innovations have been normalized (divided by their theoretical standard deviations) so that outliers can be more

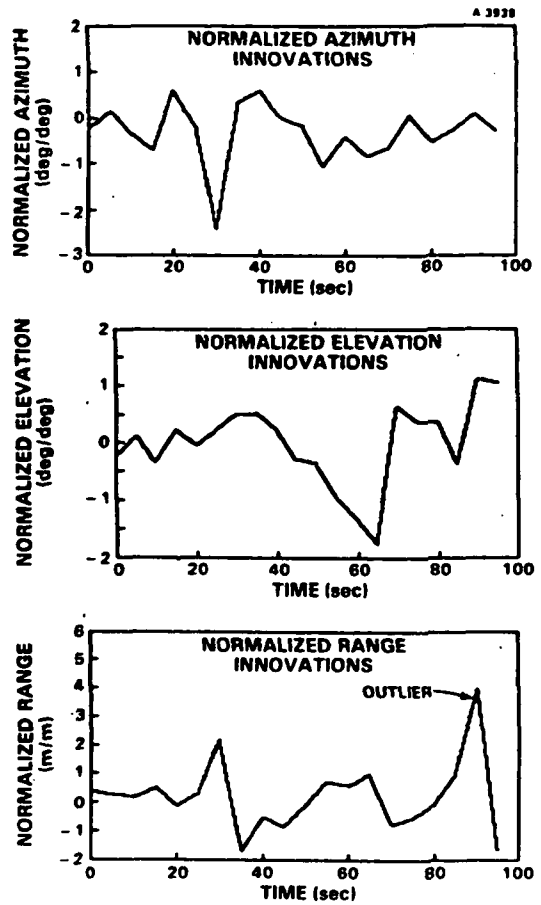

Figure 5.8-2 Kalman Filter Innovations, Nike-Orion (31.027) Trajectory, Radar No. 8

easily identified. For example, in the plot of the range innovations, there is a 4-sigma outlier (a measurement that lies 4 standard deviations away from its expected value of zero). The theoretical standard deviations of the innovations are the square roots of the diagonal elements of the innovations covariance matrix C_k. The covariance C_k is computed automatically by the Kalman filter using Eq. 5.6-4. When the stochastic error model of the Kalman filter is consistent with the tracking data, the innovations are samples of unit-variance zero-mean white noise. Statistically significant departures from this behavior indicate that the data may contain errors that are not modeled by the filter.

Figure 5.8-3 shows the outputs of the smoother module. In the first column of Fig. 5.8-3, the position of the payload relative to the nominal trajectory is plotted as a function of time. The solid lines are the smoothed estimates, and the dotted lines are the 1-sigma uncertainties (one-standard-deviation error bounds) of these estimates. The estimated payload velocity relative to the nominal trajectory is plotted on the right side of Fig. 5.8-3. Both position and velocity are expressed in earth-centered Cartesian inertial coordinates.

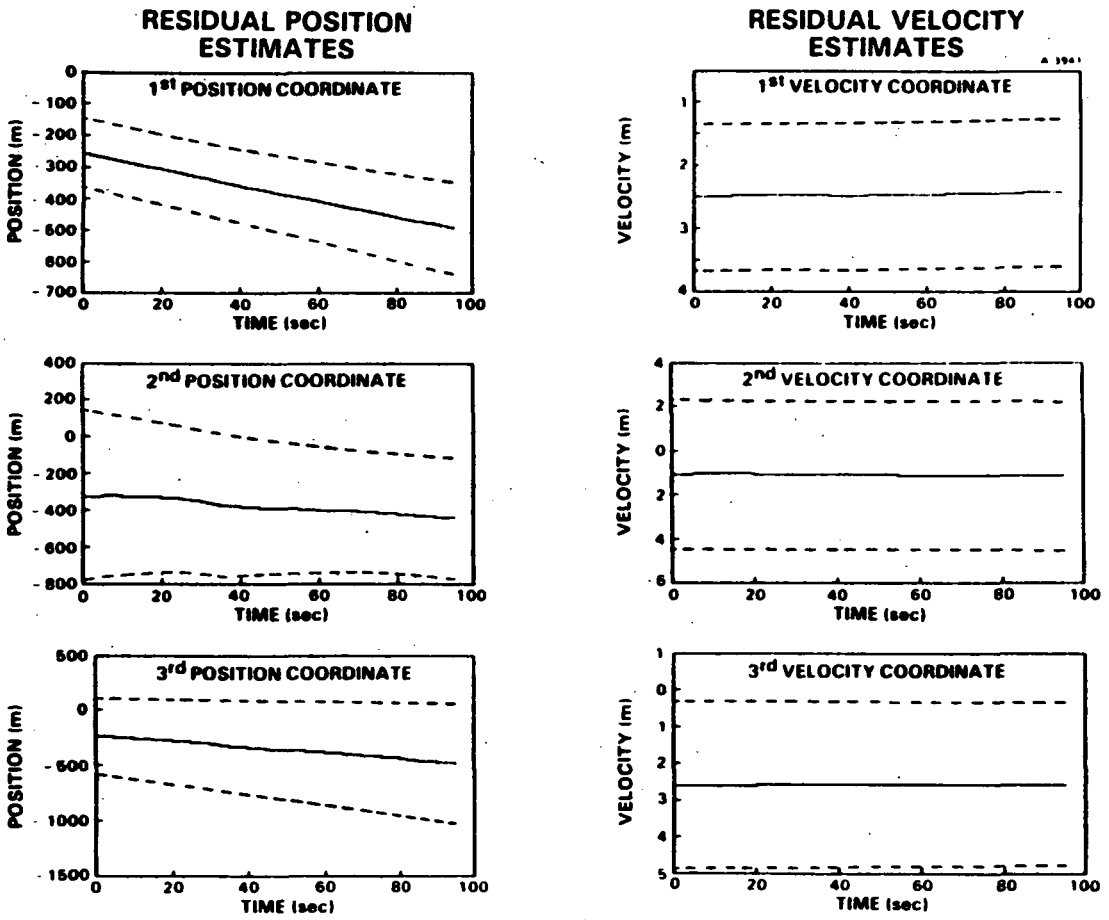

Figure 5.8-3 Smoothed Trajectory Estimates, Nike-Orion (31.027) Trajectory, Radar No. 8

The following comments apply to Fig. 5.8-3:

- The rms position accuracy ranges from 110 m to 540 m, depending on the position coordinate and the time
- The rms velocity accuracy ranges from 1.2 m/s to 3.4 m/s with very little dependence on the time
- The rms accuracy estimates are computed by the algorithm, based on the error covariances generated by the Kalman filter/smoother
- The algorithm was processing the data in mode 3 for automatic outlier detection and handling. Therefore, the outlier in the range innovations was automatically detected and appropriately processed.

The algorithm also estimated the systematic bias and ramp errors in the radar measurements. The smoothed estimates (σ = theoretical standard deviation of the estimation error) are as follows:

Azimuth Bias	=	0.05 deg	(σ = 0.46 deg)
Range Ramp	=	1.8 m/s	(σ = 3.5 m/s)
Range Bias	=	200 m	(σ = 470 m)

These results indicate that the bias and ramp estimates are imprecise (because the standard deviations are larger than the estimates of the biases and the ramp). The reason for this is that data from a single radar provides insufficient information for the precise estimation of radar errors. Better precision can be obtained by simultaneously processing the tracking data from two or more radars tracking a single payload. The Kalman filter/smoother can be extended to handle data from multiple radars, but such an extension was not part of this investigation.

Radar No. 41 Data - The residual data from Radar No. 41, tracking the Nike-Orion 31.027 trajectory are depicted in Fig. 5.8-4. An extremely large outlier occurs at 15 s in the range data. This outlier is caused by a data processing error and would normally be edited manually. However, as a demonstration of the algorithm's automatic outlier processing (mode 3 processing), the outlier is intentionally left in the data. As with Radar No. 8, the data in Fig. 5.8-4 are sampled at 5-s intervals.

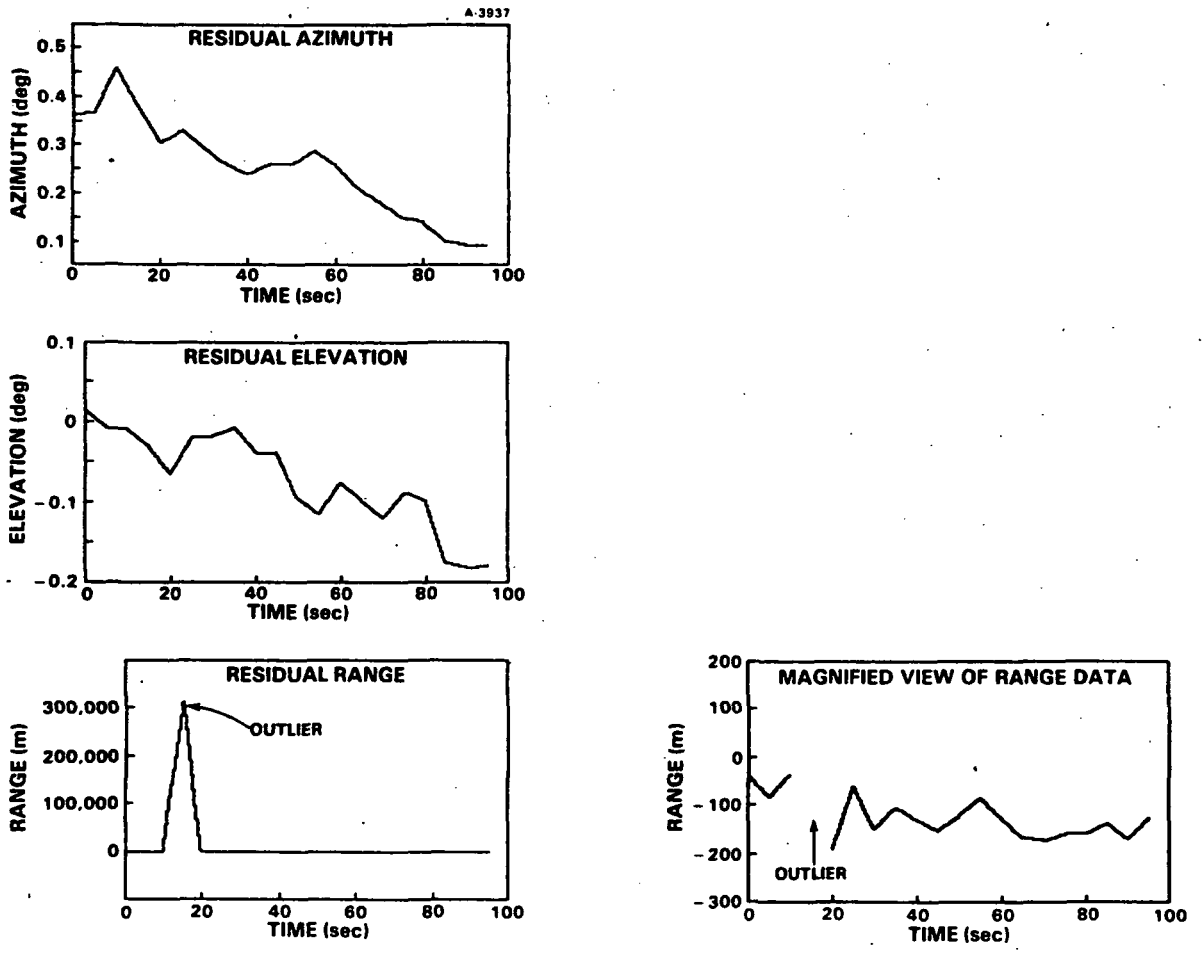

Figure 5.8-4 Residual Tracking Data, Nike-Orion (31.027) Trajectory, Radar No. 41

Three error states were used to model systematic bias errors in the three radar channels. The a priori rms uncertainties of these errors were 0.5 deg for azimuth and elevation and 1000 m for range. In addition the random errors in each channel were modeled as white noise with the following rms values: 0.04 deg in azimuth; 0.03 deg in elevation; and 45 m in range.

The innovations from the Kalman filter are depicted in Fig. 5.8-5. The data are normalized by their theoretical standard deviations. Except for the isolated outlier in the range data, the innovation values lie in the expected range.

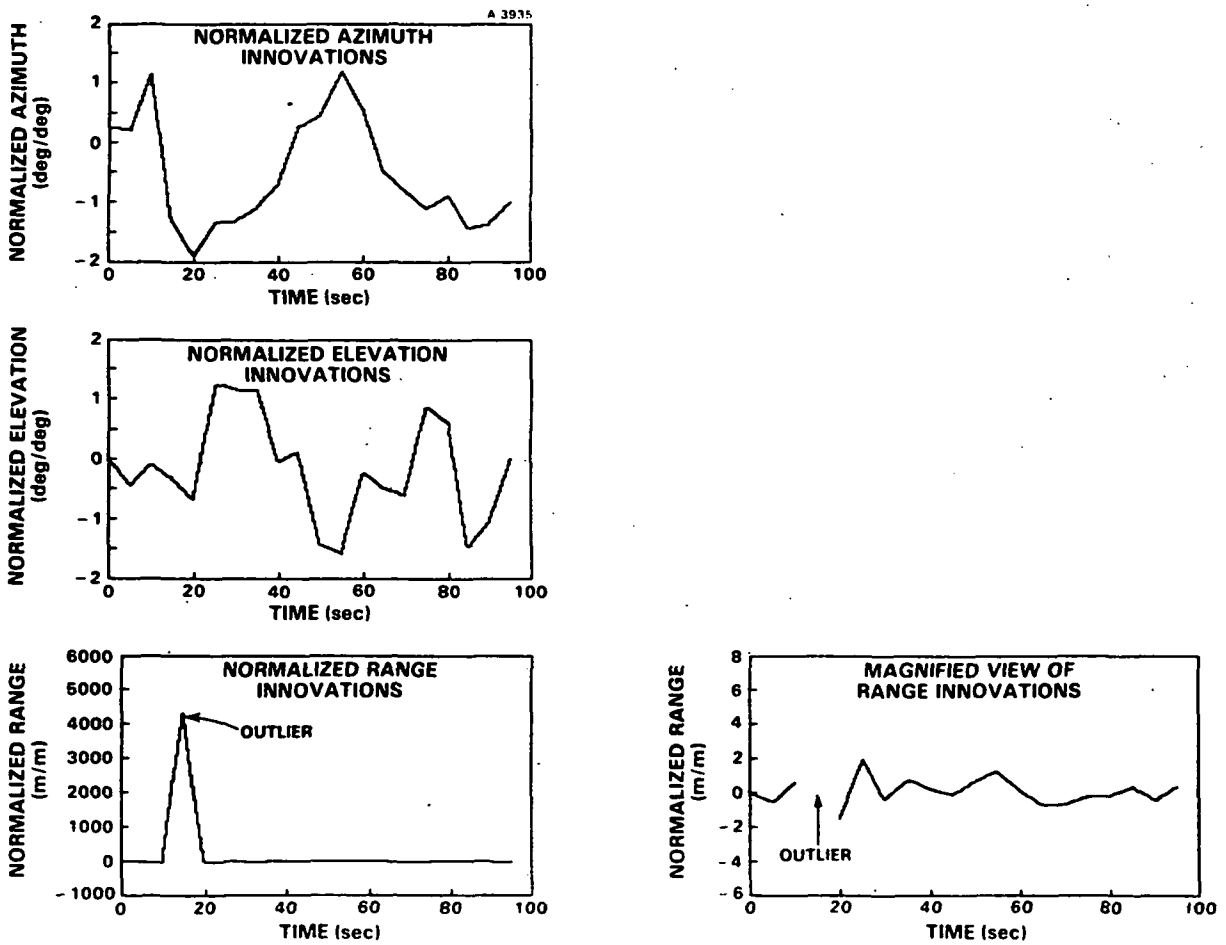

Figure 5.8-5 Kalman Filter Innovations, Nike-Orion (31.027) Trajectory, Radar No. 41

The smoothed position and velocity estimates, and their 1-sigma error bounds, are presented in Fig. 5.8-6. The following comments apply to these results:

- The rms position accuracy is in the range from 370 m to 580 m
- The rms velocity accuracy is in the range from 1.6 m/s to 2.2 m/s
- The algorithm was operating in mode 3 and therefore automatically ignored the extreme outlier in the range data.

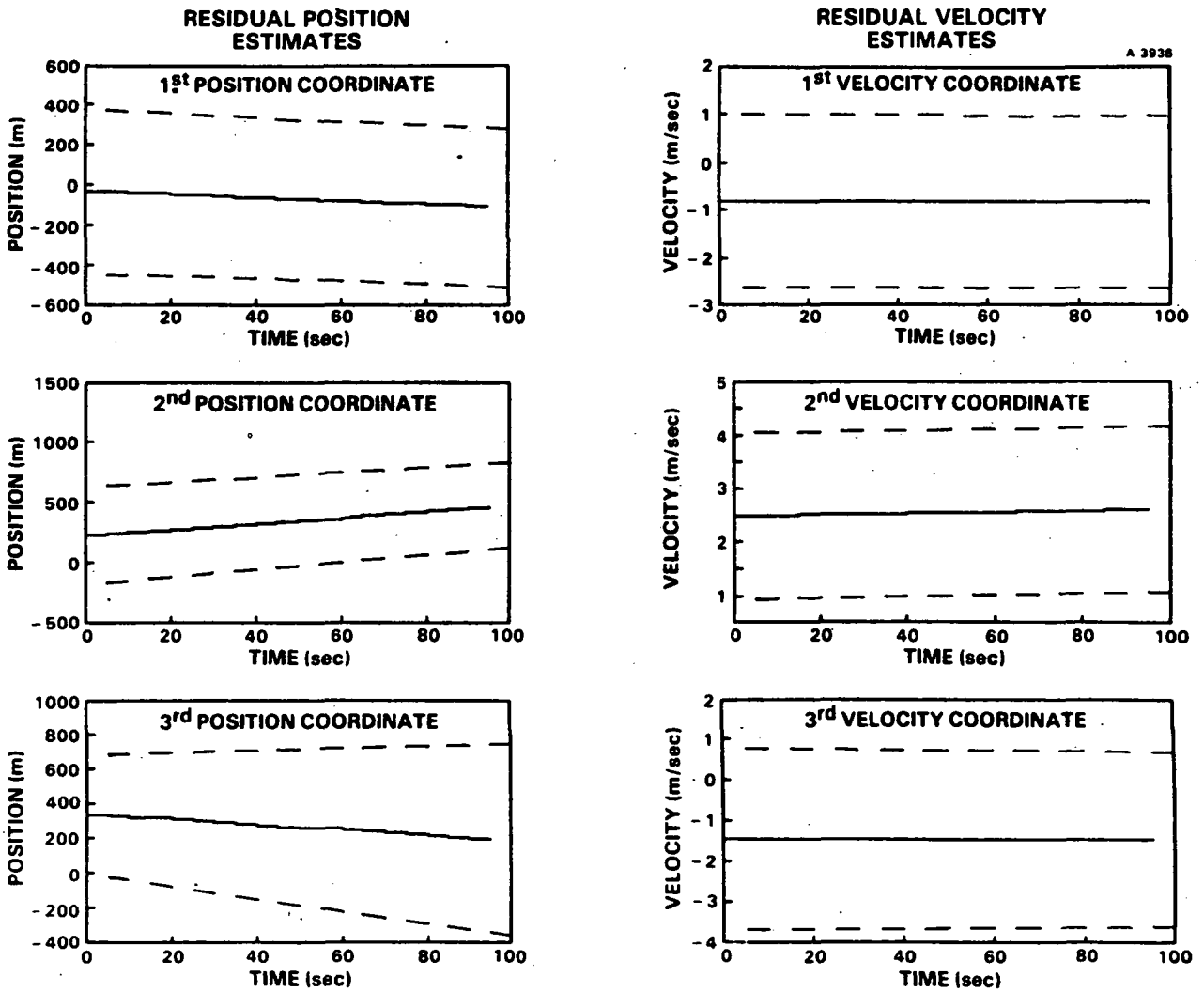

Figure 5.8-6 Smoothed Trajectory Estimates, Nike-Orion (31.027) Trajectory, Radar No. 41

The smoother also provided the following estimates of the radar biases (σ = theoretical standard deviation of the estimation error):

Azimuth Bias	= 0.05 deg	(σ = 0.46 deg)
Elevation Bias	= 0.04 deg	(σ = 0.18 deg)
Range Bias	= 220 m	(σ = 420 m)

The conclusion to be drawn from these results is that the data provided by Radar No. 41 alone are not sufficient for precise estimates of the radar biases.

Comparison of Trajectory Estimates - The data from Radars No. 8 and No. 41 were processed separately to provide two independent estimates of the Nike-Orion trajectory. In this section, the two trajectory estimates are compared with each other. The comparison shows that the two trajectory estimates are statistically consistent with each other.

Table 5.8-1 lists the mean differences between the two trajectory estimates (expressed as individual position and velocity coordinates averaged over the span of the data processed). If the trajectory estimates from the two radars are consistent, then the mean differences between them should be less than, say, two standard deviations of the difference. The theoretical standard deviation (σ) of each mean difference is also listed in Table 5.8-1. In the last column of the table, the normalized mean differences are listed. These normalized quantities express each difference as a multiple of its theoretical standard deviation. For consistency at a 2-σ level, the numbers in the last column of Table 5.8-1 should be less than 2. An examination of the table shows that this criterion

TABLE 5.8-1

STATISTICS OF DIFFERENCES BETWEEN
TWO NIKE-ORION (31.027) TRAJECTORY ESTIMATES

ESTIMATED QUANTITY	MEAN DIFFERENCE	THEORETICAL STD. DEV. (σ)	NORMALIZED MEAN DIFFERENCE
1st Position Coordinate	300 m	410 m	0.7 σ
2nd Position Coordinate	730 m	550 m	1.3 σ
3rd Position Coordinate	620 m	620 m	1.0 σ
1st Velocity Coordinate	1.6 m/s	2.1 m/s	0.8 σ
2nd Velocity Coordinate	3.7 m/s	3.6 m/s	1.0 σ
3rd Velocity Coordinate	1.1 m/s	3.1 m/s	0.4 σ

for consistency is easily met; the largest normalized difference between the two trajectory estimates is only 1.3 σ. The conclusion to be drawn from this comparison is that the trajectories estimated from the two radar data sets are statistically consistent.

5.8.2 Terrier-Malemute Trajectory

The final set of test data used for validating the trajectory estimation algorithm was obtained from Radar No. 8 tracking a Terrier-Malemute (29.019) trajectory. An initial analysis of the raw tracking data disclosed a significant growing oscillation in the range rate having a frequency of 0.5 Hz and a peak magnitude of 300 m/s. The cause of this oscillation is unknown.

Therefore, the range data were smoothed by computing the 2-s running mean of the data to suppress the 0.5-Hz error signal. The radar data were then resampled at 10-s intervals for processing with the trajectory estimation algorithm. In an operational setting this resampling would not necessarily be recommended. But for validating the trajectory estimation algorithm, the resampling is advantageous because it permits a realistic test of the algorithm with a smaller data processing effort.

WFF data on the nominal velocity at time k = 0 (nominal apogee) were not available for this analysis. Therefore, the inital conditions for the nominal trajectory were determined by iteration as explained in the following paragraphs.

The raw radar data (sampled at 1-s intervals) were first transformed to earth-centered Cartesian inertial coordinates. Second, linear trends were fitted to the first 20 s of the data. Finally, the linear trends were used to estimate the payload velocity coordinates at time step k = 0. The nominal trajectory was computed using this estimate of the initial payload velocity together with the nominal payload position determined from WFF documentation. The nominal measurements and residual measurements were computed using the nominal trajectory, and the residual measurements were filtered and smoothed. The a priori state error covariance was the same one used for processing data from Radar No. 41 on the Nike-Orion trajectory, and the radar error model had three bias states (one for each measurement channel) and additive white noise. The initial rms uncertainties of the bias states were 0.5 deg in angle and 1000 m in range. The rms of the white noise for each channel was determined using the method recommended in Section 4.3.2 (based on the level at high frequencies of the estimated power spectrum for each data channel). The

filter and smoother were operated in mode 1 (no outlier detection) so that the measurement noise model had a fixed covariance matrix. It is important to use mode 1 processing (and mode 2 processing if there are gaps caused by missing data) because large innovations may be produced during the first iterations, when the nominal trajectory is inaccurate. In mode 3 processing, these large innovations would be interpreted as outliers and the speed of convergence of the iterative process would be reduced.

The smoothed estimate of the initial payload vector was then used to update the original initial conditions for computing the nominal trajectory. Using the updated initial position and velocity, a new nominal trajectory was computed, and the whole process was repeated using the same a priori state error covariance and measurement noise covariance. The smoothed estimates of the state vector were significantly smaller than in the previous iteration, which indicated that the second nominal trajectory was closer to the true trajectory than the first one.

The resulting smoothed estimate of the payload's initial state was again used to update the initial position and velocity to compute a third nominal trajectory, and the data analysis was repeated a third time. However, this time the covariance matrix of the measurement noise model was adjusted so that the innovations would have the expected 1-2 sigma range of values. The resulting rms measurement noise model was 0.3 deg in azimuth, 0.02 deg in elevation, and 15 m in range. The results of this last iteration are discussed in the following.

The residual tracking data from Radar No. 8 are depicted in Fig. 5.8-7, with a sampling interval of 10 s between measurements. To model the offsets in the data, three radar

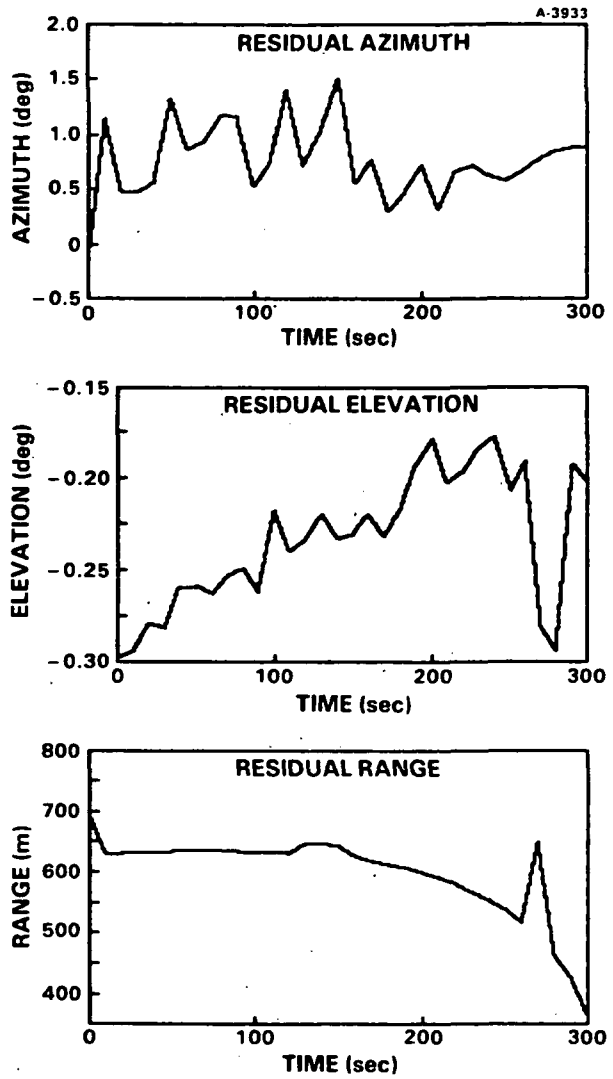

Figure 5.8-7 Residual Tracking Data, Terrier-Malemute (29.019) Trajectory, Radar No. 8

error states were used to model possible biases in each of the three channels. The innovations produced by the Kalman filter operating in mode 1 are shown in Fig. 5.8-8. Three-sigma outliers occur in the elevation and range data near the end of the data set. Since the filter was operating in mode 1, it used a measurement noise model with a fixed covariance matrix. Therefore, the outliers were processed suboptimally in this example. Nevertheless, the smoothed trajectory estimates depicted in Fig. 5.8-9 are free of jumps and are qualitatively

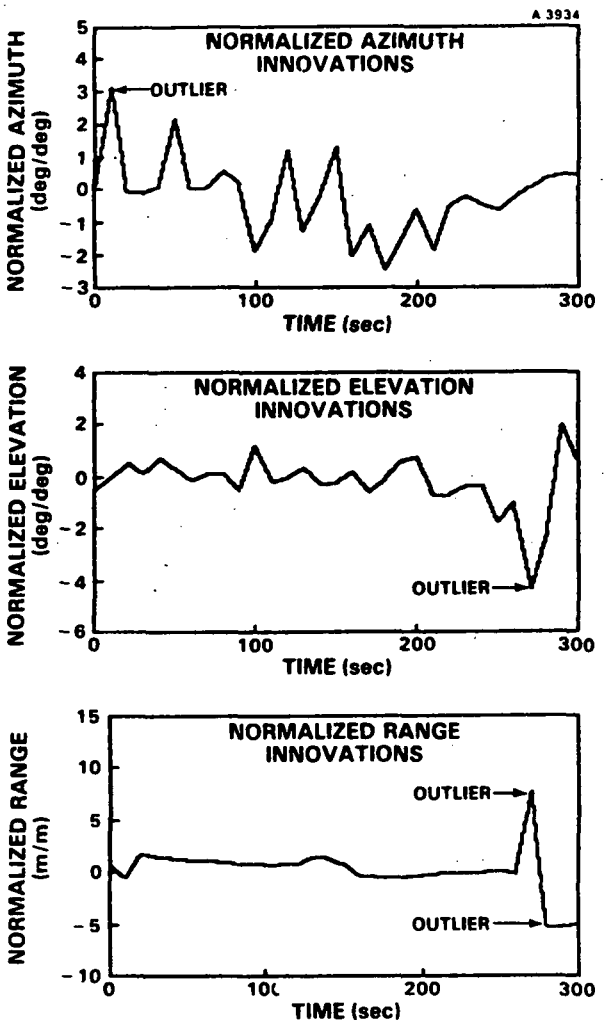

Figure 5.8-8 Kalman Filter Innovations, Terrier-Malemute (29.019) Trajectory, Radar No. 8

similar to the results of mode-3 processing for the Nike-Orion trajectory discussed in Section 5.8.1. Smooth trajectory estimates are produced in this case because the filter/smoother produces a trajectory estimate that is consistent with the physics of a massive payload in free fall.

An examination of Fig. 5.8-9 leads to the following conclusions:

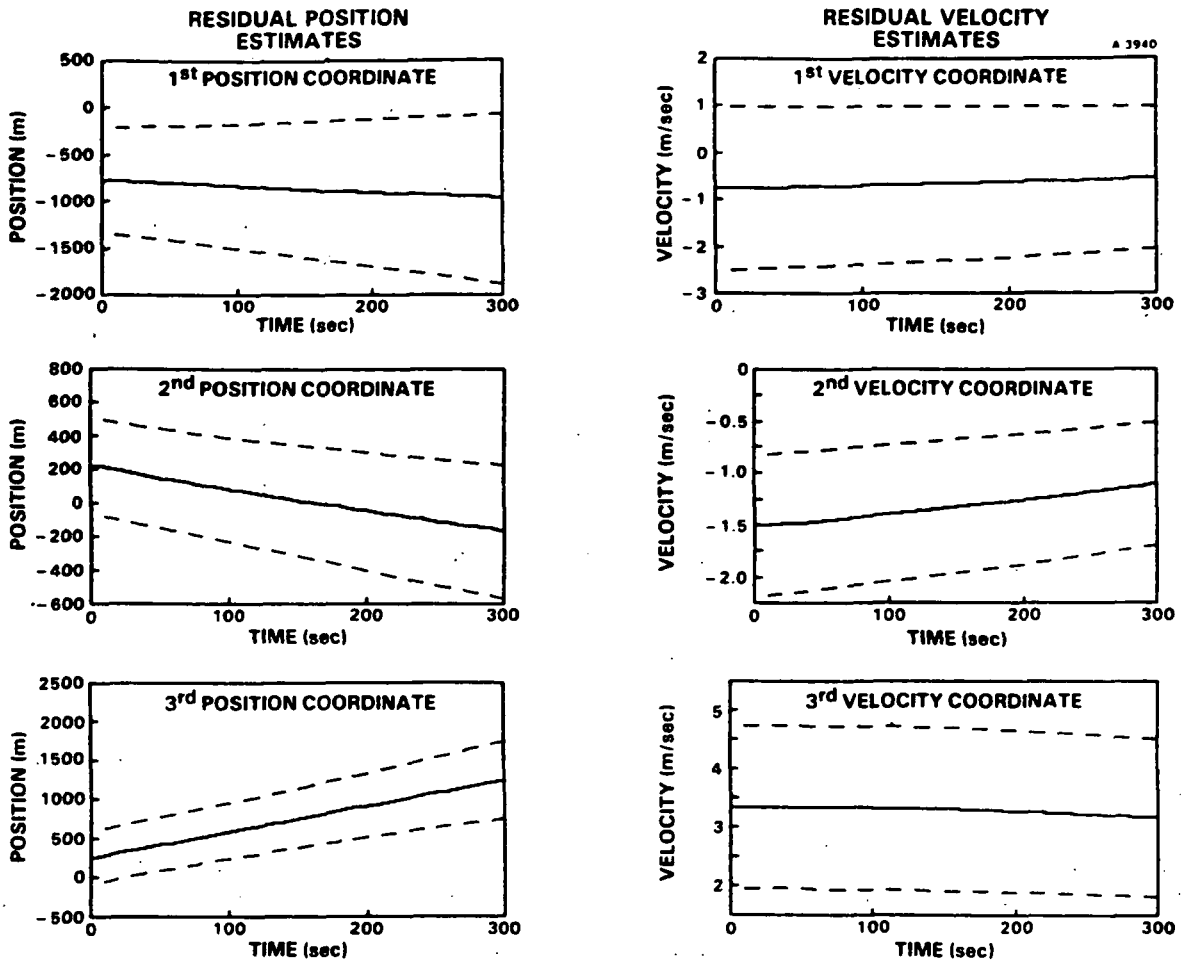

Figure 5.8-9 Smoothed Trajectory Estimates, Terrier-Malemute (29.019) Trajectory, Radar No. 8

- The rms position accuracy ranges from 280 m to 570 m, depending on the position coordinate and the time
- The rms velocity accuracy ranges from 0.6 m/s to 1.7 m/s with very little dependence on the time.

The smoothed estimates of the radar biases are listed in the following (σ = theoretical standard deviation of the estimation error):

Azimuth Bias	=	0.24 deg	(σ = 0.40 deg)
Elevation Bias	=	-0.24 deg	(σ = 0.03 deg)
Range Bias	=	1040 m	(σ = 200 m)

These results indicate that the elevation and range biases have been estimated with reasonable precision because the one-sigma error bounds are much smaller than the magnitudes of the estimated biases.

5.8.3 Conclusions

The validation tests described in Section 5.8 verify that the trajectory estimation algorithm yields consistent results when it is used to estimate the trajectory of a single payload that was tracked simultaneously by two radars. The validation tests also verify that the algorithm automatically handles isolated data outliers and provides estimates of the rms accuracies of the estimated position and velocity coordinates of the payload. The test results include a demonstration of using the algorithm iteratively to estimate the initial velocity of a payload when only nominal position data were available.

5.9 SUMMARY

An algorithm has been developed for processing radar tracking data to estimate payload trajectories above the atmosphere (altitude > 50 km). The algorithm is based on Kalman filtering and smoothing techniques and is optimal with respect to models for gravitation, atmospheric drag, radar measurement errors, and errors in the assumed initial position and velocity of the payload.

The algorithm has three operating modes:

- The first mode employs a radar noise model having a fixed noise covariance matrix. This mode is used for iteratively refining an initial poor estimate of the payload initial position or velocity.

- The second mode employs a variable radar noise model having a very large noise covariance for specified measurements in the tracking data. This mode is used for optimally processing data having gaps caused by missing data, or very noisy data.

- The third mode employs a variable radar noise model which employs a noise covariance that is automatically increased in a continuous fashion when the filter innovations indicate data outliers. This mode is used for optimally processing data having isolated data errors, as opposed to intervals of many missing or noisy data, which are better processed using mode 2.

The algorithm is optimal in the sense that it computes unbiased minimum-variance estimates based on the following error models:

- The initial payload position and velocity coordinates of the payload are random variables with a specified error covariance matrix

- The radar noise is modeled as additive white noise with a specified baseline covariance matrix. In mode 2 or mode 3 processing, the noise model covariance is increased from the baseline values as appropriate

- The systematic radar errors are modeled as biases and ramps. The initial uncertainty about the magnitudes of these systematic errors is represented by an error covariance matrix.

In addition to the error models, the algorithm also uses an accurate model of the dynamics of the payload as it falls in the earth's gravitational field subject to nominal atmospheric drag forces. The Kalman filter and smoother algorithms are linear time-varying data processors that process residual radar measurements (residual data = raw data - nominal data, where the nominal data correspond to an ideal radar tracking the nominal payload trajectory based on nominal initial conditions, the normal gravitational field of an ellipsoidal earth model, and nominal atmospheric drag forces).

Because the algorithm is optimized with respect to the physics of the falling payload and the statistics of the important error sources, the estimated trajectories are smooth even when the tracking data are noisy. Moreover, the algorithm automatically computes the error covariance of the estimated payload state and radar error states at each time step.

Using radar data provided by WFF from Radars No. 8 and No. 41 in Peru, the performance of the algorithm has been successfully demonstrated. In particular, the algorithm provided two mutually consistent estimates of a Nike-Orion trajectory that had been simultaneously tracked by the two radars.

6. SUMMARY, CONCLUSIONS, AND RECOMMENDATIONS FOR FUTURE STUDY

6.1 SUMMARY

The principal accomplishments of this study are summarized in the following:

- The accuracy of the current WFF data smoothing technique was analyzed for a variety of radars and payloads, using tracking data provided by WFF for this study
- Alternative data noise reduction techniques were assessed and recommendations were made for improving radar data processing at WFF
- A data-adaptive algorithm, based on Kalman filtering and smoothing techniques, was developed for estimating payload trajectories above the atmosphere from noisy time-varying radar data
- The new trajectory estimation algorithm was tested and verified using radar tracking data provided by WFF.

6.2 CONCLUSIONS

The principal conclusions of this study are summarized in the following. More detailed discussions are provided in Sections 2.4, 3.7, 4.4, and 5.9.

Rms noise levels in smoothed radar data vary with payload.

- The estimated rms noise levels of positional data products (for Zuni, Super Loki Optical, and Super Loki Sphere trajectories tracked by radars Nos. 3 and 5) produced by the current WFF smoothing filters have the following range of values for the data sets analyzed in this study:

  Latitude and Longitude: 3 μdeg to 73 μdeg
  Height: 1.3 ft to 6.9 ft

Current WFF smoothing techniques can be improved by using the following recommended techniques:

- Subtracting orthogonal polynomials from the radar data before smoothing, to reduce possible distortion of the nominal trajectory by the smoothing filter

- Estimating the high-frequency rms noise levels in smoothed tracking data using an autoregressive modeling algorithm, to monitor data quality and provide quantitative error estimates with the existing smoothing filters

- Replacing the current midpoint smoothing filters with an alternative Kalman filter/smoother, to process radar data optimally when the data contain significant time-varying noise, measurement gaps caused by missing data, or large uncertainties on radar calibration errors.

The Kalman filter/smoother algorithm yielded reasonable trajectory estimates and error analyses when it was tested using radar tracking data provided by WFF.

- The algorithm is data-adaptive, automatically handles data outliers, and can optimally smooth data sets having measurement gaps caused by missing data.

6.3 RECOMMENDATIONS FOR FUTURE STUDY

Based on the results of this study, the following recommendations are made for future study:

The Kalman filter/smoother algorithm can be extended to increase its flexibility:

- To process data from two or more radars simultaneously
- To model data errors that are more complex than data gaps, additive white noise, linear trends, and isolated outliers
- To estimate automatically the initial payload position or velocity from the radar tracking data alone
- To calibrate radars based on future Geosat satellite tracking techniques.

A smart preprocessor for radar tracking data can be developed:

- To select and setup appropriate error models automatically for the Kalman filter/smoother algorithm
- The preprocessor could employ artificial intelligence techniques together with automated stochastic state-space modeling algorithms.

APPENDIX A
ORTHOGONAL POLYNOMIALS

The purpose of this appendix is to describe the recommended way of using least squares to fit orthogonal polynomials to time-series data. In this study, the orthogonal polynomials are used to model nominal payload trajectory signals in radar tracking data.

The polynomials used in this study are optimal in the following sense (Ref. 12):

Given the N data:

$$y_k = k^{th} \text{ datum}, \quad k = 0, 1, \ldots, N-1 \tag{A-1}$$

and given the polynomial $p^m(x)$ of degree m in the variable x:

$$p^m(x) = c_m x^m + c_{m-1} x^{m-1} + \ldots + c_o \tag{A-2}$$

Find the coefficients $c_o, c_1, \ldots, c_m$ that minimize the sum-squared error e^2:

$$e^2 = \sum_{k=o}^{N-1} [y_k - p^m(k)]^2 \tag{A-3}$$

This is a conventional least-squares problem using ordinary polynomials. The equations for computing the optimal coefficients become ill conditioned as N and m increase. This leads to serious numerical difficulties in practice. To reduce these numerical problems, the problem is reformulated using

polynomials $f^n(x)$ of degree n that are orthogonal on the discrete interval k = 0, 1, ..., N-1 and normalized so that their values are in the range from -1 to +1. A linear combination of these polynomials is used in place of the formula for $p^n(x)$ given in Eq. A-2. They are called Chebyshev polynomials on a discrete domain (Ref. 12) and are computed recursively as follows.

$$f^o(x) = 1 \qquad \text{(A-4)}$$

$$f^1(x) = 1 - (2x)/N \qquad \text{(A-5)}$$

and for n = 1, 2, ..., N-1

$$f^{n+1}(x) = [(2n+1)(N-2x)f^n(x) - n(N+n+1)f^{n-1}(x)](n+1)^{-1}(N-n)^{-1} \qquad \text{(A-6)}$$

The optimal polynomial $p^m(x)$ of degree m is expressed in terms of the orthogonal polynomials as follows:

$$p^m(x) = \sum_{n=o}^{m} a_n f^n(x) \qquad \text{(A-7)}$$

In Eq. A-7, the coefficients a_n are computed as follows:

$$a_n = \frac{(y,f^n)}{(f^n,f^n)}, \qquad n = 0, 1, \ldots, m \qquad \text{(A-8)}$$

where the numerator is the inner product

$$(y,f^n) = \sum_{k=o}^{N-1} y_k f^n(k) \qquad \text{(A-9)}$$

and the denominator of Eq. A-8 is given by the following expression involving factorials

$$(f^n, f^n) = \frac{(N+n+1)!(N-n)!}{(2n+1)(N!)^2} \qquad \text{(A-10)}$$

APPENDIX B
AUTOGRESSIVE MODELING

This appendix describes an effective method for using autoregressive (AR) modeling to estimate the power spectra of time series. The AR models are used in this study to estimate the power spectra of noise-like errors in radar tracking data.

An autoregressive model of order p for time series y_k, k = 0, 1, ..., N-1, is the difference equation

$$y_k = \sum_{j=1}^{p} c_j \cdot y_{k-j} + w_k, \qquad k = p, p+1, \ldots, N-1 \qquad \text{(B-1)}$$

Equation B-1 is driven by the residual noise w_k. AR models are developed from time series by choosing the coefficients c_j, j = 1 to p, so that the sample mean square (VAR) of the residuals is minimized:

$$\text{VAR} = \frac{1}{N-p} \sum_{k=p}^{N-1} w_k^2 \qquad \text{(B-2)}$$

In Eq. B-2, the limits of the summation are chosen to avoid running off the ends of the time series. Choosing the AR coefficients to minimize VAR is known as the covariance method of AR modeling.

If the AR model is appropriate for the process generating the data y_k, then the residuals w_k are a sample of approximately white noise. It follows that the power spectral density (power spectrum) of the discrete-time process generating the data y_k can be estimated as follows:

$$S_o(F) = \frac{VAR}{\left| 1 - \sum_{k=1}^{P} c_k \cdot e^{i2\pi Fk} \right|^2} \qquad \text{(B-3)}$$

where F [cycles/sampling interval] is the normalized frequency variable. F = 0.5 is the folding frequency. The variance of the random process having the power spectrum $S_o(F)$ is given by the area under the spectrum (including negative frequencies):

$$\text{variance} = \int_{1/2}^{1/2} S_o(F) \cdot dF \qquad \text{(B-4)}$$

A natural estimate for the power spectrum of the underlying continuous-time process (of which the data y_k are uniformly-spaced sample values, i.e., $y_k = y(k \cdot \delta t)$ with δt = sampling interval) is

$$S(f) = \frac{S_o(f/f_s)}{f_s} \quad \text{for } |f| \leq \frac{f_s}{2} \qquad \text{(B-5)}$$

where

$f_s = 1/(\delta t)$ = sampling frequency [Hz]

f = spectrum frequency [Hz]

$S(f)$ = power spectrum [variance/Hz]

For each time series y_k, k = 0, 1, ..., N-1, the best choise of the order p is estimated by computing the Akaike information criterion (Refs. 2-4) for each model in a family of AR models.

Each model in the family corresponds to a different model order $p = 0, 1, \ldots, N/20$. For each of these models the AIC is computed:

$$AIC = N \cdot \log_e(VAR) + 2 \cdot p \qquad \text{(B-6)}$$

That model for which the AIC is smallest is chosen as the best AR model in the family for the purpose of modeling the underlying process that generated the observed data y_k. An algorithm (ACOVAR) for efficiently computing the family of AR models and selecting the model order using the AIC is specified in Ref. 13.

APPENDIX C
STOCHASTIC STATE-SPACE MODELING

C.1 INTRODUCTION

This appendix describes a canonical-variates (CV) technique for the stochastic modeling of vector time series. (This is a modification and extension of ideas originally presented in Ref. 14). The CV method differs significantly from the one-step linear prediction techniques that are now commonly used to develop autoregressive (AR all-pole) and autoregressive-moving-average (ARMA pole-zero) models from empirical data. The technique has been used successfully with a variety of geophysical data sets for spectrum estimation, reduced-order modeling, and optimal filtering. The CV algorithm is recursive in the data. Therefore the data may consist of several short time series instead of one contiguous sequence.

The modeling technique was motivated by Akaike's original work (summarized and extended in Ref. 3), which describes an ARMA modeling technique based on a canonical-variates analysis (Ref. 15) in the time domain. W.E. Larimore modified and extended Akaike's approach to state-space modeling (Ref. 16). In this appendix the CV technique is interpreted as a form of multi-step linear prediction. This leads to a simplified derivation of the algorithm and shows that the technique does not reduce to conventional one-step rediction-error modeling.

An important advantage of the CV approach is that a family of optimal state-space models is generated by solving a finite number of linear equations for the state-space model parameters. This fact distinguishes the CV technique from

other approaches, such as Gaussian maximum likelihood and conventional one-step prediction, which all require that nonlinear equations be solved for state-space modeling. These nonlinear equations lead to iterative calculations that may or may not converge, depending on the particular data being analyzed. In contrast, the only iteration in the CV approach occurs while computing Singular Value Decompositions (SVDs). The SVD is well understood and can be implemented with dependable algorithms (Ref. 17).

C.2 SUMMARY OF RESULTS

The CV approach to state-space modeling consists of three steps. The first step is to solve a family of least-squares multi-step linear prediction problems with different rank constraints on the predictors. This is a canonical-variates analysis of the joint behavior of the local past and local future of the time series, in which several future vectors of the time series are being simultaneously predicted using several past vectors. The entire family of predictors is computed at one time by using the SVD. The output of this analysis is the definition of the canonical states in terms of the observed data. The state vector is expressed as a linear combination of the local past, and the individual states are canonical variates.

The second step is to solve a family of linear least-squares problems that use the state vectors from Step One as given quantitites. This yields the parameter matrices of a family of state-space models for the time series. These models differ from each other in their complexities, ranging from the simplest white-noise model containing no states, to a model of maximum complexity containing the largest number of states

permitted by the CV analysis. For the number of states it contains, each of these models is optimal in a least-squares sense.

The third step is to select one of the state-space models from the family generated during Step Two. For the purpose of modeling the underlying process that generated the empirical data, the Akaike information criterion (Refs. 2-4) is used to select that model which is best supported by the data. Alternatively, a model with a reduced number of states is selected for reduced-order modeling. A formula is given in Section C.3 for computing the amount of mutual information between the future and past that is lost by reducing the number of states when modeling Gaussian processes.

C.3 ANALYSIS

C.3.1 Step One: Canonical Variates

A time series of empirical data is denoted by the sequence of m-vectors $\underline{y}_k$ for k = 1 to n'. An ergodic state-space model (in innovations form) for the data process is represented by the following equations:

$$\underline{x}_{k+1} = \Phi\underline{x}_k + G\underline{\nu}_k \qquad \text{(C-1)}$$

$$\underline{y}_k = H\underline{x}_k + \underline{\nu}_k \qquad \text{(C-2)}$$

$$R = E[\underline{\nu}_k\underline{\nu}_k^T] \qquad \text{(C-3)}$$

The n×1 state vector is $\underline{x}_k$, and $\underline{y}_k$ is the observed m×1 output vector at time step k. The n×n state-transition matrix is Φ, while G is the n×m noise-gain matrix, and H is the m×n output

matrix. The m×m covariance matrix of the zero-mean white noise (steady-state) innovations process $\underline{\nu}_k$ is R. The noise vector $\underline{\nu}_j$ is uncorrelated with $\underline{\nu}_k$ for all $j \neq k$; $\underline{\nu}_j$ is also uncorrelated with $\underline{x}_k$ for all $j \geq k$.

The primary objective of state-space modeling is to use observations of $\underline{y}_k$ for k = 1, 2, ..., n' to estimate values for the model order, n, and the parameter matrices Φ, G, H, and R. The CV technique for doing this is based on a local past and local future for $\underline{y}_k$. The local past $\underline{z}_k^-(p)$, of length p, is the pm×1 vector containing the p most recent predecessors of $\underline{y}_k$:

$$\underline{z}_k^-(p) = \begin{bmatrix} \underline{y}_{k-1} \\ \underline{y}_{k-2} \\ \vdots \\ \underline{y}_{k-p} \end{bmatrix} \qquad k = p+1, \ldots, n'+1 \qquad \text{(C-4)}$$

The local future $\underline{z}_k^+(f)$, of length f, is the fm×1 vector containing $\underline{y}_k$ and the next f-1 data vectors:

$$\underline{z}_k^+(f) = \begin{bmatrix} \underline{y}_k \\ \underline{y}_{k+1} \\ \vdots \\ \underline{y}_{k+f-1} \end{bmatrix} \qquad k = 1, \ldots, n'-f+1 \qquad \text{(C-5)}$$

In many applications the lengths of the local future and past are equal (f=p).

The state vector $\underline{x}_k$ contains n numbers: the states at time k. These states contain all the information available from the entire past $\underline{z}_k^-(\infty)$ about the entire future $\underline{z}_k^+(\infty)$. In

other words, $\underline{x}_k$ is a sufficient statistic of $\underline{z}_k^-(\infty)$ for optimally predicting $\underline{z}_k^+(\infty)$.

The empirical data are the finite sequence $\underline{y}_k$ for k = 1 to n'. To estimate the corresponding sequence of state vectors, $\underline{x}_k$ is expressed as a linear transformation L(n) of the local past $\underline{z}_k^-(p)$:

$$\underline{x}_k = L(n)\ \underline{z}_k^-(p), \qquad k = p+1, \ldots, n' \tag{C-6}$$

In Eq. C-6, the n×pm matrix L(n) is to be defined so that three conditions are satisified:

- Given n, the vector $\underline{x}_k$ is optimal for predicting the local future $\underline{z}_k^+(f)$. That is, for some fm×n matrix M(n), the following estimates of the local future are optimal in a weighted least-squares sense:

$$\hat{\underline{z}}_k^+(f) = M(n)\ \underline{x}_k, \quad k = p+1, \ldots, n'-f+1 \tag{C-7}$$

- The state vector $\underline{x}_k$ is standardized (for convenience) so that the n states are uncorrelated with each other, and each state has zero mean and unit sample variance. This means that the sample covariance matrix of $\underline{x}_k$ (defined in Eq. C-8 and denoted $(\underline{x},\underline{x})$) is the n×n identity matrix as indicated in Eq. C-9:

$$(\underline{x},\underline{x}) \triangleq \sum_{k=p+1}^{n'-f+1} \underline{x}_k\ \underline{x}_k^T \cdot [n'-f-p+1]^{-1} \tag{C-8}$$

$$(\underline{x},\underline{x}) = I_n \tag{C-9}$$

- The states in $\underline{x}_k$ are arranged in the order of their importance for predicting the future (as measured by a weighted least-squares error criterion). The first state is most important, the second state is second most important, etc.

The optimal L(n) and M(n) matrices are determined by solving the following linear prediction problem. Fix the positive integers n, f, and p, with $n \leq \min[fm,pm]$. Find the $n \times pm$ matrix L(n) and the $fm \times n$ matrix M(n), such that the following estimate of the local future

$$\hat{\underline{z}}_k^+(p) = M(n)\, L(n)\, \underline{z}_k^-(p), \qquad k = p+1 \text{ to } n'-f+1 \tag{C-10}$$

has the error vector

$$\underline{e}_k(n) = \hat{\underline{z}}_k^+(f) - \underline{z}_k^+(f) \tag{C-11}$$

with the smallest weighted sum-square error J(n):

$$J(n) \triangleq \sum_{k=p+1}^{n'-f+1} \underline{e}_k^T(n)\, W(f)^{-1}\, \underline{e}_k(n) \tag{C-12}$$

The $fm \times fm$ weighting matrix W(f) is the sample covariance matrix of the local future:

$$W(f) \triangleq \sum_{k=p+1}^{n'-f+1} \underline{z}_k^+(f) \cdot [\underline{z}_k^+(f)]^T \cdot [n'-p-f+1]^{-1} \tag{C-13}$$

This choice of the weighting matrix leads to a definition of the state vector that maximizes the mutual information between the local future and the local past. Moreover, W(f) makes the

canonical analysis independent of the units in which the observed data $\underline{y}_k$ are expressed. (In Eq. C-13), if W(f) is singular, then f is larger than it needs to be, and its value should be reduced.)

Fragmented data sets, consisting of several time series, are handled in Eqs. C-12 and C-13 by summing over all contiguous data segments, taking care to avoid running off the ends of the segments, and then dividing by the total number of terms in each sum.

The optimal choices for L(n) and M(n) are found by defining the standardized future vectors (with their dependencies on p and f suppressed):

$$\underline{s}_k^+ \triangleq (\underline{z}^+,\underline{z}^+)^{-T/2} \cdot \underline{z}_k^+, \quad k = p+1, \ldots, n'-f+1 \tag{C-14}$$

In Eq. C-14, the notation $(\underline{z}^+,\underline{z}^+)^{-T/2}$ represents the transposed inverse of any matrix square root of the sample covariance of the local future. The covariance matrix and its square-root matrix are defined by the following equations:

$$(\underline{z}^+,\underline{z}^+) \triangleq \sum_{k=p+1}^{n'-f+1} \underline{z}_k^+ [\underline{z}_k^+]^T \cdot [n'-p-f+1]^{-1} \tag{C-15}$$

$$(\underline{z}^+,\underline{z}^+) = (z^+,z^+)^{T/2} \cdot (\underline{z}^+,\underline{z}^+)^{1/2} \tag{C-16}$$

The standardized past vectors are defined the same way:

$$\underline{s}_k^- \triangleq (\underline{z}^-,\underline{z}^-)^{-T/2} \cdot \underline{z}_k^-, \quad k = p+1, \ldots, n'-f+1 \tag{C-17}$$

(If the inverse matrix in Eq. C-17 does not exist, then p is larger than it needs to be, and its value should be reduced.) This standardization forces the sample covariance matrices of $\underline{s}_k^+$ and $\underline{s}_k^-$ to be identity matrices.

Consider the predictor P of $\underline{s}_k^+$ given $\underline{s}_k^-$:

$$\hat{\underline{s}}_k^+ = P\underline{s}_k^-, \quad k = p+1, \ldots, n'-f+1 \tag{C-18}$$

Choosing the matrix P in Eq. C-18 to minimize the sum-square error J'(n)

$$J'(n) = \sum_{k=p+1}^{n'-f+1} (\hat{\underline{s}}_k^+ - \underline{s}_k^+)^T (\hat{\underline{s}}_k^+ - \underline{s}_k^+) \tag{C-19}$$

is equivalent to minimizing the sum-square weighted error J(n) in Eq. C-12, provided that the matrix P is constrained to have a rank of n. From least-squares theory, it is known that the optimal P (with no rank constraint) is

$$P = (\underline{s}^+, \underline{s}^-) = (\underline{z}^+, \underline{z}^+)^{-T/2} \, (\underline{z}^+, \underline{z}^-) \, (\underline{z}^-, \underline{z}^-)^{-1/2} \tag{C-20}$$

To find the optimal P for the present problem (for which the rank of P is n), factor the P in Eq. C-20 by using the singular value decomposition:

$$P = U \, S \, V^T \tag{C-21}$$

In Eq. C-21, U is an fm×fm orthogonal matrix, V is a pm×pm orthogonal matrix, and S is an fm×pm matrix. The diagonal elements S(k,k), for k = 1 to min[fm,pm], contain the singular values arranged in order, from largest to smallest. The optimal rank-n predictor is denoted P(n) and is given by the formula

$$P(n) = U(n) \, S(n) \, V^T(n) \tag{C-22}$$

In Eq. C-22, S(n) is the upper-left n×n submatrix of S. The pm×n submatrix V(n) contains the first n columns of V, and the fm×n submatrix U(n) contains the first n columns of U.

By replacing the P in Eq. C-18 with the P(n) defined in Eq. C-22 and then solving Eq. C-18 for the predicted local future, the optimal rank-n predictor of $\underline{z}_k^+$ is found to satisfy the following equation:

$$\hat{\underline{z}}_k^+ = (\underline{z}^+,\underline{z}^+)^{T/2}\ U(n)\ S(n)\ V^T(n)\ (\underline{z}^-,\underline{z}^-)^{-T/2}\ \underline{z}_k^- \qquad \text{(C-23)}$$

By comparing Eq. C-23 with Eq. C-10, the optimal prediction matrices M(n) and L(n) are identified:

$$L(n) = V^T(n)\ (\underline{z}^-,\underline{z}^-)^{-T/2} \qquad \text{(C-24)}$$

$$M(n) = (\underline{z}^+,\underline{z}^+)^{T/2}\ U(n)\ S(n) \qquad \text{(C-25)}$$

This is the only grouping of terms which guarantees that the state vector, defined as

$$\underline{x}_k \triangleq L(n)\ \underline{z}_k^- \qquad \text{(C-26)}$$

has the following two properties: (1) its sample covariance matrix $(\underline{x},\underline{x})$ (as defined by Eq. C-8) is the n×n identity matrix; and (2) it contains the states arranged with the most important state first, the second most important state second, etc.

In the parlance of canonical-variates theory, the states defined by Eq. C-26 are canonical variates, and the singular values S(k,k), for k = 1 to n, are the first n canonical correlations between the past and the future. For

Gaussian processes, the mutual information rate I(n) between the future and past conveyed by $\underline{x}_k$ is given by the formula (Ref. 18)

$$I(n) = -\sum_{k=1}^{n} \log_2[1-S^2(k,k)]/2 \quad \text{[bit/sample]} \qquad \text{(C-27)}$$

C.3.2 Step Two: State-Space Parameters

The output of Step One is the definition of the canonical state vector $\underline{x}_k$, for times k = p+1 to n'-f+1, and for state orders n = 1 to min[fm,pm]. The object of Step Two is to use these state vectors and the observed data ($\underline{y}_k$ for k = 1 to n') to estimate the parameters of a family of ergodic state-space models for the underlying stochastic process that generated the $\underline{y}_k$ vectors. Each model corresponds to a different choice for n. The state-space parameter matrices Φ, G, H, and R are estimated by using least squares, as outlined in the following.

For each state order, n = 1 to min(fm,pm), the m×n measurement matrix H in Eq. C-2 is selected to minimize J"(n), the sum of squares of the innovations $\underline{\nu}_k$ (which are defined by their occurrence in Eqs. C-1 to C-3):

$$J"(n) = \sum_{k=p+1}^{n'-f+1} \underline{\nu}_k^T \underline{\nu}_k \qquad \text{(C-28)}$$

The H that minimizes J"(n) is given by least-squares theory as follows:

$$H = (\underline{y},\underline{x})(\underline{x},\underline{x})^{-1} = (\underline{y},\underline{x}) \qquad \text{(C-29)}$$

$$(\underline{y},\underline{x}) \triangleq \sum_{k=p+1}^{n'-f+1} \underline{y}_k \, \underline{x}_k^T \cdot [n'-f-p+1]^{-1} \qquad \text{(C-30)}$$

$$(\underline{x},\underline{x}) \triangleq \sum_{k=p+1}^{n'-f+1} \underline{x}_k \, \underline{x}_k^T \cdot [n'-f-p+1]^{-1} \qquad \text{(C-31)}$$

In Eq. C-29, the simplified right side is valid because the sample covariance matrix $(\underline{x},\underline{x})$ of the canonical state vector is an n×n identity matrix. The sample covariance matrix $(\underline{\nu},\underline{\nu})$ of the innovation is then given by the following equation:

$$(\underline{\nu},\underline{\nu}) = (\underline{y},\underline{y}) - HH^T \qquad \text{(C-32)}$$

It is known from the theory of least squares that Eq. C-29, together with Eq. C-2, imply that $\underline{\nu}_k$ is uncorrelated with $\underline{x}_k$ for k = p+1 to n'-f+1. Therefore, the optimal linear estimate of $\underline{x}_{k+1}$, given $\underline{x}_k$ and $\underline{\nu}_k$, is given by Eq. C-1 if, and only if, the Φ and G matrices are selected as follows:

$$\Phi = (\underline{x}_1,\underline{x})(\underline{x},\underline{x})^{-1} = (\underline{x}_1,\underline{x}) \qquad \text{(C-33)}$$

$$G = (\underline{x}_1,\underline{\nu})(\underline{\nu},\underline{\nu})^{-1} = [(\underline{x}_1,\underline{y}) - (\underline{x}_1,\underline{x})H^T] \cdot (\underline{\nu},\underline{\nu})^{-1} \qquad \text{(C-34)}$$

In Eqs. C-33 and C-34, the covariance matrix $(\underline{\nu},\underline{\nu})$ is defined by Eq. C-32 and the sample lagged covariance matrices are defined as follows:

$$(\underline{x}_1,\underline{x}) \triangleq \sum_{k=p+1}^{n'-f+1} \underline{x}_{k+1} \, \underline{x}_k^T \cdot [n'-f-p+1]^{-1} \qquad \text{(C-35)}$$

$$(\underline{x}_1,\underline{y}) \triangleq \sum_{k=p+1}^{n'-f+1} \underline{x}_{k+1} \, \underline{y}_k^T \cdot [n'-f-p+1]^{-1} \qquad \text{(C-36)}$$

The parameter matrices Φ, G, and H of the model represented by Eqs. C-1 and C-2 are defined in Eqs. C-29, C-33, and C-34. The innovation covariance matrix R for the model is estimated as follows. First Eq. C-2 is solved for $\underline{\nu}_k$, and this expression is substituted into Eq. C-1; this yields the following pair of equations in which $\underline{y}_k$ is the input and $\underline{\nu}_k$ is the output:

$$\underline{x}_{k+1} = [\Phi - GH]\,\underline{x}_k + G\underline{y}_k \qquad \text{(C-37)}$$

$$\underline{\nu}_k = \underline{y}_k - H\underline{x}_k \qquad \text{(C-38)}$$

Equations C-37 and C-38 are used to process the observed data $\underline{y}_k$ for k = p+1 to n' to compute the innovations time series ν_k for the same range of k. In this calculation, the initial state $\underline{x}_{p+1}$ is computed from $\underline{y}_1$, $\underline{y}_2$, ..., $\underline{y}_p$ using Eq. C-26. The $\underline{\nu}_k$, computed from Eq. C-38, are then used to compute the sample covariance matrix R for the (steady-state) innovations:

$$R = \sum_{k=p+1}^{n'} \underline{\nu}_k \, \underline{\nu}_k^T \cdot [n'-p]^{-1} \qquad \text{(C-39)}$$

Equation C-39 is a more accurate way of selecting the model noise covariance matrix R than Eq. C-32. The reason for this is that Eq. C-32 is based on the fact that the state covariance matrix $(\underline{x},\underline{x})$ is the n×n identity matrix <u>when the $\underline{x}_k$ vectors are computed using Eq. C-26 from the CV analysis of Step One</u>. However, the matrix R should be selected to model the behavior of the state process defined by Eqs. C-1 to C-3 <u>when the matrices Φ, G, and H are defined by Eqs. C-29, C-33, and C-34</u>. This state process would normally not have an identity covariance matrix, although it may be close to being an identify matrix. Equation C-39, being a direct calculation based on the model equations, is the preferred estimate of the steady-state innovations covariance matrix.

In Eq. C-39, as in all other summations over the data, fragmented data sets are handled by summing over all available contiguous segments of data, with care taken to avoid running off the boundaries of the data. Each sum is then divided by the number of terms in the sum.

C.3.3 Step Three: Model Selection

The output of Step Two is a family of state-space models. Each model is optimal in a least-squares sense, given the state order n, the state vectors from Step One, and the empirical data. But which of these models is best for modeling the underlying stochastic process that generated the empirical data? A logical criterion for model selection is to select that model which has the largest expected value for its Gaussian log likelihood evaluated on future data sets. The Akaike information criterion (AIC) is an asymptotically (as the number of data increases) unbiased estimator of this measure of fit. (The AIC is not, and was never intended to be, an estimate of "true" model order. It is, however, a rational criterion for selecting that model which is most likely to be the best model in the family for modeling the underlying data process, as opposed to a model for the detailed kinks and wrinkles of the available data $\underline{y}_k$ for k = 1 to n'.)

The AIC(n) is evaluated for each model (i.e., each state order n). The model having the smallest AIC(n) is selected as the best model in the family:

$$AIC(n) = \sum_{k=1}^{n'} \log_e \left[\det[C_k(n)] \right] + 4mn \qquad \text{(C-40)}$$

In Eq. C-40, $\det[C_k(n)]$ is the determinant of the time-varying innovations covariance matrix at time k for the model with n states. The innovations covariance matrix $C_k(n)$ is rigorously computed by using a time-varying Kalman filter (Ref. 5) that optimally predicts $\underline{y}_k$ for k = 1 to n', given the available past data $\underline{y}_j$ for j = 1 to k - 1. A less accurate, but much easier to compute approximation is to use R, the steady-state innovations covariance matrix of the model, in place of $C_k(n)$ in Eq. C-40.

Equation C-40 is derived from the fact that the state-space model defined by Eqs. C-1 to C-3, with n states and m outputs, has $2mn + m(m+1)/2$ independent parameters (which is not the number of literal scalars in the matrices Φ, G, H, and R). The 4mn term in Eq. C-40 is twice the number of independent parameters to within the constant term m(m+1). (This neglected term is constant, i.e., independent of how many states are being considered for a model.)

Choosing n to minimize AIC(n) may yield a larger value of n than is necessary or desirable for reduced-order modeling. In this case a smaller value of n is selected to reduce the complexity of the model. An estimate of the mutual information between the local past and local future that is lost by omitting a specified number of states can be computed using Eq. C-27.

C.4 CONCLUDING COMMENTS

This appendix has described a practical method of developing state-space models for the underlying random processes that generate observed vector time-series data. When only n' data vectors are availble for analysis, there is a limit to how large the local future and local past can be.

The larger the length f of the future and the length p of the past, the more complicated the state-space models can be. But at the same time, increasing f and p also decreases the number of predictions that can be performed on the available data. For a fixed number of data vectors, there is a limit to the number of states n that can be usefully estimated from the data. As a practical guideline, the total number of data n' should satisfy the following inequality:

$$n' \geq 22n + f + p$$
$$n = \text{number of states} \leq \min(fm, pm) \qquad \text{(C-41)}$$

It can be shown that if the lengths f and p of the local future and past and the number of states n are restricted in accordance with inequality C-41, then there will be at least 10 statistical degrees of freedom for each free parameter in the canonical variates analysis. When f, p, and n are too large for the amount of time-series data available, the resulting stochastic model is not a reliable model for the underlying random process. Instead, it is a representation (in the sense of curve fitting) for the particular kinks and wrinkles in the observed time-series. Another reason for requiring sufficient degrees of freedom is that the minimum-AIC rule for selecting the number of states is rigorous for large data samples, which provide many degrees of freedom in the model parameter estimates.

APPENDIX D
COORDINATES, TRANSFORMATIONS, AND COVARIANCES

The purpose of this appendix is three fold: (1) to define the coordinate systems used in this study; (2) to present the equations for transforming between these coordinates; and (3) to present the formulas for computing covariance matrices of transformed position vectors.

D.1 COORDINATES AND TRANSFORMATIONS

D.1.1 Earth-Centered Cartesian Inertial Coordinates

Earth-centered Cartesian inertial coordinates are defined with the aid of Fig. D.1-1, which depicts the three coordinate axes and their relation to the earth at time t = 0. Axes No. 1 and No. 2 span the equatorial plane, while axis No. 3 is directed north. The orientation of these coordinate axes is fixed and is defined by the orientation of the earth at time t = 0 as follows: axis No. 1 passes through the prime meridian and axis No. 2 passes through the equator at 90 deg east longitude. The origin of the coordinate axes is fixed to the center of the earth. Although this coordinate frame translates with the earth, it is an accurate approximation to an inertial frame for the purpose of analyzing the motion of a payload near the earth.

D.1.2 Geocentric Coordinates

Geocentric (earth-centered and earth-fixed Cartesian coordinates are defined with the aid of Fig. D.1-2, which

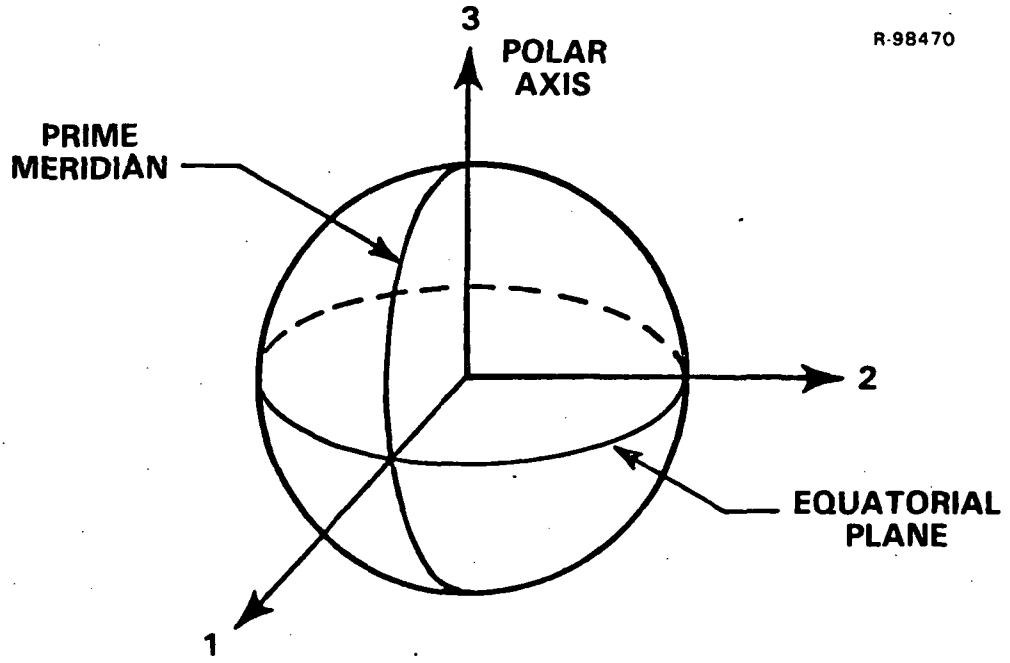

Figure D.1-1 Orientation with Respect to the Earth of the Earth-Centered Inertial Coordinate Axes at Time t = 0.

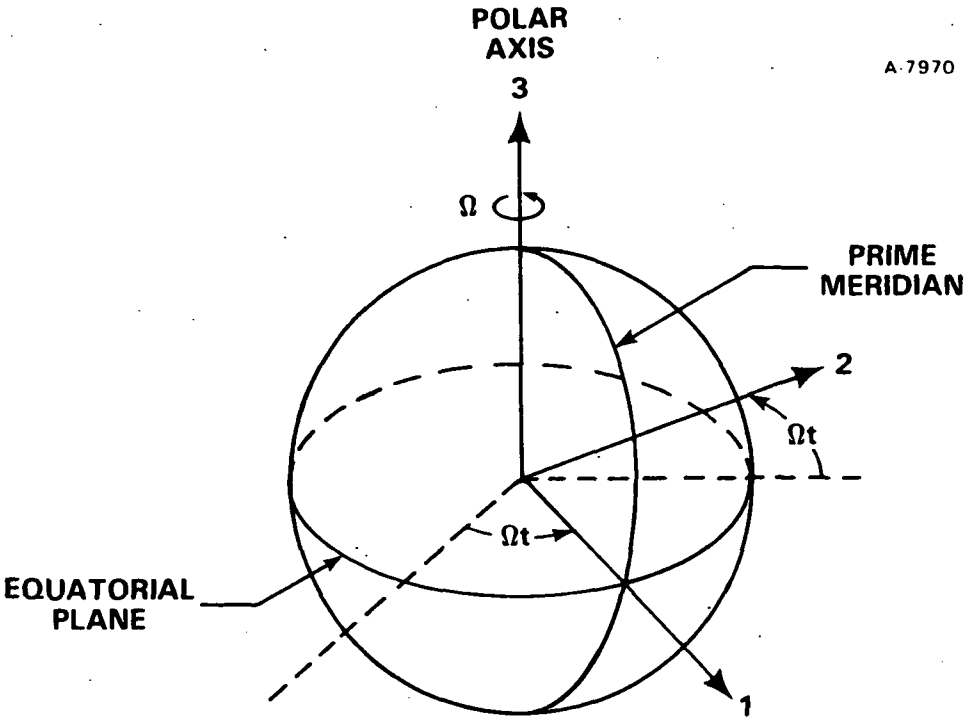

Figure D.1-2 Orientation with Respect to the Earth of the Geocentric Coordinate Axes at Time t.

depicts the coordinate axes and their fixed relation with respect to the earth. At time t = 0, the geocentric coordinate axes Nos. 1, 2, and 3 correspond to the earth-centered Cartesian inertial coordinate axes defined in Section D.1.1. At any other time t, the geocentric axes Nos. 1 and 2 rotate with the earth about the axis No. 3 through an angle Ωt with respect to the inertial axes, where Ω is the rotational velocity of the earth about axis No. 3.

The relation between the inertial and geocentric Cartesian coordinates at time t is given by the following equations:

$$\underline{r}_t^{(geo)} = \begin{bmatrix} r_{1,t}^{(geo)} \\ r_{2,t}^{(geo)} \\ r_{3,t}^{(geo)} \end{bmatrix} = \text{geocentric position coordinates} \qquad \text{(D-1)}$$

$$\underline{r}_t^{(in)} = \begin{bmatrix} r_{1,t}^{(in)} \\ r_{2,t}^{(in)} \\ r_{3,t}^{(in)} \end{bmatrix} = \text{inertial position coordinates} \qquad \text{(D-2)}$$

$$\underline{r}_t^{(geo)} = T_{t,(in)}^{(geo)} \cdot \underline{r}_t^{(in)} \qquad \text{(D-3)}$$

$$\underline{r}_t^{(in)} = T_{t,(geo)}^{(in)} \cdot \underline{r}_t^{(geo)} \qquad \text{(D-4)}$$

$$T^{(geo)}_{t,(in)} = \begin{bmatrix} \cos(\Omega t) & \sin(\Omega t) & 0 \\ -\sin(\Omega t) & \cos(\Omega t) & 0 \\ 0 & 0 & 1 \end{bmatrix} \qquad \text{(D-5)}$$

$$T^{(in)}_{t,(geo)} = \left[T^{(geo)}_{t,(in)} \right]^T \qquad \text{(D-6)}$$

Geocentric spherical coordinates (north latitude, east longitude, and radial distance) are defined with the aid of Fig. D.1-3. The relation between the Cartesian (r_1, r_2, r_3) and spherical (Φ, λ, R) geocentric coordinates are given by the following transformation equations:

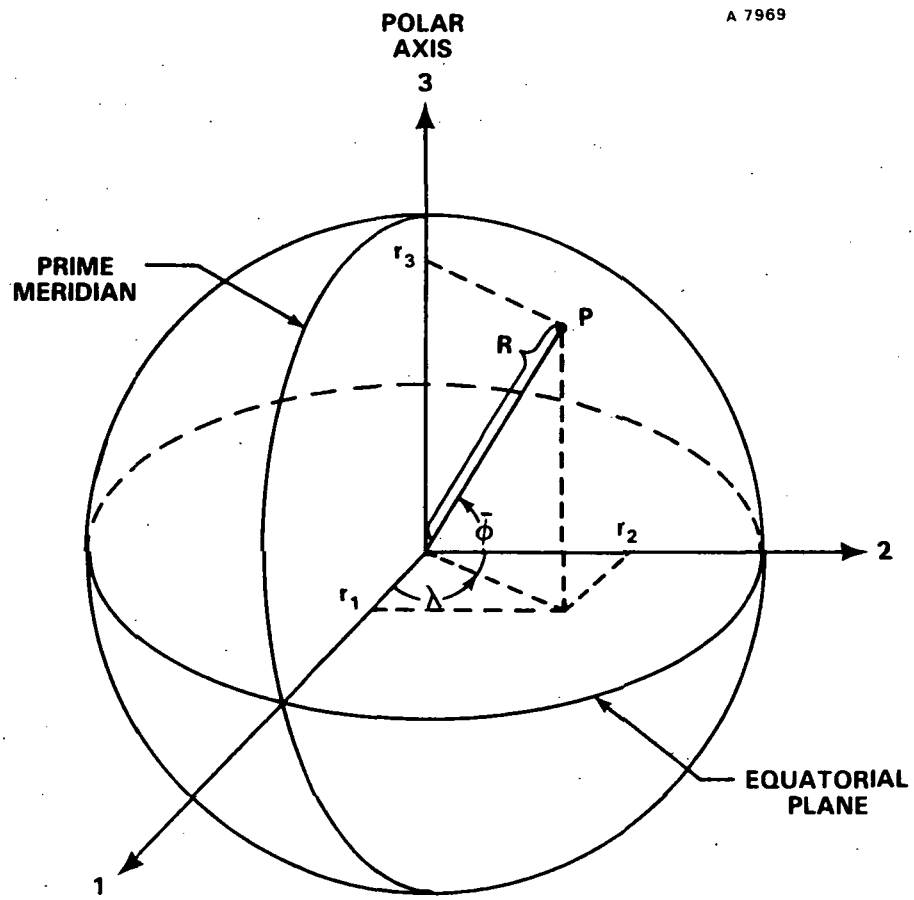

Figure D.1-3 Spherical Geocentric Coordinates of Point P. λ = East Longitude, $\bar{\Phi}$ = North Latitude, R = Radial Distance

$$R = [r_1^2 + r_2^2 + r_3^3]^{1/2} = \text{radial distance} \qquad \text{(D-7)}$$

$$R_{12} = [r_1^2 + r_2^2]^{1/2} = \text{equatorial distance} \qquad \text{(D-8)}$$

$$\bar{\Phi} = \tan^{-1}\left[\frac{r_3}{R_{12}}\right] = \text{geocentric north latitude} \qquad \text{(D-9)}$$

$$\lambda = \tan^{-1}\left[\frac{r_2}{r_1}\right] = \text{geocentric east longitude} \qquad \text{(D-10)}$$

$$r_1 = R_{12} \cdot \cos\lambda \qquad \text{(D-11)}$$

$$r_2 = R_{12} \cdot \sin\lambda \qquad \text{(D-12)}$$

$$r_3 = R \cdot \sin\bar{\Phi} \qquad \text{(D-13)}$$

D.1.3 Geodetic Coordinates

Geodetic coordinates (north latitude, east longitude, and height) are defined with respect to a reference ellipsoid. The geodetic north latitude Φ and the height h above the ellipsoid are defined for a point P with the aid of Fig. D.1-4. In this figure, the semi-major and semi-minor axes of the ellipsoid are denoted by a and b. Line AP is normal to the ellipsoid at point B and has the length N+h. The geodetic coordinates Φ and h are related to the geocentric Cartesian coordinates (r_1, r_2, r_3) of point P by the following equations (Ref. 9, p. 182) in which λ is the east longitude of point P (geodetic and geocentric longitudes are the same):

$$r_1 = (N + h) \cdot \cos\Phi \cdot \cos\lambda \qquad \text{(D-14)}$$

$$r_2 = (N + h) \cdot \cos\Phi \cdot \sin\lambda \qquad \text{(D-15)}$$

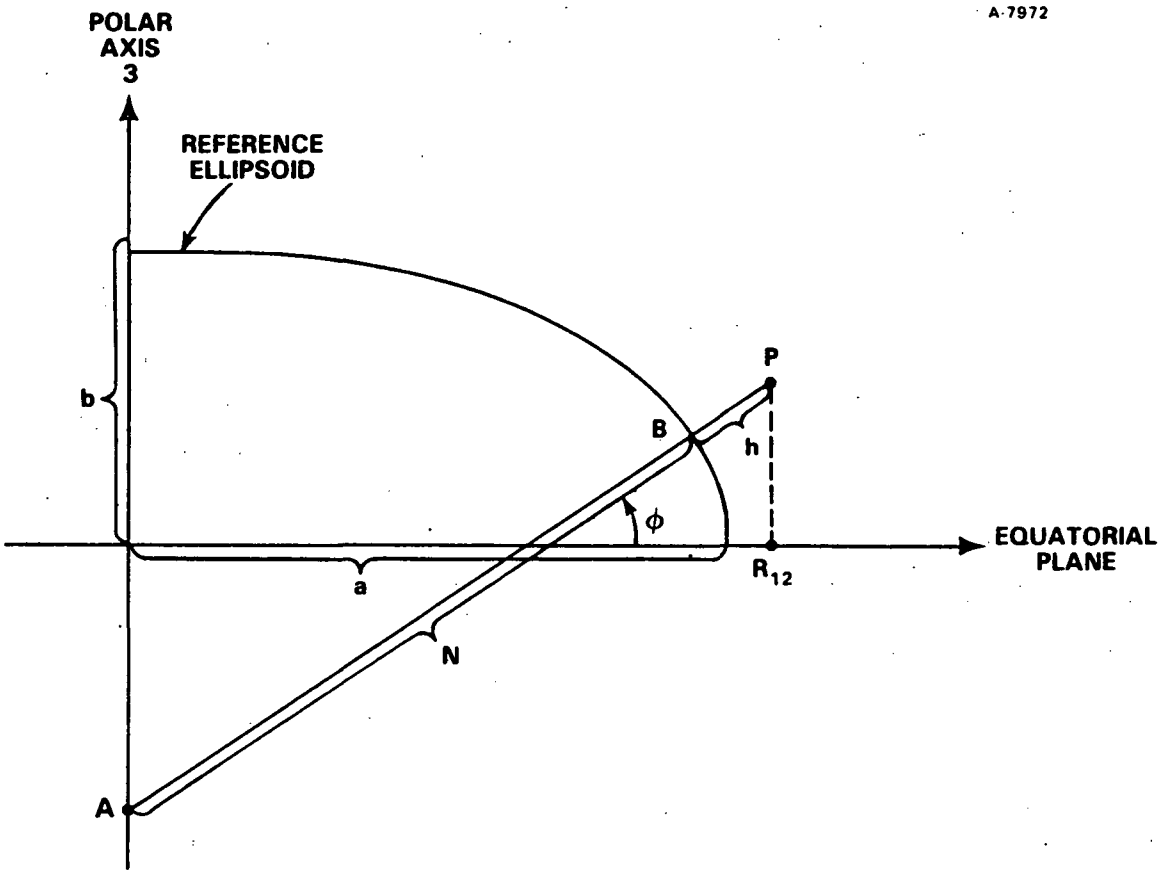

Figure D.1-4 Cross-section of Reference Ellipsoid and Point P. Geodetic Coordinates of P are Φ = North Latitude and h = Height

$$r_3 = \left[\frac{b^2}{a^2} \cdot N + h\right] \cdot \sin\Phi \qquad \text{(D-16)}$$

$$N = \frac{a^2}{\sqrt{a^2 \cdot \cos^2\Phi + b^2 \cdot \sin^2\Phi}} \qquad \text{(D-17)}$$

D.1.4 Topocentric Cartesian Coordinates

Topocentric Cartesian coordinates (north, east, down) are defined for any point P (not on the polar axis of the reference ellipsoid). They are natural Cartesian coordinates for

the local tangent space at P associated with the reference ellipsoid. The origin of the coordinates is at point P, which has height h above the reference ellipsoid, and has the geodetic east longitude λ and the north latitude Φ. The north coordinate axis points toward the polar axis of the ellipsoid, the east coordinate axis is parallel to the equatorial plane and points east, and the down axis points into the ellipsoid along the normal. The equations for transforming between topocentric Cartesian coordinates and geocentric Cartesian coordinates (for the position of any point P' relative to P) are given in the following:

$$\underline{r}^{(geo)} = \begin{bmatrix} r_1^{(geo)} \\ r_2^{(geo)} \\ r_3^{(geo)} \end{bmatrix} = \text{position of P' relative to P in geocentric coordinates} \quad \text{(D-18)}$$

$$\underline{r}^{(ned)} = \begin{bmatrix} r_{north}^{(ned)} \\ r_{east}^{(ned)} \\ r_{down}^{(ned)} \end{bmatrix} = \text{position of P' relative to P in topocentric NED coordinates} \quad \text{(D-19)}$$

$$\underline{r}^{(geo)} = T_{(ned)}^{(geo)} \cdot \underline{r}^{(ned)} \quad \text{(D-20)}$$

$$\underline{r}^{(ned)} = T_{(geo)}^{(ned)} \cdot \underline{r}^{(geo)} \quad \text{(D-21)}$$

$$T_{(geo)}^{(ned)} = \left[T_{(ned)}^{(geo)} \right]^T \quad \text{(D-22)}$$

$$T^{(geo)}_{(ned)} = \begin{bmatrix} -\sin\Phi\cdot\cos\lambda & -\sin\lambda & -\cos\Phi\cdot\cos\lambda \\ -\sin\Phi\cdot\sin\lambda & \cos\lambda & -\cos\Phi\cdot\sin\lambda \\ \cos\Phi & 0 & -\sin\Phi \end{bmatrix} \qquad \text{(D-23)}$$

D.1.5 Radar Coordinates

Radar coordinates (azimuth, elevation, and range) for a point P' are the topocentric spherical coordinates of P' realtive to the radar. Azimuth (AZ) is measured positive eastward, with AZ = 0 for due north. Elevation (EL) is measured positive toward the zenith, with EL = 0 for the horizontal. Range (RA) is measured positive away from the radar, with RA = 0 at the radar. For this discussion, the radar is located at point P, which is the origin of the radar coordinate system. The relationship between $\underline{r}^{(ned)}$, the topocentric Cartesian coordinates of P' relative to P, and the radar coordinates of P' are given by the following equations:

$$r^{(ned)}_{north} = RA \cdot \cos(AZ) \cdot \cos(EL) \qquad \text{(D-24)}$$

$$r^{(ned)}_{east} = RA \cdot \sin(AZ) \cdot \cos(EL) \qquad \text{(D-25)}$$

$$r^{(ned)}_{down} = -RA \cdot \sin(EL) \qquad \text{(D-26)}$$

D.2 COVARIANCES

D.2.1 Introduction

In this section, equations are derived for computing the covariance of a position vector in geodetic coordinates when the covariance of the position vector is given in radar coordinates. These equations are used in this investigation

to study the propagation of radar measurement noise into positional data products expressed in geodetic latitude, longitude, and height above the reference ellipsoid.

The technical approach is to linearize the coordinate transformation equations for radar measurements and then compute the covariance relations governing small perturbations about a nominal position vector. This approach is accurate for the statistical analysis of radar measurement noise because the rms of the noise signal is a small percent of the rms of the trajectory signal in the radar tracking data. The following coordinate transformations are used in this analysis: (1) radar coordinates to topocentric Cartesian coordinates; (2) topocentric Cartesian coordinates to geocentric Cartesian coordinates; and (3) geodetic coordinates to geocentric Cartesian coordinates.

In the following discussion, $\underline{\rho}$ denotes a 3×1 matrix of radar measurements:

$$\underline{\rho} = \begin{bmatrix} AZ \\ EL \\ RA \end{bmatrix} \qquad \text{(D-27)}$$

The radar coordinates $\underline{\rho}$ specify a point P', which has the topocentric Cartesian coordinates given by the nonlinear transformation defined in Eqs. D-24 to D-26. This transformation of coordinates is represented by the function $\underline{f}(\underline{\rho})$ as follows:

$$\underline{r}^{(ned)} = \underline{f}(\underline{\rho}) \qquad \text{(D-28)}$$

The topocentric Cartesian coordinates (north, east, down) in Eq. D-28 can be transformed to geocentric Cartesian coordinates as follows:

$$\underline{r}^{(geo)} = T^{(geo)}_{(ned)} \cdot \underline{r}^{(ned)} + \underline{R}^{(geo)}_{radar} \qquad \text{(D-29)}$$

$\underline{R}^{(geo)}_{radar}$ = geocentric Cartesian coordinates of the radar position

The geocentric coordinates of point P' in Eq. D-29 can also be represented in closed form as a nonlinear function $\underline{g}(\underline{\gamma})$ of the geodetic coordinates $\underline{\gamma}$:

$$\underline{\gamma} = \begin{bmatrix} \Phi \\ \lambda \\ h \end{bmatrix} = \begin{bmatrix} \text{north latitude} \\ \text{east longitude} \\ \text{height} \end{bmatrix} \qquad \text{(D-30)}$$

$$\underline{r}^{(geo)} = \underline{g}(\underline{\gamma}) \qquad \text{(D-31)}$$

The function $\underline{g}(\underline{\gamma})$ in Eq. D-31 is defined by Eqs. D-14 to D-17.

D.2.2 Perturbation Analysis

Equations D-28, D-29, and D-31 are used to solve the following problem. Given the radar coordinates $\underline{\rho}$ and the corresponding geodetic coordinates $\underline{\gamma}$ of a point P', determine the linear transformation that maps small perturbations of $\underline{\rho}$ into corresponding perturbations of $\underline{\gamma}$. With $\delta\underline{\rho}$ and $\delta\underline{\gamma}$ denoting the small perturbations, the problem is to find the 3×3 matrix T such that the following equation is satisfied in the limit as the norms of the perturbations go to zero:

$$\delta\underline{\gamma} = T \cdot \delta\underline{\rho} \qquad \text{(D-32)}$$

As shown in the sequel, the solution to this problem is given as follows:

$$T = A^{-1}(\underline{\gamma}) \cdot B \cdot C(\underline{\rho}) \qquad \text{(D-33)}$$

In Eq. D-33, the 3×3 matrix $A(\underline{\gamma})$ is defined as the derivative of vector $\underline{g}(\underline{\gamma})$ with respect to vector $\underline{\gamma}$:

$$A(\underline{\gamma}) \triangleq \frac{\partial \underline{g}(\underline{\gamma})}{\partial \underline{\gamma}} \qquad \text{(D-34)}$$

The vector differentiation in Eq. D-34 is defined as follows:

$$A_{i,j} = \frac{\partial g_i}{\partial \gamma_j} , \quad \text{for } i,j = 1, 2, 3 \qquad \text{(D-35)}$$

$$\underline{g} = [g_1 \; g_2 \; g_3]^T \qquad \text{(D-36)}$$

$$\underline{\gamma} = [\gamma_1 \; \gamma_2 \; \gamma_3]^T \qquad \text{(D-37)}$$

$$A = \begin{bmatrix} A_{11} & A_{12} & A_{13} \\ A_{21} & A_{22} & A_{23} \\ A_{31} & A_{32} & A_{33} \end{bmatrix} \qquad \text{(D-38)}$$

In Eq. D-33, the 3×3 matrix B is the transformation matrix defined by Eq. D-23 in terms of the geodetic north latitude Φ and east longitude λ of the radar's position:

$$B \triangleq T^{(geo)}_{(ned)} \qquad \text{(D-39)}$$

The 3×3 matrix $C(\underline{\rho})$ in Eq. D-33 is defined as the derivative of vector $\underline{f}(\underline{\rho})$ with respect to vector $\underline{\rho}$:

$$C(\underline{\rho}) \triangleq \frac{\partial \underline{f}(\underline{\rho})}{\partial \underline{\rho}} \qquad \text{(D-40)}$$

D.2.3 Covariance Analysis

In the following, $cov(\delta\underline{\rho})$ denotes the 3×3 covariance matrix of the perturbed radar coordinates of point P', and $cov(\delta\underline{\gamma})$ denotes the 3×3 covariance matrix of the perturbed geodetic coordinates.

From Eq. D-32, it follows that the geodetic covariance can be computed from the radar covariance as follows:

$$cov(\delta\underline{\gamma}) = T \cdot cov(\delta\underline{\rho}) \cdot T^T \qquad \text{(D-41)}$$

$$T = A^{-1}(\underline{\gamma}) \cdot T^{(geo)}_{(ned)} \cdot C(\underline{\rho}) \qquad \text{(D-42)}$$

D.2.4 Transformation Matrices

The following expressions for computing matrices $A(\underline{\gamma})$ and $C(\underline{\rho})$ are obtained by computing the derivatives indicated in Eqs. D-34 and D-40:

$$A(\gamma) = \begin{bmatrix} -(N+h)\cos\Phi\sin\lambda & -(N+h)\sin\Phi\cos\lambda & \cos\Phi\cos\lambda \\ (N+h)\cos\Phi\cos\lambda & -(N+h)\sin\Phi\sin\lambda & \cos\Phi\sin\lambda \\ 0 & [(b^2/a^2)\cdot N+h]\cos\Phi & \sin\Phi \end{bmatrix} \qquad \text{(D-43)}$$

In Eq. D-43, the quantity N is defined in terms of the semi-major and semi-minor axes (a and b) of the reference ellipsoid:

$$N = \frac{a^2}{\sqrt{a^2\cdot\cos^2(\Phi) + b^2\cdot\sin^2(\Phi)}} \qquad \text{(D-44)}$$

$$C(\underline{\rho}) = \begin{bmatrix} -RA\cdot CL\cdot SZ & -RA\cdot SL\cdot CZ & CL\cdot CZ \\ RA\cdot CL\cdot CZ & -RA\cdot SL\cdot SZ & CL\cdot SZ \\ 0 & -RA\cdot CL & -SL \end{bmatrix} \quad \text{(D-45)}$$

$$CL = \cos(EL) \quad \text{(D-46)}$$

$$SL = \sin(EL) \quad \text{(D-47)}$$

$$CZ = \cos(AZ) \quad \text{(D-48)}$$

$$SZ = \sin(AZ) \quad \text{(D-49)}$$

D.2.5 Derivation of Linear Transformation

The key linear transformation in Eq. D-32, which relates a small perturbation $\delta\underline{\rho}$ in the radar coordinates $\underline{\rho}$ of point P' to the corresponding perturbation $\delta\underline{\gamma}$ in its geodetic coordinates $\underline{\gamma}$, is derived as follows. The linearized form of Eq. D-28 is computed by expanding $\underline{f}(\underline{\rho}+\delta\underline{\rho})$ in a Taylor series about $\underline{\rho}$, and then equating the terms that are linear in the perturbation $\delta\underline{\rho}$. The result is the following linear transformation between the perturbation of the topocentric Cartesian coordinates and the radar coordinates (matrix $C(\underline{\rho})$ is defined by Eq. D-40):

$$\delta\underline{r}^{(ned)} = C(\underline{\rho}) \cdot \delta\underline{\rho} \quad \text{(D-50)}$$

Equations D-29 and D-31 are also linearized to yield the two additional linear transformations (matrices B and $A(\underline{\gamma})$ are defined by Eqs. D-39 and D-34):

$$\delta\underline{r}^{(geo)} = B \cdot \delta\underline{r}^{(ned)} \quad \text{(D-51)}$$

$$\delta\underline{r}^{(geo)} = A(\underline{\gamma})\cdot\delta\underline{\gamma} \quad \text{(D-52)}$$

Substituting Eq. D-50 in D-51 and solving Eqs. D-51 and D-52 for $\delta\underline{y}$ yields the desired linear transformation:

$$\delta\underline{y} = A^{-1}(\underline{y}) \cdot B \cdot C(\underline{\rho}) \cdot \delta\underline{\rho} \qquad \text{(D-53)}$$

APPENDIX E
RADAR MEASUREMENT EQUATIONS

The purpose of this appendix is to derive Eqs. 5.6-33 to 5.6-45, which specify the linearized measurement equations for an ideal (error-free) tracking radar. The 3×1 vector $\underline{Z}_k$ of ideal radar measurements at time k is a nonlinear function $\underline{h}_k(\underline{R}_k)$ of the earth-centered Cartesian inertial coordinates $\underline{R}_k$ of the payload position:

$$\underline{Z}_k = \begin{bmatrix} Z_k^{(\text{azimuth})} \\ Z_k^{(\text{elevation})} \\ Z_k^{(\text{range})} \end{bmatrix} = \begin{bmatrix} AZ_k \\ EL_k \\ RA_k \end{bmatrix} \tag{E-1}$$

$$\underline{R}_k = \begin{bmatrix} R_k^{(1)} \\ R_k^{(2)} \\ R_k^{(3)} \end{bmatrix} \tag{E-2}$$

$$\underline{Z}_k = \underline{h}_k(\underline{R}_k) \tag{E-3}$$

The position and measurement vectors are analyzed using nominal (nom) and small residual (δ) components:

$$\underline{R}_k = \underline{R}_k^{(\text{nom})} + \delta\underline{R}_k \tag{E-4}$$

$$\underline{Z}_k \equiv \underline{Z}_k^{(\text{nom})} + \delta\underline{Z}_k \tag{E-5}$$

The goal of this analysis is to determine the linear transformation that relates the residual measurement $\delta\underline{Z}_k$ to

the residual payload position $\delta\underline{R}_k$, in the limit as the norm of the residual position goes to zero. This linear transformation is represented by the 3×3 matrix H_k^o in Eq. 5.6-33; it satisfies the following equation for arbitrary small residual position vectors:

$$\delta\underline{Z}_k = H_k^o \cdot \delta\underline{R}_k \qquad \text{(E-6)}$$

The linear transformation is derived as the product of three simpler transformations:

$$H_k^o = A_k^{-1} \cdot B \cdot C_k \qquad \text{(E-7)}$$

In Eq. E-7, the 3×3 matrices A_k, B, and C_k have the following meanings:

C_k is the linear transformation that maps the residual payload position (in earth-centered Cartesian inertial coordinates) $\delta\underline{R}_k$ into geocentric Cartesian coordinates $\delta\underline{R}_k^{(geo)}$. This matrix is a function of the time step k.

B is the linear transformation that maps geocentric Cartesian coordinates $\delta\underline{R}_k^{(geo)}$ into the topocentric Cartesian coordinates (north, east, down) $\delta\underline{R}_k^{(ned)}$ of the radar. The matrix is a fixed function of the geodetic coordinates of the radar's location.

A_k^{-1} is the linear transformation that maps the topocentric Cartesian coordinates $\delta\,\underline{R}_k^{(ned)}$ into radar measurement coordinates $\delta\,\underline{Z}_k$. This matrix is a function of the nominal payload position expressed in radar coordinates $\underline{Z}_k^{(nom)}$.

The derivation of Eq. E-7 consists in two steps: (1) expanding the coordinate transformations (between the inertial, geocentric, and radar coordinates) in Taylor series about the nominal payload position and measurement vectors $\underline{R}_k^{(nom)}$ and $\underline{Z}_k^{(nom)}$; and (2) retaining only those terms which are linear in the residual (δ) quantities. The calculations are summarized in the following.

From Eq. D-3 (in Appendix D), the geocentric Cartesian coordinates are related to the Cartesian inertial coordinates by a linear transformation which is defined in Eq. D-5:

$$\underline{R}_k^{(geo)} = T_{t,(in)}^{(geo)} \cdot \underline{R}_k, \quad t = k \cdot \delta t \qquad \text{(E-8)}$$

The linearization of Eq. E-8 in terms of residual vectors is

$$\delta\underline{R}_k^{(geo)} = C_k \cdot \delta\underline{R}_k \qquad \text{(E-9)}$$

$$C_k = T_{t,(in)}^{(geo)}, \quad t = k \cdot \delta t \qquad \text{(E-10)}$$

The geocentric Cartesian coodinates of the payload position relative to the radar are denoted $\underline{r}_k^{(geo)}$:

$$\underline{r}_k^{(geo)} = \underline{R}_k^{(geo)} - \underline{R}_{radar}^{(geo)} \qquad \text{(E-11)}$$

$\underline{R}_{radar}^{(geo)}$ = radar location in geocentric Cartesian coordinates

Since the radar location vector is fixed, the linearized form of Eq. E-11 is

$$\delta\underline{r}_k^{(geo)} = \delta\underline{R}_k^{(geo)} \qquad \text{(E-12)}$$

According to Eq. D-21, the topocentric Cartesian coordinates of the payload position relative to the radar are related to the geocentric Cartesian coordinates by the following linear transformation, which is defined by Eqs. D-22 and D-23:

$$\underline{r}_k^{(ned)} = T_{(geo)}^{(ned)} \cdot \underline{r}_k^{(geo)} \qquad \text{(E-13)}$$

The linearization of Eq. E-13 is written as follows:

$$\delta\underline{r}_k^{(ned)} = B \cdot \delta\underline{r}_k^{(geo)} \qquad \text{(E-14)}$$

$$B = T_{(geo)}^{(ned)} \qquad \text{(E-15)}$$

The relation between the topocentric Cartesian coordinates of the payload position (relative to the radar) and the radar measurement coordinates $\underline{Z}_k$ is represented by the nonlinear transformation defined in Eqs. D-24 to D-26. This transformation is represented as the function $\underline{f}(\underline{Z}_k)$:

$$\underline{r}_k^{(ned)} = \underline{f}(\underline{Z}_k) \qquad \text{(E-16)}$$

The linearized form of Eq. E-16 is written as follows:

$$\delta\underline{r}_k^{(ned)} = A_k \cdot \delta\underline{Z}_k \qquad \text{(E-17)}$$

$$A_k = \left[\frac{\partial \underline{f}(\underline{Z})}{\partial \underline{Z}}\right]_{\underline{Z} = \underline{Z}_k^{(nom)}} \qquad \text{(E-18)}$$

The vector derivative in Eq. E-18 is defined by Eqs. D-34 to D-38.

The desired expressions given by Eqs. E-6 and E-7 are derived by solving Eq. E-17 for the residual radar measurements $\delta \underline{Z}_k$. Equations E-14, E-12, and E-9 are then used to express $\delta \underline{Z}_k$ as a function of $\delta \underline{R}_k$.

REFERENCES

1. "Information Processing Handbook," National Aeronautics and Space Administration, Wallops Flight Center, Information Processing Laboratory, November 1978.

2. Akaike, H., "A New Look at the Statistical Model Identification," IEEE Trans. Automatic Control, Vol. AC-19, No. 6, Dec. 1974, pp. 716-723.

3. Akaike, H., "Canonical Correlation Analysis of Time Series and the Use of an Information Criterion," System Identification: Advances and Case Studies, R.K. Mehra and D.G. Lainiotis (Editors), Academic Press, New York, 1976, pp. 27-96.

4. Akaike, H., "A Bayesian Extension of the Minimum AIC Procedure of Autoregressive Model Fitting," Biometrica, Vol. 66, No. 2, 1979, pp. 237-242.

5. Gelb, A. (Editor), "Applied Optimal Estimation," M.I.T. Press, Cambridge, 1974.

6. "U.S. Standard Atmosphere, 1976," National Oceanic and Atmospheric Administration, National Aeronautics and Space Administration, United States Air Force, October 1976.

7. Brouwer, D. and Clemence, G.M., Methods of Celestial mechanics, Academic Press, New York, 1961.

8. Goldstein, J.D., "Evaluation of Gravity-Induced Impact Errors Using Inflight Transfer Functions (U)," The Analytic Sciences Corporation, Report No. TR-4423-2, August 1983, pp. 2-1 - 2-6 (U) and pp. A-1 - A-10 (U), (SECRET).

9. Heiskanen, W.A. and Moritz, H., Physical Geodesy, W.H. Freeman and Co., San Francisco, 1967.

10. Bierman, G.B., Factorization Methods for Discrete Sequential Estimation, Academic Press, New York, 1977, p. 29.

11. Bryson, A.E., Jr., and Ho, Y.C., Applied Optimal Control, John Wiley and Sons, New York, Hemisphere Publishing Corp., 1975, pp. 393-395.

REFERENCES (Continued)

12. Hochstrasser, U.W., "Orthogonal Polynomials," Handbook of Mathematical Functions with Formulas, Graphs, and Mathematical Tables, Abramowitz, M. and Stegun, I.A. (Editors), Department of Commerce, National Bureau of Standards, 1964, p. 791.

13. White, J.V., "NOSS Algorithm Specifications for Ocean Current Mapping, Volume 1," National Aeronautics and Space Administration, Goddard Space Flight Center, Wallops Flight Center, NASA Contractor Report 156886(1), July 1982, pp. 2-1 - 2-6.

14. White, J.V., "Stochastic State-Space Models from Empirical Data," Proceedings ICASSP 83, Vol. 1, IEEE Intern. Conf. Acoustics, Speech and Signal Processing, Paper No. 6.3, April 1983, pp. 243-246.

15. Hotelling, H., Biometrica, Vol. 28, 1936, pp. 321-377.

16. Larimore, W.E., "System Identification, Reduced-Order Filtering and Modeling via Canonical Variate Analysis," American Control Conference, San Francisco, June 1983.

17. Kelma, V.C., and Laub, A.J., IEEE Trans. Automatic Control, Vol. AC-25, April 1980, pp. 164-176.

18. Gelfand, I.M., and Yaglom, A.M., Amer. Math. Soc. Translations, Series (2), Vol. 12, pp. 199-246, 1959.

19. Brammer, R.F., "Real-Time Shipboard Orbit Determination Using Kalman Filtering Techniques," IEEE Transactions on Aerospace and Electronic Systems, Vol. AES-10, No. 4, July 1974, pp. 492-496.

20. Herrick, S., Astrodynamics, Vol. 1, Van Nostrand Reinhold Co., London, 1971.

1. Report No.	2. Government Accession No.	3. Recipient's Catalog No.
NASA CR-168347		

4. Title and Subtitle	5. Report Date
RADAR DATA SMOOTHING FILTER STUDY	May 1984
	6. Performing Organization Code

7. Author(s)	8. Performing Organization Report No.
James V. White	
	10. Work Unit No.

9. Performing Organization Name and Address	11. Contract or Grant No.
The Analytical Sciences Corporation One Jacob Way Reading, Massachusetts 01867	NAS5-27425
	13. Type of Report and Period Covered
12. Sponsoring Agency Name and Address	NASA Contractor Final Report
NASA/Goddard Space Flight Center/Wallops Flight Facility Wallops Island, Virginia 23337	14. Sponsoring Agency Code

15. Supplementary Notes

16. Abstract

This reports presents an assessment of the accuracy of the current WFF data smoothing techniques for a variety of radars and payloads. Alternative data reduction techniques are given and recommendations are made for improving radar data processing at WFF. A data adaptive algorithm, based on Kalman filtering and smoothing techniques, was also developed for estimating payload trajectories above the atmosphere from noisy time-varying radar data. This algorithm is tested and verified using radar tracking data from WFF.

17. Key Words (Suggested by Author(s))	18. Distribution Statement
Radar,Smoothing,Kalman,Trajectory	Unclassified - unlimited STAR Category 35

19. Security Classif. (of this report)	20. Security Classif. (of this page)	21. No. of Pages	22. Price*
Unclassified	Unclassified	172	

*For sale by the National Technical Information Service, Springfield, Virginia 22151

National Aeronautics and
Space Administration

Goddard Space Flight Center
Wallops Flight Facility
Wallops Island, Virginia 23337

SPECIAL FOURTH CLASS MAIL
BOOK

Postage and Fees Paid
National Aeronautics and
Space Administration
NASA-451

Official Business
Penalty for Private Use, $300

NASA

POSTMASTER: If Undeliverable (Section 158
Postal Manual) Do Not Return